Genome-wide analysis of trimethylated lysine 4 of histone H3 (H3K4me3) in *Aspergillus niger*

Christina Sawchyn

A Thesis
in
The Department
of
Biology

Presented in Partial Fulfillment of the Requirements
for the Degree of Master of Science (Biology) at
Concordia University
Montreal, Quebec, Canada

April 2014

CONCORDIA UNIVERSITY

School of Graduate Studies

This is to certify that the thesis prepared

By: Christina Sawchyn

Entitled: Genome-wide analysis of trimethylated lysine 4 of histone H3 (H3K4me3) in *Aspergillus niger*

and submitted in partial fulfillment of the requirements for the degree of

Master of Science (Biology)

complies with the regulations of the University and meets the accepted standards with respect to originality and quality.

Signed by the final Examining Committee:

_____ Chair
Dr Malcolm Whiteway

_____ External Examiner
Dr Reginald Storms

_____ Examiner
Dr Alisa Piekny

_____ Examiner
Dr Justin Powlowski

_____ Supervisor
Dr Adrian Tsang

Approved by _____
Dr Selvadurai Dayanandan, Graduate Program Director

May 29, 2014 _____
Joanne Locke, Interim Dean of Faculty

Abstract

Aspergillus niger is a commercially important producer of enzymes and organic acids. In this study, I have examined the distribution of trimethylated lysine 4 of histone H3 (H3K4me3) in the *A. niger* genome. I performed chromatin immunoprecipitation followed by sequencing (ChIP-seq) to determine the genomic regions enriched for nucleosomes with this histone modification. I have conducted an analysis of the resulting peaksets to determine the optimal peak finding parameters for use in the detection of H3K4me3 ChIP-enriched regions in *A. niger*. As H3K4me3 was previously widely reported to mark actively transcribed genes, genome-wide ChIP-seq maps for maltose and xylose growth were compared with transcriptome data generated under the same growth conditions. Almost all genes that contained H3K4me3 are actively transcribed. However, nearly a third of all actively transcribed genes are not associated with H3K4me3. In addition, H3K4me3 is not associated with the majority of genes differentially expressed on maltose or xylose growth. Chromosomal maps revealed that this histone modification is non-randomly distributed in the genome. In particular, H3K4me3 is enriched at pericentromeric regions, but absent at the centromere and at regions proximal to the telomeres. Finally, H3K4me3 occasionally localized to actively transcribed regions not predicted to contain a gene model. The results of this study suggest that H3K4me3 is positively correlated with transcriptional activity, but is not a definitive marker of active gene expression. Furthermore, this modification is highly locally organized along *A. niger* chromosomes. Epigenetic phenomena in *A. niger* warrant further study to determine their significance in genome regulation.

Acknowledgements

Firstly and most importantly, I thank my supervisor, Dr Adrian Tsang. I am grateful for the opportunity to pursue graduate studies under his supervision and in a state-of-the-art laboratory environment: I benefited greatly from the outstanding facilities at the Centre for Structural and Functional Genomics (CSFG). I would also like to thank Dr Tsang for the opportunity to perform a ChIP-seq experiment for the first time in *Aspergillus niger*. This is a fascinating area of research at the frontier of molecular biology and I am privileged to have been part of this project. In particular, I am indebted to Dr Tsang for his instruction in experimental design and execution for generating high-quality results. As well, in the preparation of this Thesis, Dr Tsang provided me with a great deal of feedback, which has greatly impacted my writing skills in scientific communication. Finally, Dr Tsang has supported me in presenting my research at several conferences, experiences for which I am extremely grateful.

It has been a pleasure working with my committee members. I thank Dr Justin Powlowski for attending lab meetings where I presented results. Dr Alisa Piekny was instrumental in providing direction to the project, most importantly in suggesting the use of an antibody against a histone modification.

I had the opportunity to collaborate with many outstanding individuals at the CSFG. I thank Dr Marcos Di Falco for his assistance with the mass spectrometry analysis as well as his support and encouragement. Dr Ian Reid performed sequence mapping and Dr Emmet O'Brien assisted with aspects of the bioinformatics analysis. Dr Marie-Jean Meurs was extremely helpful with R Bioconductor and statistical testing. Truly, all members of the staff at the CSFG have been kind and always ready to lend a hand. I am fortunate to have worked with each and every one of them.

Without the immeasurable contribution of Vincent Lau, the data analysis portion of this work would not have been possible. Vincent was always brilliant, patient, enthusiastic and ready to assist.

I would like to acknowledge and thank Vanessa Blandford, not only for providing RNA-seq data integral to this project, but also for her companionship as a fellow graduate student and friend.

I am especially thankful for support and mentorship from Miriam Posner. Miriam has encouraged and supported me for many years and I owe her my deepest gratitude.

Last but not least, I would like to offer my special thanks to all of my family and friends for supporting me through thick and thin. I thank Danny Baum for his friendship, support and love, particularly in the final stages of this process. Most significantly, thanks to my parents, who have supported me materially and spiritually in all of my endeavours.

Table of Contents

List of Figures vii
List of Tables viii
List of Abbreviations viii

Section 1: Introduction 1

1.1 The epigenetic regulation of genomes 1

1.2 Organization of chromatin 2

1.3 Epigenetic modifications of histones 2

1.4 Epigenetic regulation of gene expression 4

1.5 Histone methylations as epigenetic markers 6

1.6 Trimethylation of lysine 4 on histone H3 (H3K4me3) 9

1.7 Chromatin immunoprecipitation followed by sequencing: ChIP-seq 11

1.8 ChIP-seq data analysis to determine significantly enriched regions 14

1.9 *Aspergillus niger*, a cell factory 15

1.10 Rationale for studying comparative ChIP-seq of *A. niger* H3K4me3 in growth on maltose and xylose 16

Section 2: Methods 19

2.1 *Aspergillus niger* strains, media and growth conditions 19

2.2 Formaldehyde crosslinking of *A. niger* mycelia 19

2.3 Cell lysis and crude separation of cytosolic and nuclear fractions 20

2.4 Determination of DNA in pellet and supernatant fractions 21

2.5 Assessment of formaldehyde crosslinking 21

2.6 Protein digestion 22

2.7 LC-MS/MS analysis 22

2.8 Mass spectrometry bioinformatics data processing 23

2.9 Lysis of crude nuclei enriched pellet and determination of sonication conditions 23

2.10 Chromatin immunoprecipitation (ChIP) 24

2.11 Immunoblotting to determine the reactivity of the anti-H3K4me3 antibody and sequencing of immunoprecipitated chromatin 25

2.13 Identification of H3K4me3 peaks 26
2.14 Peakset and differential binding analysis with the DiffBind package for R Bioconductor 27
2.17 File conversions, ChIP peak intersections, annotation and analysis of peaksets 27
2.19 Statistical testing of differences between distributions of FPKM values 27
2.20 Data visualization 27

Section 3: Results 28
3.1 Protocol development for ChIP-seq in *Aspergillus niger* 28
3.1.1 Enrichment of nuclear fraction for ChIP-seq analysis 28
3.1.2 Demonstration of suitable crosslinking conditions 31
3.1.4 H3K4me3 chromatin immunoprecipitation followed by sequencing (ChIP-seq) 33
3.2 H3K4me3 ChIP-seq data processing 36
3.2.1 H3K4me3 peak finding 36
3.2.2 Analysis of SICER peakset correlation between replicates 38
3.2.3 SICER peakset analysis 38
3.3 H3K4me3 patterns and distribution in the *Aspergillus niger* genome 47
3.3.1 A majority of actively transcribed genes contain H3K4me3 47
3.3.2 Differential H3K4me3 binding analysis 53
3.3.3 Comparison of differential H3K4me3 binding and levels of transcript accumulation 55
3.3.4 Genes with and without H3K4me3 are not randomly distributed along the chromosome 61
3.3.5 H3K4me3 is associated with potential non-coding RNA 66

Section 4: Discussion 70
4.1 Development of a method for enrichment of nuclei in *Aspergillus niger* 70
4.2 Technical considerations for *A. niger* ChIP-sequencing and data analysis 70
4.3 H3K4me3 is not a definitive marker of active gene transcription in *A. niger* 72
4.4 Non-random distribution of H3K4me3 in the chromosome 75
4.5 H3K4me3 supports the annotation of genomic features 76

Section 5: Conclusion 77

Section 6: References 78

List of Figures

Figure 1. Post-translational modifications on histones 3
Figure 2. Suggested modes of genome regulation by histone modifications 5
Figure 3. Summary of a ChIP-seq experiment.....12
Figure 4. Representation of xylose and maltose metabolic pathways in *Aspergillus niger* 17
Figure 5. DNA content of nuclear and cytosolic fractions 29
Figure 6. Distribution of marker proteins in pelleted and supernatant fractions 30
Figure 7. Chromatin crosslinking and de-crosslinking 32
Figure 8. Determination of sonication conditions.....34
Figure 9. H3K4me3 antibody specificity.....35
Figure 10. Control sonicated DNA as a control for H3K4me3 ChIP-seq 37
Figure 11. Correlation heatmap of peaksets 39
Figure 12. Peak finding parameters and the number of H3K4me3 modified genes detected 43
Figure 13. The effect of smaller window and gap sizes on peak detection 44
Figure 14. Effects of gap size on fragmented peak regions.....46
Figure 15. Comparing gene expression of *A. niger* and presence of H3K4me3 for growth on maltose and xylose.....48
Figure 16. Comparing expression and presence of H3K4me3 across functional categories.....49
Figure 17. Presence of H3K4me3 in constitutively transcribed genes 54
Figure 18. Visual representation of significantly differentially bound sites.....56
Figure 19. Maltose growth and xylose growth peak occupancy analysis 58
Figure 20. Comparison of differentially expressed genes and H3K4me3 modification.....59
Figure 21. Chromosomal distribution of H3K4me3 62
Figure 22. Genes with and without H3K4me3 in regions surrounding the centromeres and telomeres.....64
Figure 23. H3K4me3 marks regions of non-coding transcripts 67

List of Tables

Table 1. Proposed regulatory functions of histone methylations 7
Table 2. Published histone modification ChIP-seq studies in fungi 13
Table 3. Pearson correlation values of SICER peaksets from sample replicates.....40
Table 4. Genes marked or unmarked by H3K4me3 categorized by protein function 52
Table 5. Differentially bound sites identified in DiffBind.....57
Table 6. Differentially transcribed genes with differential H3K4me3 60
Table 7. H3K4me3 distribution at regions proximal to the centromeres and telomeres 65
Table 8. Genome coordinates for ChIP-enriched regions not intersecting with a known gene model.....68

List of Abbreviations

ACN	acetonitrile
bp	base pair
CCAT	Control based ChIP-seq Analysis Tool
ChIP	chromatin immunoprecipitation
ChIP-seq	chromatin immunoprecipitation-sequencing
chr	chromosome
CID	collision-induced disassociation
DTT	dithiothreitol
ECL	enhanced chemiluminescence
EDTA	ethylenediaminetetraacetic acid
FA	formic acid
FDR	false discovery rate
FPKM	fragments per kilobase of exon per million fragments mapped
G	gap size
GC	guanine-cytosine
GH	glycosyl hydrolase
H1	histone H1
H2A	histone H2A
H2B	histone H2B
H3	histone H3
H3K4me3	tri-methylated Lysine 4 on histone H3
H4	histone H4
H5	histone H5

HPLC	high performance liquid chromatography
IgG	immunoglobulin G
K	lysine
kb	kilobase
kbp	kilobase pair
kDa	kilodalton
kV	kilovolt
LC	liquid chromatography
LiCl	lithium chloride
MA	M (log ratios) and A (mean average)
Me	methyl group
MgOAc	magnesium acetate
MM	minimal media
MS	mass spectrometry
NaCl	sodium chloride
NADP	nicotinamide adenine dinucleotide phosphate
NaHCO3	sodium bicarbonate
NP-40	Nonidet P-40
PAGE	polyacrylamide gel electrophoresis
PBS	phosphate-buffered saline
PCI	phenol/chloroform/isoamyl alcohol
PCR	polymerase chain reaction
PHD	plant homeodomain
PMSF	phenylmethanesulfonyl fluoride
R	arginine
RCDC	reducing agent and detergent compatible
RNA	ribonucleic acid
RNAP	RNA polymerase
RNase A	ribonuclease A
rRNA	ribosomal RNA
SD	standard deviation
SDS	sodium dodecyl sulfate
SICER	spatial clustering approach for identification of ChIP-enriched regions
TAF3	TATA-box binding protein associated factor 3
TE	Tris-EDTA
TFIID	transcription factor II D
Tris-HCl	Tris hydrochloride
tRNA	transfer RNA
Ub	ubiquitin
W	window size

Section 1: Introduction

1.1 The epigenetic regulation of genomes

Despite the availability of a wide variety of whole genome sequences, biologists are still unable to resolve differences in biological characteristics of different cell types, individuals or species based solely on heritability of gene sequence or DNA mutations. It has become clear that certain phenomena are governed by other determinants not contained within the DNA sequence.

The term "epigenetics" (derived from the Greek "epi", meaning "above" or "on top"), coined by the British biologist Conrad Waddington (Waddington, 1942), is the study of clonally heritable alterations that direct expression in genomes, unrelated to primary DNA sequence. These differences include, among others, DNA methylation, paramutation, DNA damage, and histone modifications.

The biological consequences of epigenetic phenomena, seen in all eukaryotes, are varied. In mammals, totipotent cells are guided to a differentiated state via epigenetic changes (Boyer et al. 2006). Once a cell is fully differentiated into a specific cell type, the genome needs to be stabilized to realize long-term stable gene expression patterns, achieved here again by imparting epigenetic changes (Ng and Gurdon, 2008). Changes in the epigenome are linked to various types of cancer and have led to targets for therapeutics (Højfeldt et al. 2013). Epigenetic modifications have also been implicated in the mediation of DNA repair mechanisms (Li et al. 2013; Tang et al. 2013). In the plant genome, epigenetic mechanisms are involved in developmental processes, stress-responses and phytohormone signaling (Chen and Zhou, 2013). In filamentous fungi, the epigenome has become important in the study of secondary metabolite synthesis (Gacek and Strauss, 2012). For example, the sterigmatocystin gene cluster in *Aspergillus nidulans* is regulated by competition between an activating epigenetic modification that promotes gene expression and a repressing epigenetic marker that mediates genome silencing (Reyes-Dominguez et al. 2010).

The study of epigenetics has moved to the forefront of molecular biology and has been a dynamic and productive area of research in the last decade. Advances in epigenetics hold multiple implications for understanding previously inexplicable changes in eukaryotic gene expression and chromosome structure.

1.2 Organization of chromatin

The basic packaging unit of DNA in nuclear chromatin is the nucleosome. Crystal structure analysis has revealed that the nucleosome is formed by a core particle consisting of 146 base pairs of DNA superhelix wrapped around the histone octamer, which is made up of two H2A/H2B heterodimers and two H3 and H4 dimers (Luger et al. 1997). These are immediately followed by short stretches of linker DNA, which complex with H1 and H5 linker histones. The nucleosome particles wrapped in DNA form 10 nm linear "beads-on-a-string" structures, known as chromatin "fibers". Linear chromatin can assemble into larger 30 nm fibers and even higher order structures, a phenomenon termed "chromatin compaction". The properties and fundamental structure of these arrangements is still controversial (Grigoryev and Woodcock, 2012). Although many aspects of chromatin biology remain ambiguous, there is clear evidence that the chromatin fiber is a dynamic and flexible structure that moves inside living cells (Lanctot et al. 2007). Furthermore, some chromatin loci are more mobile than others and this can depend on their location within the nucleus.

1.3 Epigenetic modifications of histones

The histones that assemble into nucleosomes and chromatin fibers are subject to a number of modifications and mediate the epigenetic process. Most histone modifications occur in the first 25 N-terminal amino acids protruding from the nucleosome core. Several types of histone modifications have been identified, including phosphorylation of serine, threonine and tyrosine residues; lysine acetylation, ubiquitylation and sumoylation; and lysine and arginine methylation (Bannister and Kouzarides, 2011).

Figure 1. Post-translational modifications on histones

A depiction of the histone "code", made up of DNA methylations and other post-translational histone modifications, read by chromatin binding proteins. (Image source: Scharf and Imhof, 2011)

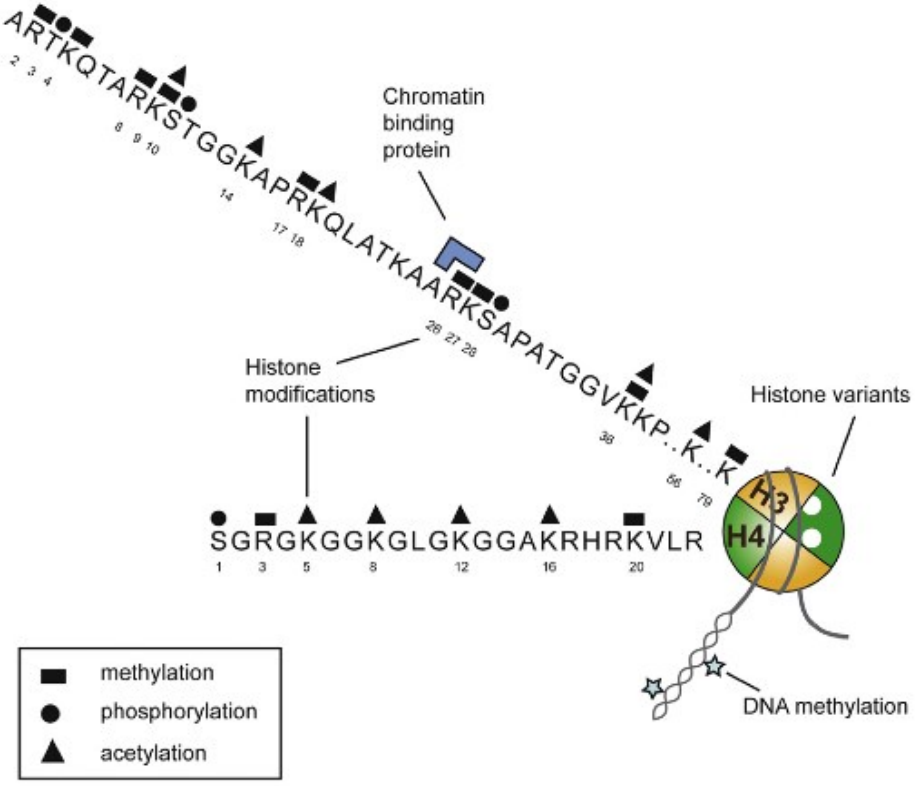

The "histone code" theory proposes that combinations of post-translational covalent modifications on nucleosomal histones distributed along chromatin (Figure 1) confer a particular regulatory state or functional properties for that region (Strahl and Allis, 2000; Gardner et al. 2011). Chromatin-binding molecules can recognize this histone "barcode" and facilitate the recruitment of other factors to alter the chromatin structure (Taverna et al. 2007).

However, due to the lack of experimental support, the "histone code" theory has been questioned (Henikoff and Shilatifard, 2011). The central question is whether histone modifications cause a biological response or occur as a result of dynamic cellular processes. In other words, it has not yet been shown whether histone modifications dictate chromatin changes that result in a defined output, such as transcriptional activation or repression.

1.4 Epigenetic regulation of gene expression

Two general concepts of possible signaling by histone modifications and their effect on chromatin structure and transcriptional control have been proposed: direct (or *cis*) and indirect (or *trans*). An overview of these mechanisms is shown in Figure 2 (review of Greer and Shi, 2012).

In *cis* regulation, histone modifications influence higher order structures of chromatin, which impact nucleosome positioning, stability and assembly. One theory suggests the occurrence of chromosomal "looping" by interacting histone modifications (Figure 2, Panel a), physically bringing together separate, non-adjacent compartments of chromatin (Dekker et al. 2002), which could include gene activating enhancer elements or repressing insular regions (Deng and Blobel, 2010). The phenomenon known as "gene kissing", in which distant regulatory elements and target genes co-localize (occasionally between different chromosomes) has been demonstrated in *Drosophila*, mouse and human cells (Lanctot et al. 2007). Precisely how histone methylations mediate this process remains thus far untested (Allis and Muir, 2011).

In *trans* regulation, histone modifications facilitate the recruitment or release of specific binding proteins, such as chromatin remodeling complexes, which mediate their function. One proposed mechanism suggests that inaccessible chromatin domains can be "opened" by DNA sequence-specific "pioneering" transcription factors (Cirillo et al. 2002) such as forkhead box proteins (Figure 2, Panel b). After this binding event, DNA methylation and other histone

Figure 2. Suggested modes of genome regulation by histone modifications.

A representation of proposed mechanisms for transcriptional regulation by histone methylations. Panel a) depicts a *cis* model and various proposed *trans* models are shown in Panels b)-d). (Image source: Greer and Shi, 2012)

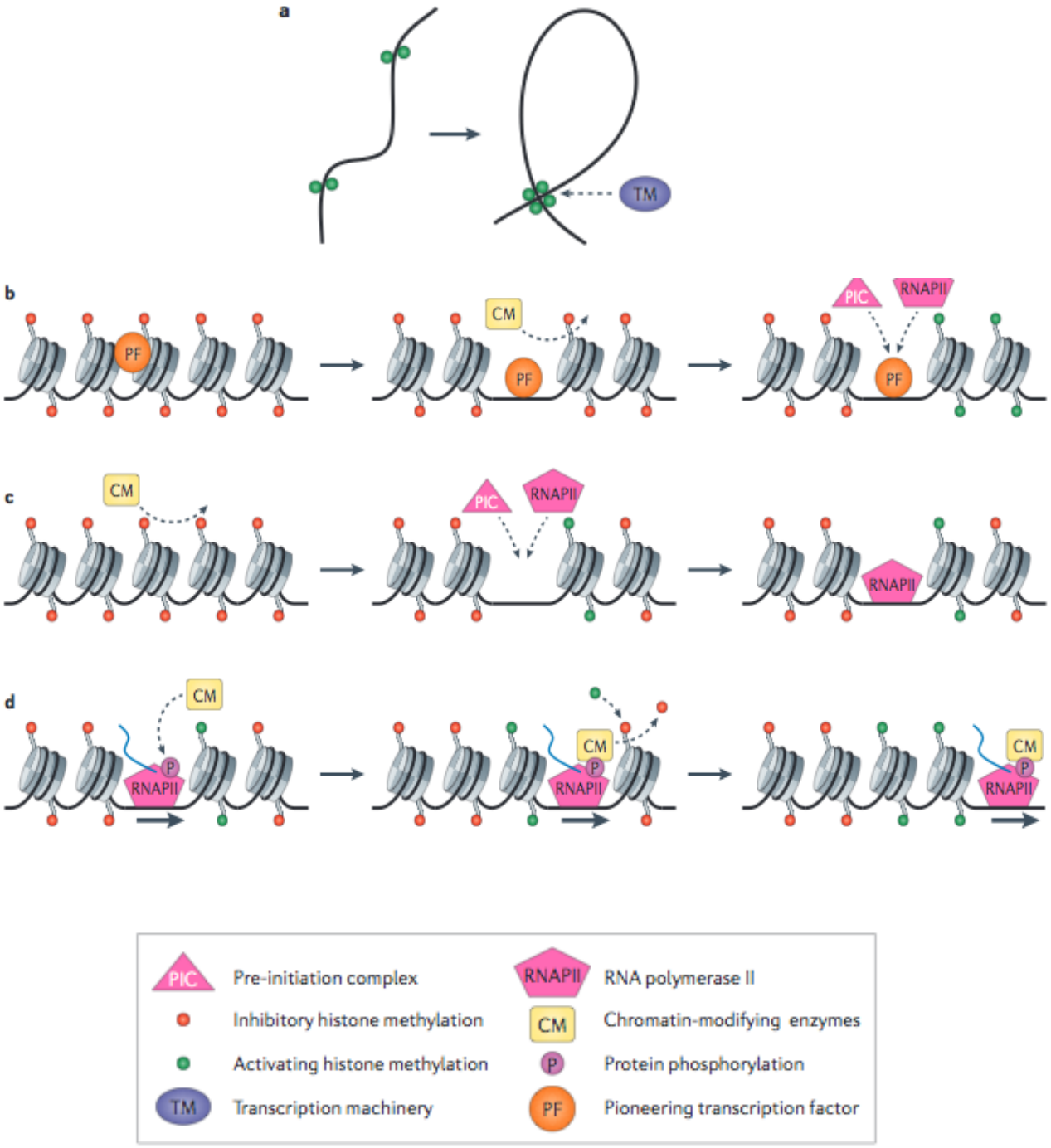

modifications participate in making the chromatin more accessible to other transcription factors, the pre-initiation complex and RNA polymerase II (Serandour et al. 2011). Stretches of certain histone methylation patterns may be a requirement for the binding of transcription factors (Figure 2, Panel c), as has been demonstrated for the human Myc transcription factor binding to promoter regions (Guccione et al. 2006), although the mechanism for this is unclear. Finally, histone modifications can facilitate recruitment of chromatin remodeling complexes (Fuda et al. 2009) to potentially regulate transcriptional efficiency and/or elongation (Figure 2, Panel d). Despite recent advances made in understanding indirect regulation by histone modifications, much remains to be understood about the precise functions and order of events that link them to transcription control (Greer and Shi, 2012).

1.5 Histone methylations as epigenetic markers

Post-translational modifications on histones H1, H2A, H2B, H3 and H4 have been experimentally correlated with diverse biological functions and processes, including development and differentiation, cell-cycle regulation, DNA repair, RNA splicing and transcriptional processes (Kouzarides, 2007; Pederesen and Helin, 2010; Greenberg, 2011; Eissenberg and Shilatifard, 2010).

As reviewed by Fischle (2013), the most complex epigenetic modification is histone methylation. Histones are mainly methylated on their arginines and lysines, and rare methylation of histidines has been described (Gershey et al. 1969, Borun et al. 1972). All methylations of lysines occur on the ε-amine group, which can be mono- (me), di- (me2) or tri-methylated (me3). Peptidylarginine methyltransferases methylate arginines once or twice, the latter either asymmetrically (both methyl groups on one terminal nitrogen) or symmetrically (one methyl group on each terminal nitrogen). Table 1 summarizes the epigenetic effects of histone methylations that have been experimentally characterized to date. Methylations of histones have been implicated in both activation and silencing of global gene expression. The most studied methylations are those occurring on histones H3 and H4. In general, transcriptional activation is associated with symmetrical dimethylation of arginine 2 on histone H3 (H3R2me2), H3K4me3,

Table 1. Proposed regulatory functions of histone methylations

Histone and modified residue	Methyl (me) groups	Organism(s)	Proposed function(s)	References (PMID)
H1.4K26	me2	*H. sapiens*	transcriptional silencing	16127177 15099518
H2AR3	me2	*H. sapiens*	regulation of DNA repair response	22761421
H2BK5	me1	*H. sapiens*	transcriptional activation	17512414
H3R2	me2a*	*H. sapiens, S. cerevisiae*	transcriptional repression	17898714 17898715
H3R2	me2s*	*M. musculus,* *D. melanogaster, X. laevis,* *S. cerevisiae*	transcriptional activation	22720264
H3K4	me1	*H. sapiens*	transcriptional repression; maintenance of promoter structure	24656132
H3K4	me1	*D. melanogaster*	transcriptional activation	23166019 23560912
H3K4	me1	*C. reinhardtii*	transcriptional repression	16100335
H3K4	me1	*S. cerevisiae*	transcriptional repression	15949446
H3K4	me2	*H. sapiens*	transcriptional activation	17512414
H3K4	me2	*S. cerevisiae*	transcriptional repression	23028359
H3K4	me2	*H. sapiens*	establishment of transcription factor binding regions	24530516
H3K4	me2	*D. melanogaster*	transcriptional de-repression	15031712 15175259
H3K4	me3	*H. sapiens, O. sativa*, *S. cerevisiae*	transcriptional activation	17043231 17512414 20086188 12060701 12353038 14636589
H3K4	me3	*D. melanogaster*	transcriptional de-repression	15031712 15175259
H3K4	me3	*S. cerevisiae*	establishment of repressive chromatin structure	23028359
H3K4	me3	*A. thaliana*	transcriptional elongation	23284292
H3R8	me2	*H. sapiens*	transcriptional repression	15485929 17043109 17627275 18694959 21447565
H3K9	me1	*H. sapiens*	transcriptional activation	17512414

*'s': symmetrical methylation; 'a': asymmetrical methylation

Histone and modified residue	Methyl groups	Organism(s)	Proposed function(s)	References (PMID)
H3K9	me3	*M. musculus, H. sapiens*	propagation of heterochromatin; transcriptional silencing	11242053 17512414
H3K9	me3	*H. sapiens*	transcriptional repression	11959841
H3K9	me3	*N. crassa, A. thaliana*	DNA methylation	11713521 12194816
H3K9	me3	*N. crassa*	normal distribution of centromeric histone variant	21505064
H3K9	me3	*D. melanogaster*	transcriptional activation	12397363
H3R17	me1	*H. sapiens*	transcriptional activation	11747826 11751582 12498683
H3R17	me2a*	*H. sapiens*	transcriptional de-repression	22723830
H3R17	me2a*	*H. sapiens*	transcriptional activation	22451921
H3R26	me2a*	*H. sapiens*	transcriptional de-repression	22723830
H3K27	me1	*H. sapiens*	transcriptional activation	17512414
H3K27	me3	*H. sapiens*	transcriptional repression	17512414
H3K36	me2	*S. cerevisiae, S. pombe, D. melanogaster*	transcriptional elongation; chromatin deacetylation	15798214 16087749 18007591 24004944
H3K36	me3	*D. melanogaster*	transcriptional elongation; chromatin deacetylation	18007591
H3K36	me3	*H. sapiens*	regulation of DNA repair response	23622243
H3K79	me2	*S. cerevisiae*	inhibition of heterochromatin propagation	15920479 12574507
H3K79	me2	*D. melanogaster, M. musculus*	transcriptional activation	15175259 18285465
H3K79	me2	*H. sapiens*	transcriptional elongation	17135274 17855633
H3K79	me3	*D. melanogaster*	transcriptional activation	20203130
H4R3	me2s*	*H. sapiens*	regulation of DNA repair response	22761421
H4R3	me2s*	*H. sapiens*	DNA methylation; transcriptional silencing	19234465
H4K16	me1	*H. sapiens*	unknown	21925322
H4K20	me1	*D. melanogaster*	transcriptional silencing	12086618
H4K20	me1	*H. sapiens*	DNA replication	20953199
H4K20	me2	*S. pombe, H. sapiens, M. musculus*	regulation of DNA repair response	15550243 23377543
H4K20	me3	*M. musculus*	transcriptional silencing	15145825

*'s': symmetrical methylation; 'a': asymmetrical methylation

H3K9me1 and H3K79me3. Transcriptional repression is correlated with H3K9me3 and H3K27me3. H3K9me3 is also involved in genome silencing by heterochromatin formation and H3K79me2 inhibits heterochromatin formation. H3K36me2/3 and H3K79me2 function in transcriptional elongation. Other proposed functions of histone methylations include DNA repair (H2AR3me2, H3K36me3 and H4K20me2), DNA methylation (H3K9me3 and H4R3me2s) and DNA replication (H4K20me1). Some histone methylations were shown to behave differently between species or to have dual roles. For example, H3K4me1 is an activating marker in fruit fly, but is correlated with transcriptional repression in yeast and human. The best-studied chromatin modification, tri-methylation of lysine 4 of histone 3 (H3K4me3), is in yeast associated with active transcription, but has also been implicated in transcriptional repression.

1.6 Trimethylation of lysine 4 on histone H3 (H3K4me3)

H3K4me3 is a well-conserved modified histone found universally in eukaryotes (Strahl et al. 1999; Fuchs et al. 2006). In yeast, the Set1/COMPASS complex is responsible for catalyzing methylations on H3 and was the first histone methylase to be identified (Miller et al. 2001). These modifications were first thought to be irreversible, due to the thermodynamic stability of the N-CH_3 bond. The discovery of H3K4 demethylases (Shi et al. 2004, Trewick et al. 2005, Christensen et al. 2007) changed this perception. It has since been demonstrated that histone methylation, including trimethylation of H3K4me3 (Maltby et al. 2012), is a biochemically dynamic modification.

Several different proteins with a variety of biological functions can bind H3K4me3. These include transcriptional activators, chromatin remodeling factors, histone acetylation proteins, chromatin silencing factors, and proteins involved in splicing efficiency (reviewed by Vermeulen and Timmers, 2010). An important question is how specific recruitment of these factors is achieved, given their functional diversity and sometimes opposing effects. Currently, it is thought that this can be achieved by the interaction of H3K4me3 with specific transcription factors to recruit the appropriate binding molecule (Vermeulen et al. 2007). Another model suggests that H3K4me3 stabilizes the interaction between transcription factors and other proteins or facilitates the interaction of the H3K4me3 binding complexes with the DNA sequence (Tu et al. 2008). Finally, the proteins that can bind H3K4me3 have varying levels of affinity for this histone modification, which may also play a role in recruitment specificity (Sims and Reinberg, 2006; Huang et al. 2006; Vermeulen et al. 2007).

In general, H3K4me3 is localized to promoter regions or 5' regions of genes and binding sites decrease in number over the next few kilobases (Schneider et al. 2004; Bernstein et al. 2005; Barski et al. 2007). This pattern is specific to trimethylation of lysine 4, as di- and monomethyl K4 modifications show distinct distributions. In yeast, H3K4me2 marks were shown to localize to the middle of gene coding regions and H3K4me1 is found at the end of genes (Pokholok et al. 2005).

Over the past decade, a number of studies investigating a role for H3K4 methylation in gene expression have been published for a wide range of eukaryotic species (Table 1). The first studies to describe a role for H3K4me3 reported that this histone modification was characteristic of genes undergoing transcriptional activation in yeast (Bernstein et al. 2002; Santos-Rosa et al. 2002). This finding was subsequently echoed for many other species in (reviewed by Sims et al. 2003). In metazoans, H3K4me3 was proposed to play a role in active gene transcription by serving as a high affinity binding platform for the general transcription initiation factor TFIID, which is shown to interact directly with the TAF3 subunit (Vermeulen et al. 2007, Lauberth et al. 2013). As a result, it has been suggested that H3K4me3 stabilizes the pre-initiation complex at the promoter and increases the probability of transcription initiation.

H3K4me3 is thought to function differently in yeast, as its TAF3 subunit lacks the PHD finger domain (Gangloff et al. 2001). There is emerging evidence supporting alternative

explanations for the relationship between H3K4me3 and gene expression in yeast. For instance, the yeast Set1p methyltransferase, responsible for the methylation of histone H3, was shown to bind to the initiating form of RNA polymerase II, suggesting that H3K4me3 could occur as a consequence rather than a cause of transcription (Ng et al. 2003). In addition, more recent studies exploring the role of H3K4me3 in yeast transcription have described a role for H3K4me3 in both active and repressed subsets of genes, suggesting that the role of histone modifications in gene expression may be context-dependent (Guillemette et al. 2011; Margaritis et al. 2012).

In filamentous fungi, studies describing the role and patterns of H3K4me3 are limited. To date, there have been two reports: in *Neurospora crassa* (Smith et al. 2011) and *Trichoderma reesei* (Seiboth et al. 2012). Each of these studies performed chromatin immunoprecipitation followed by sequencing (ChIP-seq) to describe the DNA binding sites of H3K4me3. Descriptions for the role of H3K4me3 in these studies are brief and the authors did not explore the link between this histone modification and gene expression. A list of all ChIP-seq publications describing genome-wide patterns of histone modifications in fungi is shown in Table 2.

1.7 Chromatin immunoprecipitation followed by sequencing: ChIP-seq

Chromatin immunoprecipitation (ChIP) followed by sequencing, known as ChIP-seq, generates a genome-wide binding map of a given transcription factor, modified histone or DNA binding protein. This method employs the pull-down of a target protein using an antibody specific for a DNA binding protein, followed by massively parallel sequencing of the DNA fragments bound to the protein of interest (originally described by Barski et al. 2007, Johnson et al. 2007 and Roberston et al. 2007.) A summary of the steps of a ChIP-seq experiment is illustrated in Figure 3.

ChIP-seq experimental design requires some key considerations. Most importantly, specificity and sensitivity of antibodies, including commercially available ChIP-grade antibodies are required to be validated. According to the ENCODE and modENCODE consortia, which

Figure 3. Summary of a ChIP-seq experiment

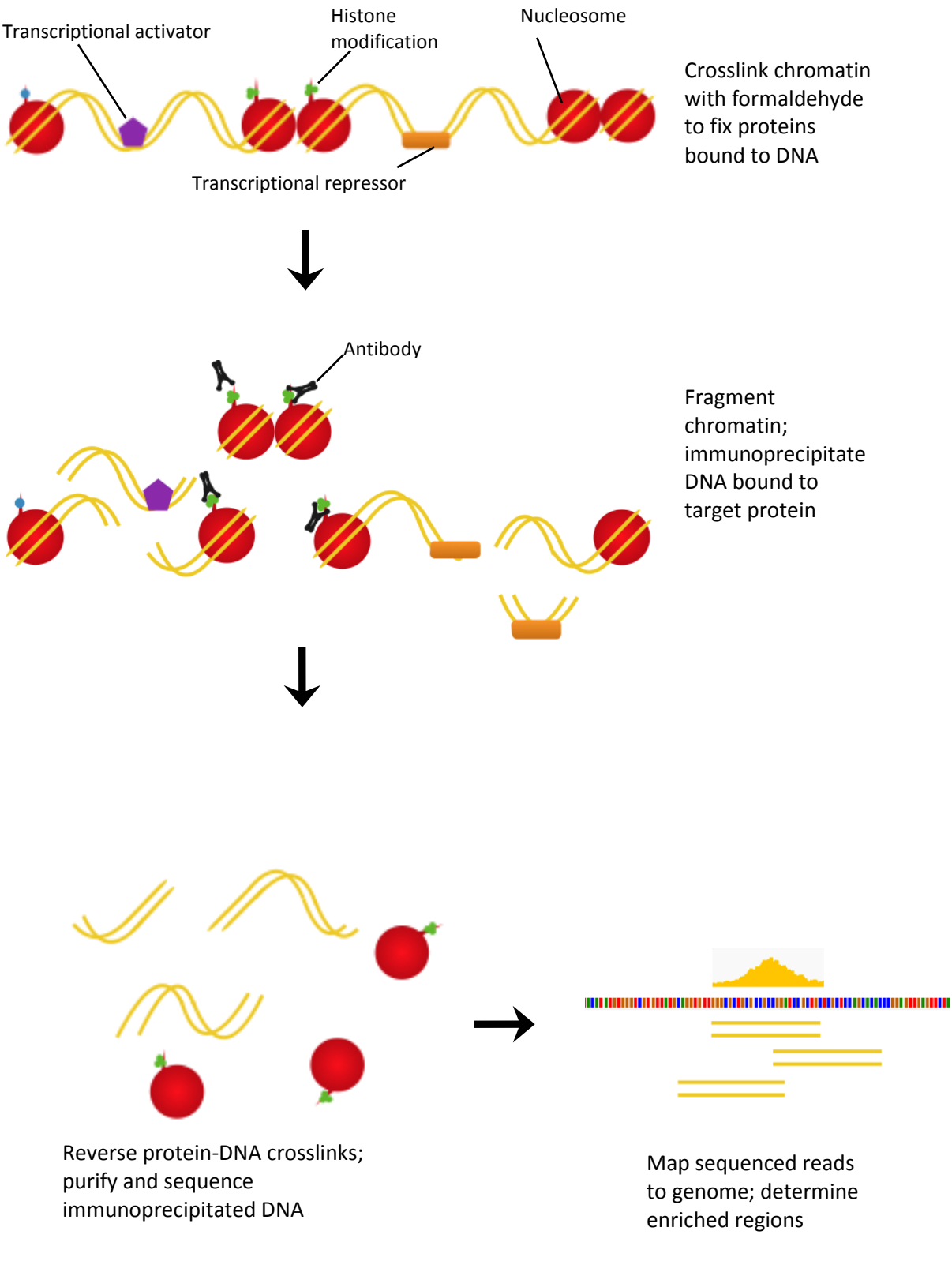

Table 2. Published histone modification ChIP-seq studies in fungi

A list of publications (derived from PubMed), which have reported histone modification data from a ChIP-sequencing (ChIP-seq) experiment. This list includes all published ChIP-seq studies to-date from yeast (*Saccharomyces cerevisiae*) and filamentous fungi.

Species	Histone modification	Year	Authors	Major findings
S. cerevisiae	H3K36me2 H3K36me3 H2BK123Ub	2011	Batta et al.	H3K36me2 is more frequent in the genome than H3K36me3; H3K36 methylation is not linked to transcription frequency; H3K36 methylation contributes indirectly to nucleosome stability in transcribed regions
S. cerevisiae	H3K4me3	2012	Maltby et al.	H3K4me3 is dependent on histone H3 acetylation; H3K4 demethylation is negatively regulated by histone H3 acetylation
S. cerevisiae	H3K4me3	2014	Thornton et al.	H2B ubiquitylation protein complexes play a context-dependent role in the deposition of H3K4me3
S. cerevisiae	H4K16Ac	2014	Thurtle and Rine	Telomeres contain a continuous domain of hypoacetylated H4K16; H4K16 is uniformly hypoacetylated at the mating-type loci
Neurospora crassa	H3K9me3 H3K4me3 H3K4me2	2011	Smith et al.	H3K9me3 co-localizes with centromeric histone variants; H3K4me3 and H3K4me2 are not enriched at centromeric DNA
Cryptococcus neoformans	H3K9Ac	2011	Haynes et al.	Ada2 acetylates K9 on H3; H3K9Ac is proximal to transcription start sites
Trichoderma reesei	H3K9me3 H3K4me3 H3K4me2	2012	Seiboth et al.	The heterochromatin methyltransferase LaeA is not involved in the methylation of H3K4 or H3K9
Fusarium fujikuroi	H3K4me2 H3K9me3 H3K9Ac	2013	Wiemann et al.	Presence of H3K4me2 and H3K9Ac is correlated with gene expression in secondary metabolism gene clusters; presence of H3K4me2 and H3K9Ac correlates poorly with gene expression overall

have independently performed over 140 experiments in more than 100 cell types in four different organisms (ENCODE Project Consortium, 2004, 2011; Celniker et al. 2009, Landt et al. 2012), antibodies against histone modifications are required to pass two separate tests in order to be considered appropriate for use in ChIP: validation on immunoblot and another secondary test, such as a peptide-binding assay. Background controls for ChIP-seq are critical. A mock immunoprecipitation using non-specific immunoglobulin could be performed; but as suggested Kidder et al. (2011), sonicated genomic DNA from the same experimental source is preferred as this control provides a more appropriate background for subtraction of biased chromatin regions that are preferentially sheared during the sonication process and consequently overrepresented in the genome. Other technical considerations are sufficient sequencing depth of immunoprecipitated DNA, and the use of a minimum of two biological replicates.

1.8 ChIP-seq data analysis to determine significantly enriched regions

Following the ChIP-sequencing procedure, the resulting mapped reads can then be viewed in a genome browser, which provides a first impression of enriched regions in the genome. This is an important step in the process and it provides the end-user with a preliminary idea of the quality of the experiment and of the tag distribution in relation to genomic features (Kidder et al. 2011). An analysis is then performed to identify the presence of significant "peaks". As programs may differ in how they detect peaks, it is important to choose a ChIP-seq "peak-calling" algorithm appropriate for the type of DNA binding protein being studied (broad regions typically associated with histone modifications and sharp regions with transcription factors). In general, all software for peak finding include the following components: 1) defining a signal profile along the genome, 2) determining or modeling the background signal, 3) establishing peak calling criteria, 4) filtering of artifacts and 5) significance ranking or scoring of individual peaks (Pepke et al. 2009). Although new programs for peak finding in ChIP-seq experiments are being developed at a very rapid rate, only a few have been demonstrated for their effectiveness in histone modification data. Peak callers were initially largely developed for use in detection of peaks at transcription factor binding sites, which are short (<50bp) and sharp in appearance and sparsely located throughout the genome (Chen et al. 2008; Valouev et al. 2008; Jothi et al. 2008; Kharchenko et al. 2008; Zhang et al. 2008; Rozowsky et al. 2009).

Furthermore, different peak callers have, in various benchmarking studies, shown unequal performances on different data sets (Laajala et al. 2009; Wilbanks and Facciotti, 2010; Micsinai et al. 2012), emphasizing the importance of testing different peak callers and comparing the results.

1.9 *Aspergillus niger*, a cell factory

Aspergillus niger is a black spored, mitosporic filamentous fungal organism known for its efficient production of citric acid and other primary metabolites. It is sometimes referred to as a microbial cell factory for production of gluconic and citric acid (Rujiter et al. 2002), the latter considered to be one of the most efficient and highest yield industrial bioprocesses (Baker, 2006). *Aspergillus niger* is also known for producing high quantities of commercially important proteins, due to its inherent high enzyme secretion capacity. In addition, *A. niger* is a host for production of a number of heterologous proteins (Punt et al. 2002; Archer and Turner, 2006). Other important enzymes secreted by *A. niger* include cellulases, hemicellulases, pectinases and proteases, which are involved in plant cell wall and complex biomass decomposition. Some of these enzymes are of interest for their applications in use for degrading non-edible plant matter in the emerging market of second-generation biofuels research (Galbe and Zacchi, 2007). Today, commercial enzyme production is a multi-billion industry (Novozymes, 2008) and applications include the production of high fructose corn syrup and clarification of cider, wine, and juice.

Owing to its role in industry as a highly efficient protein and metabolite producer and the availability of its sequenced genome, *A. niger* has become an important model organism for the study of expression systems and industrial protein production (Baker, 2006). However, precisely how *A. niger* is able to produce protein at a high and efficient rate is unclear. Upon genomic comparison of the elements of the secretory pathway between *A. niger* and *Saccharomyces cerevisiae*, no significant differences could be found to explain how *A. niger* is a better secretor of extracellular proteins than *S. cerevisiae* (Pel et al. 2007).

Experimental omics research, in combination with the availability of sequenced genomes, has resulted in fostering *A. niger* strain and process improvements. For example, Jacobs et al.

(2008) integrated proteomics and transcriptomics data to select protein targets for modulation, which resulted in increased production of the model β-glucuronidase gene. Together with the availability of other fully-sequenced genomes and data published from a variety of 'omics studies, the research community is provided with a basis for comparing the evolution of cellular processes in the filamentous fungi, including their versatile primary carbon metabolic systems (Flipphi et al. 2008).

Recently, Tsang et al. have generated a new assembly for the *A. niger* NRRL3 (N400) strain (unpublished data). The assembled eight telomere-to-telomere chromosomes have seven gaps corresponding to seven of the eight centromeres. The NRRL3 genome contains 34.5 Mbp and a thorough manual curation has defined 11,846 protein-coding genes.

1.10 Rationale for studying comparative ChIP-seq of *A. niger* H3K4me3 in growth on maltose and xylose

In the catabolism of biomass, filamentous fungi liberate monomeric sugars, which are efficiently metabolized by cells. The *Aspergilli* have become the most widely studied group of filamentous fungi for their potential in degrading complex plant polysaccharides from biomass (Culleton et al. 2013). Thus, primary carbon metabolism in *Aspergillus niger* and other filamentous fungi has been the subject of a number of investigations. The monosaccharide xylose is a product of degradation of xylan, the most abundant hemicellulose structure in the cellulosic microfibril of plant cell walls (Ebringerova and Heinze, 2000). Starch, one of the most common plant polysaccharides, is cleaved by amylases into maltose, a disaccharide. Both xylose and maltose can be used by *A. niger* as sole carbon substrates, but each of these sugars are catabolized by different metabolic routes (Figure 4). Unmodified xylose is taken up by the cell and subsequently reduced to xylitol by xylose reductase (Hondmann and Visser, 1994). Xylitol is converted to L-xylulose, which is subsequently phosphorylated and degraded in the pentose phosphate pathway. During growth on maltose, the glucoamylase gene is strongly induced and secreted for cleavage of maltose to glucose (Yuan et al. 2008; Vongsangnak et al. 2009). Glucose is then taken up by subsequent catabolic degradation by glycolysis or via the pentose phosphate pathway (Hondmann and Visser, 1994). Alternatively, glucose can be extracellularly

Figure 4. Representation of xylose and maltose metabolic pathways in *Aspergillus niger*.

(Image source: Lu et al. 2010)

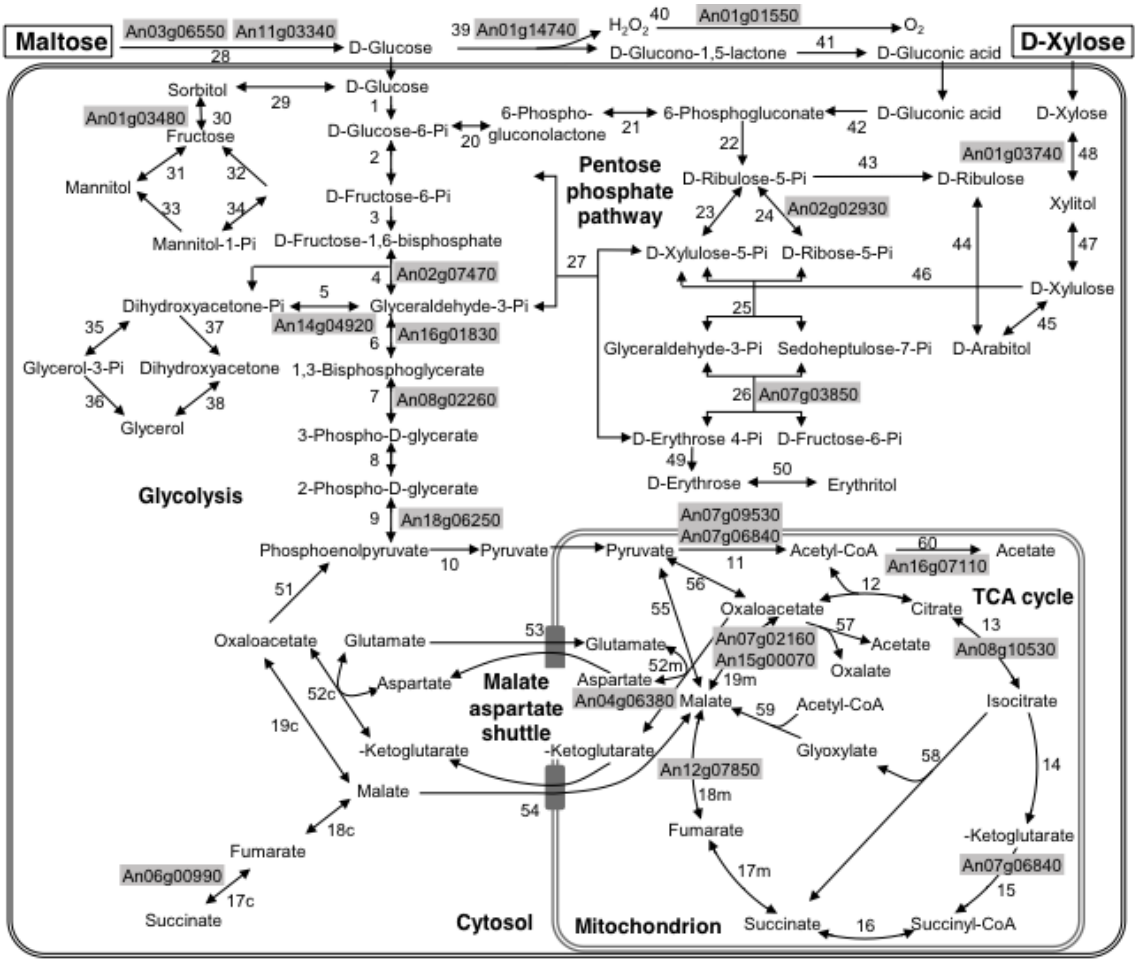

oxidized to gluconic acid by glucose oxidase, and further metabolized in the pentose phosphate pathway.

There are notable differences in gene expression for metabolism of maltose and xylose, as determined by analyses of the transcriptome (Yuan et al. 2008; Jorgensen et al. 2009) and proteome (Lu et al. 2010; Ferreira de Oliveira, 2011). At the transcriptional level, metabolism of different carbon sources is regulated by a variety of transcriptional activators and repressors. Growth on maltose induces the expression of glucoamylase (transcriptionally repressed during growth on xylose) by the transcription factor AmyR (Petersen et al. 1999). The transcription factor XlnR has been shown to regulate nearly all genes involved in the xylan and cellulose degradation pathway (de Vries and Visser, 2001). The carbon catabolite repressor CreA, represses genes involved catabolism of other carbon sources in the presence of its preferred source, glucose.

As described above, H3K4me3 has been implicated in changes in global gene expression. The genome of *A. niger* NRRL3 is the first filamentous fungal genome with a fully, manually curated set of genes. This genome resource, combined with the well-characterized metabolism of xylose and maltose, provides an excellent system to investigate the role of H3K4me3 modification in gene activity. In the present study, the genome-wide status of H3K4me3 modification was investigated in *A. niger*. First, I optimized a procedure to efficiently obtain a nuclear-enriched fraction from *A. niger* for use in the chromatin immunoprecipitation step. I performed chromatin immunoprecipitation followed by sequencing (ChIP-seq) of *A. niger* shake flask cultures grown on maltose or xylose for two hours. Immunoprecipitated DNA bound to the H3K4me3 chromatin modification was mapped to the NRRL3 *A. niger* genome. I performed a peak finding analysis to determine significantly H3K4me3-enriched sites. I obtained transcriptome data for *A. niger* growth on maltose and growth on xylose to investigate the relationship between active gene transcription and the presence of H3K4me3. Finally, I examined the distribution of H3K4me3 in the chromosomes to determine patterns of localization of this modified histone in the *A. niger* genome.

Section 2: Methods

2.1 *Aspergillus niger* strains, media and growth conditions

Aspergillus niger strain N402 (FGSC A733) was obtained from the Fungal Genetics Stock Center (Kansas City, Missouri, USA). The *A. niger* strain N402 (*cspA1*) is a morphological mutant with short conidiophores derived from the wild-type N400 (NRRL3, CBS 120.49). Conidia for this experiment were generated by plating on potato dextrose agar and harvesting after 5 days of incubation at 30°C. Conidia were collected in a saline/Tween solution, counted using a hemacytometer and stored at 4°C.

All media were based on the *Aspergillus* minimal media (MM) of Pontecorvo et al. (1953), with differing carbon sources. Primary cultures were grown on 250 mL MM containing 2% (w/v) fructose as a carbon source at 2 x 10^6 spores/mL. All cultures were incubated at 30°C in a rotary shaker at 250 rpm. Mycelia were collected by filtration under suction on Miracloth (EMD Millipore) and briefly washed with sterile water. Aliquots of 2 g of mycelia were transferred to each secondary culture flask containing 60 mL of MM with 25 mM xylose or 25 mM maltose as carbon sources. Cultures were further incubated for two hours at 250 rpm and 30°C, then collected by filtration, flash frozen in liquid nitrogen and stored at -80°C until further processing.

2.2 Formaldehyde crosslinking of *A. niger* mycelia

For mycelia used in the chromatin immunoprecipitation experiments, cultures were crosslinked as follows: after the two hour secondary culture incubation on either xylose or maltose, formaldehyde (Molecular Biology Grade, Fisher) was added directly to the culture flask to a final concentration of 0.75%. Cultures were incubated at room temperature for 8 minutes with occasional mixing. The crosslinking reaction was quenched with 1M glycine added directly to the culture to a final concentration of 0.125M. The cross-linked mycelia were harvested and kept frozen as described in Section 2.1.

2.3 Cell lysis and crude separation of cytosolic and nuclear fractions

To isolate a fraction enriched for nuclei to use in chromatin immunopreciptation from the *A. niger* cross-linked and frozen mycelia, a protocol modified from those previously described for use in the filamentous fungus *Neurospora crassa* (Loros and Dunlap 1991; Luo et al. 1998; Hong et al. 2008) was employed. First, frozen 1.5 g of mycelia were ground in liquid nitrogen to a fine powder using a mortar and pestle . Ground mycelia was transferred to a 7-mL beadbeating tube (Biospec Bioproducts) with 2.5 mL acid-washed 0.5 mm glass beads (Sigma) and 5 mL of Buffer A (1 M sorbitol, 7% Ficoll, 20% glycerol, 5 mM MgOAc, 3 mM calcium chloride, 3 mM DTT, 50 mM Tris-HCl pH 7.5) containing freshly added protease inhibitors (Complete Protease Inhibitor Tablet, EDTA-free, Roche) and 1mM PMSF. Beadbeating was performed using the Mini-Beadbeater 8 (Biospec Bioproducts) at 3200 rpm for 16 x 30s cycles. Samples were kept cool by placing on ice every 60s. After beadbeating, samples were transferred to 50-mL tubes and 10 mL of Buffer B (10% glycerol, 5 mM MgOAc, 25 mM Tris-HCl) containing protease inhibitors, taking care to rinse the beadbeating tubes with Buffer B to maximize sample recovery. Samples were gently mixed by inverting and centrifuged at 3000xg for 7 minutes in a swinging bucket rotor at 4°C to pellet mycelial debris, glass beads and unbroken mycelia. The resulting crude whole cell extract was carefully transferred to a clean, clear 30-mL ultra-centrifuge tube, taking care not to disturb the pelleted material, and centrifuged at 9400xg for 15 minutes at 4°C. Fractions of the resulting supernatant (crude cytosolic proteins) were retained for SDS-PAGE and determination of protein concentration. The resulting pelleted material (crude nuclear extract) was washed three times by carefully resuspending in 1 mL of wash buffer (5 mM MgOAc, 25 mM Tris-HCl), transferring to a 2-mL microfuge tube, centrifuging at 16000xg for 5 minutes and discarding the supernatant.

2.4 Determination of DNA in pellet and supernatant fractions

Phenol/chloroform/isoamyl alcohol (PCI, 25:24:1) DNA extractions were performed for the resulting cytosolic and pelleted material to determine DNA content. Pellet fractions were resuspended in lysis buffer and were twice purified with PCI and nucleic acid was precipitated using ethanol. Precipitated DNA pellets were resuspended in TE buffer (1mM EDTA, 10 mM Tris-HCl, pH8.0) and treated with RNase A at 30°C for 30 min. Samples were purified once more with PCI, ethanol precipitated and resuspended in TE buffer.

To determine whether any significant amount of DNA and nuclei were being lost to the supernatant fraction during the beadbeating step, samples of supernatant were subjected to phenol/chloroform/isoamyl alcohol DNA purification. In total, 6 x 500 µL fractions (3 mL total, or 20% of the whole supernatant fraction) were combined in order to concentrate them.

Four microlitres from each sample from the pellet and supernatant fractions were loaded in each lane of a 2% agarose gel for electrophoresis, followed by staining with ethidium bromide. For nuclei enriched fractions, DNA concentration was also evaluated using the PicoGreen assay (Invitrogen) following the manufacturer's instructions.

2.5 Assessment of formaldehyde crosslinking

To determine the appropriate formaldehyde concentration for chromatin crosslinking, cultures were treated as described previously (Section 2.2) with increasing final concentrations of formaldeyde (0%, 0.5%, 0.75%, 1%). To determine whether formaldehyde crosslinking of chromain was sufficient, or if material was over-crosslinked, purified DNA from crosslinked and reverse crosslinked samples were visualized on a 2% agarose gel with ethidium bromide staining (see Section 2.4 for DNA purification procedures).

2.6 Protein digestion

Following the pelleting and wash steps, the composition of the resulting supernatant liquid collected after the beadbeating step and washed pellet fraction were prepared for analysis by mass spectrometry.

Protein sample determination was carried out with the RCDC kit assay (BioRad, Mississauga, Ont). For in-gel digestions, samples containing 75 of µg of protein were loaded onto a 4-12% SDS-PAGE gradient gel and stained with Coomassie Blue. Whole lanes were evenly cut into 15 bands, subsequently destained, reduced, cysteine-alkylated, and in-gel digested with sequencing grade modified trypsin (Promega, Madison, WI) as previously described (Wasiak et al. 2002). Peptides were extracted from the gel pieces through multiple incubations in solutions of 1% formic acid (FA) and increasing concentration of acetonitrile (ACN). The extracts were dried in a speedvac and resuspended in 60 µl 5% ACN:0.1% FA.

2.7 LC-MS/MS analysis

Peptide digest (5 µL) was loaded onto a 15 cm x 75 mm i.d PicoFrit column (New Objective, Woburn, MA) packed with Jupiter 5 mm, 300 Å, C18 resin (Phenomemex, Torrance, CA) connected in-line with a Velos LTQ-Orbitrap mass spectrometer (Thermo-Fisher, San Jose, CA). Peptide separation was done using a linear gradient generated by an Easy-LC II Nano-HPLC system (Thermo Fisher) using a mixture of solvent A (3% ACN:0.1% FA) and solvent B (99.9% ACN:0.1%FA). The gradient started at 1% B, was set to reach 27% B in 21 min, ramped to 52 % B in 7 min and 90% B in 2 min, then held at 90% for 5 min.

The capillary voltage on the nanospray source was adjusted to get the best spraying plume at 10% B and typically ranged from 1.9 to 2.1 kV. MS survey scan spanning the 350 to 2000 *m*/*z* range was done at 60000 resolution. The top 10 doubly, triply or quadruply charged ions with intensity higher that 5000 counts were considered candidates to undergo CID MS/MS fragmentation in the LTQ-Velos ion trap. Optimal accumulation times were set automatically using adaptive Automatic Gain Control with a maximum accumulation time of 150 msec. Selected ions were put in a dynamic exclusion list for 15 sec and reacquired again if still detected within a 30 sec window. MS/MS scan range was automatically adjusted based on precursor m/z

and charge state. Selected ions were fragmented using a normalized collision energy set at 35% and an isolation window of 2 m/z.

2.8 Mass spectrometry bioinformatics data processing

Raw mass spectrometric data were processed for generation of peaklists using Mascot Distiller version 2.3.2.0. The peaklist data was searched against the *A. niger* protein sequence database using Mascot version 2.3.01 followed by X!Tandem version 2007.01.01.1 on the subset of identified proteins. Mascot and X!Tandem searches were done using a fragment ion mass tolerance of 0.80 Da and a parent ion tolerance of 10.0 ppm. Iodoacetamide derivative of cysteine was specified in Mascot and X!Tandem as a fixed modification. Dehydration of the N-terminus, loss of ammonia of the N-terminus, deamidation of asparagine and glutamine, methylation of aspartic acid, glutamic acid and the C-terminus, oxidation of methionine and acrylamide adduct of cysteine were specified in X!Tandem as variable modifications. Oxidation of methionine was specified in Mascot as a variable modification. Scaffold (version Scaffold_4.1.1, Proteome Software Inc.) was used to validate MS/MS based peptide and protein identifications. In order to ensure a false discovery rate of less than 1% at the peptide level, peptide identifications were accepted if they could be established at greater than 90.0% probability as specified by the Peptide Prophet algorithm (Keller et al. 2002). Protein identifications were accepted if they could be established at greater than 95.0% probability and contained at least 2 identified peptides. Protein probabilities were assigned by the Protein Prophet algorithm (Nesvizhskii, 2003). Proteins that contained similar peptides and could not be differentiated based on MS/MS analysis alone were grouped to satisfy the principles of parsimony.

2.9 Lysis of crude nuclei enriched pellet and determination of sonication conditions

After the final wash step of the crude nuclear preparation procedure, the pellet was resuspended in 600µL Buffer C (50mM HEPES-KOH pH7.5, 140mM NaCl, 1mM EDTA pH8.0, 1% Triton X-100, 0.1% sodium deoxycholate, 0.1% SDS, 1mM PMSF and protease inhibitor cocktail).

To determine optimal nuclei fraction sonication conditions for use in ChIP-seq, formaldehyde-crosslinked crude nuclear extracts were prepared as described above (Section 2.3). The lysed nuclear extracts were pooled and subjected to sonication trials on an ultrasonic homogenizer fitted with a microtip (Biologics, Inc.) performed with increasing numbers of 10-second cycles (3x10s, 4x10s, 5x10s, 6x10s). All sonications were performed at 20% output and tubes were incubated on ice throughout the sonication procedure with 15s breaks between each cycle. Following sonication, samples were reverse-crosslinked overnight by incubating in lysis buffer (Buffer C) at 65°C and purified using the phenol/chloroform method. For average size estimation, purified DNA was visualized by electrophoresis on a 2% agarose gel with ethidium bromide staining.

2.10 Chromatin immunoprecipitation (ChIP)

Aliquots of 150 µL of enriched nuclei, formaldehyde crosslinked and sonicated lysate were transferred to tubes for either DNA purification as control DNA, chromatin immunoprecipitation with 4 µg anti-H3K4me3 antibody (Ab 8580, Abcam) or incubation with beads only (no-antibody control). For ChIP, lysates were incubated with the antibody for 1.5 hrs with rotation at 4°C before the addition of 30 µL of PureProteome Protein A magnetic beads (Millipore). All samples were further incubated overnight with gentle rotation on a tube rotator at 4°C. Immunoprecipitates were washed once by addition of 1 mL Buffer C, twice using 1 mL LiCl wash buffer (0.25M LiCl, 0.5% NP-40, 0.5% sodium deoxycholate, 1 mM EDTA, 10 mM Tris-HCl pH 8.0) and once with 1 mL TE buffer, each performed for 5 minutes with rotation at 4°C. Immunoprecipitated DNA was eluted by adding 120 µL 1% SDS, 0.1M $NaHCO_3$ and incubating for 1 hour at 65°C, mixing gently every 15 minutes. The eluate was transferred to a fresh tube and further incubated with at 65°C overnight to reverse DNA crosslinks and with 2 µL 0.5 mg/mL RNase A. Immunoprecipitates were subsequently purified using a QIAquick PCR Purification Kit (Qiagen) according to the manufacturer's specifications. DNA concentration was determined for all purified samples using the PicoGreen method (Invitrogen).

One microgram RNase A (Invitrogen) was added to control DNA aliquots and incubated overnight at 65°C to reverse DNA crosslinks. Control DNA was purified twice using one volume phenol/chloroform/isoamyl alcohol, precipitated using two volumes 99% ethanol, and resuspended in 10mM Tris buffer, pH 8.5. Input DNA was visualized with ethidium bromide staining for average size estimation by electrophoresis on a 2% agarose gel.

2.11 Immunoblotting to determine the reactivity of the anti-H3K4me3 antibody and sequencing of immunoprecipitated chromatin

To determine the reactivity and specificity of the commercial H3K4me3 antibody, immunoblotting was performed on the immunoprecipitated chromatin. As negative control, crosslinked, total sonicated chromatin not subjected to immunoprecipitation was also examined. Briefly, proteins were separated on a 12% SDS-PAGE gel wet-transferred to a nitrocellulose membrane, then incubated with a 5% non-fat milk PBS solution containing 0.1% Tween-20 at room temperature with agitation for 1 hour. Anti-H3K4me3 antibody (Abcam, Ab8580) diluted 1:2000 was added to the milk solution and incubated overnight at 4°C with agitation. The membrane was then washed 3 times for 5 minutes using the milk solution. Secondary antibody incubation was performed for 1 hour at room temperature with horseradish-peroxidase conjugated mouse anti-rabbit light chain specific monoclonal IgG (Jackson ImmunoResearch Laboratories, Inc. 211-052-171). Blots were developed using the ECL Plus kit (GE Healthcare) and imaged on a Typhoon Trio Scanner (GE Healthcare).

The libraries were prepared and sequenced at the Innovation Centre at McGill University (Montreal, QC, Canada) according to the High Sample (HS) protocol (Illumina, Inc.) and with the following modifications: the fragmentation step was omitted and the preparation began instead at the end repair step of the workflow; gel purification was performed on library molecules in the range of 250-400 bp using the Sage PippinPrep system with at 1.5% gel cassette, and the enrichement PCR step consisted of 17 cycles rather than 10. Sequenced read data from ChIP and control libraries were were mapped to the NRRL3 *A. niger* genome using the Genomic Short-read Nucleotide Alignment Program (Wu and Nacu, 2010).

2.13 Identification of H3K4me3 peaks

Significant histone modification peak detection was performed using SICER (Zang et al. 2009). SICER software was downloaded from http://home.gwu.edu/~wpeng/Software.htm and the Python compilers Numpy and Scipy were obtained for running the package. Gaps are used to allow for read-count fluctuations, repetitive regions and unmodified nucleosomes. Gap size can be adjusted to the nature of the chromatin modification and the length of the gap is a bp-multiple of the window size. The following parameters were chosen to perform peak finding with SICER:

1) Window size 200 bp, gap size 200 bp (W200-G200), 2) W100-G100, 3) W40-G40, 4) W20-G20, 5) W20-G40, 6) W20-G60, 7) W20-G80

For all trials, read redundancy threshold was set to include all reads, effective genome size was set to 1, and FDR was set to 0.05.

Peak splitting with the peaksets generated with SICER was performed using the PeakSplitter utility from the PeakAnalyzer program (Salmon-Divon et al. 2010; available at http://www.ebi.ac.uk/research/bertone/software). Parameters for the peak splitting operation were set to separation float= 0.6 and minimum height = 5.

Identification of significant peaks from sequenced and mapped ChIP-seq reads was performed using the Control-based ChIP-seq Analysis Tool (or CCAT, Xu et al. 2010; available at http://cmb.gis.a-star.edu.sg/ChIPSeq/paperCCAT.htm) peak finding method and three trials were performed with the following sliding window sizes:

1) 1000 bp (as suggested by the package manual and default parameter for histone modifications), 2) 500 bp, 3) 100bp

Peak finding with Qeseq (Micsinai et al. 2012; available at http://sourceforge.net/projects/klugerlab/files/qeseq/) with the algorithm default parameters and a cutoff of 0.05.

2.14 Peakset and differential binding analysis with the DiffBind package for R Bioconductor

Differential H3K4me3 sites were identified using the DiffBind package for R Bioconductor (Stark and Brown, 2011) available at http://bioconductor.org/packages/2.13/bioc/html/DiffBind.html

Pearson correlations of peaksets were calculated and consensus binding sites for maltose or xylose replicates were determined using the overlap function in DiffBind. Reads were counted in the genomic intervals from consensus peaksets. Identification of differentially bound sites was performed using the EdgeR method (Robinson et al. 2010). DiffBind plot functions were used to draw correlation heatmaps, Venn diagrams, and MA plots.

2.17 File conversions, ChIP peak intersections, annotation and analysis of peaksets

File type conversions, gene model annotation of the resulting peaksets and in-depth analysis for counting intersecting features for peaksets was performed using the BEDTools Suite package (Quinlan and Hall, 2010, available at http://code.google.com/p/bedtools/). A minimum overlap fraction of 15% of the gene model feature was imposed for performing annotation of ChIP peaksets.

2.19 Statistical testing of differences between distributions of FPKM values

Mann-Whitney tests (Bauer, 1972; Hollander and Wolfe, 1973, 1999) were performed in R Bioconductor using the two-sample Wilcox.test{stats} function.

2.20 Data visualization

Peaksets and raw reads were visualized in the IGV Genome Browser, downloaded from the Broad Institute (available at http://www.broadinstitute.org/igv/).

Section 3: Results

3.1 Protocol development for ChIP-seq in *Aspergillus niger*

Methods for ChIP-seq have not been described for *Aspergillus*. Based on ChIP-seq protocols established for other organisms, I have established the experimental parameters for isolation, crosslinking, sonication, immunoprecipitation and de-crosslinking of chromatin for ChIP-seq for *A. niger* as described below.

3.1.1 Enrichment of nuclear fraction for ChIP-seq analysis

I developed and validated a quick method for obtaining an enriched nuclear fraction from *A. niger* mycelia for use in ChIP-seq. The protocol was adapted from that of Loros and Dunlap (1991) for isolation of nuclei in *Neurospora crassa*. Briefly, 2 g of mycelial mats recovered from *A. niger* cultures were subjected to repeated, short cycles of beadbeating with glass beads in a viscous Ficoll buffer, followed by dilution in aqueous buffer and centrifugal removal of unbroken mycelia, glass beads and debris, as described in the Methods. The resulting supernatant containing the whole cell extract was then centrifuged at high speed to pellet nuclei.

To determine potential loss of nuclei and DNA to the cytosolic fraction prior to pelleting, six fractions of 500 µL from the supernatant fraction were combined and DNA was extracted using phenol/chloroform extraction and ethanol precipitation. The precipitates were pooled and DNA was visualized on an ethidium bromide stained agarose gel. No visible band was detected in the supernatant, and strongly stained bands were seen in undiluted, 1:10 and 1:20 diluted fractions from the pellet (Figure 5). This suggested that DNA was enriched in the pelleted fractions.

Figure 5. DNA content of nuclear and cytosolic fractions. Following centrifugation of the disrupted mycelia, the pellet and supernatant fractions were resolved on 2% agarose gel and stained with ethidium bromide. Lanes for the pelleted fractions show the undiluted extract, 1:10 and 1:20 dilutions (right to left for three biological replicates). Lanes for the supernatant fractions represent undiluted samples of three biological replicates.

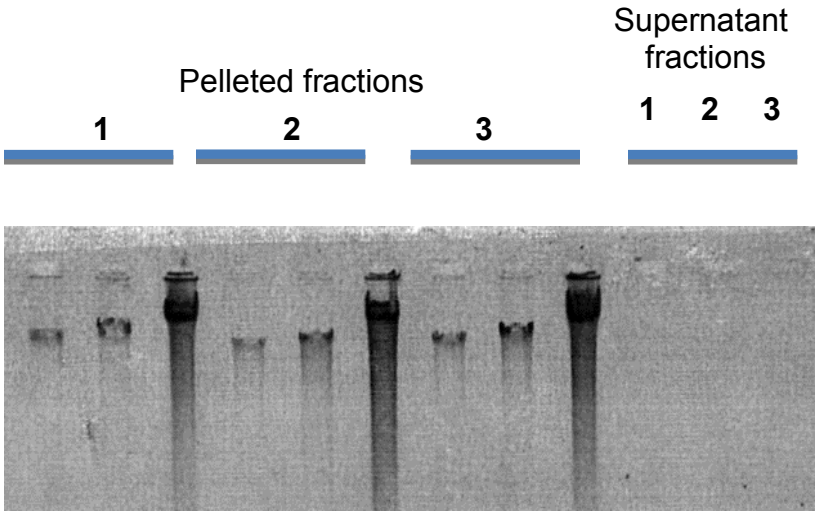

Figure 6. Distribution of marker proteins in pelleted and supernatant fractions. Supernatant and pelleted fractions were characterized by mass spectrometry to identify proteins and their

relative abundance. Spectral counts for the pelleted fraction (red bars) and for the supernatant fraction (blue bars) are shown for five protein markers specific for subcellular locations.

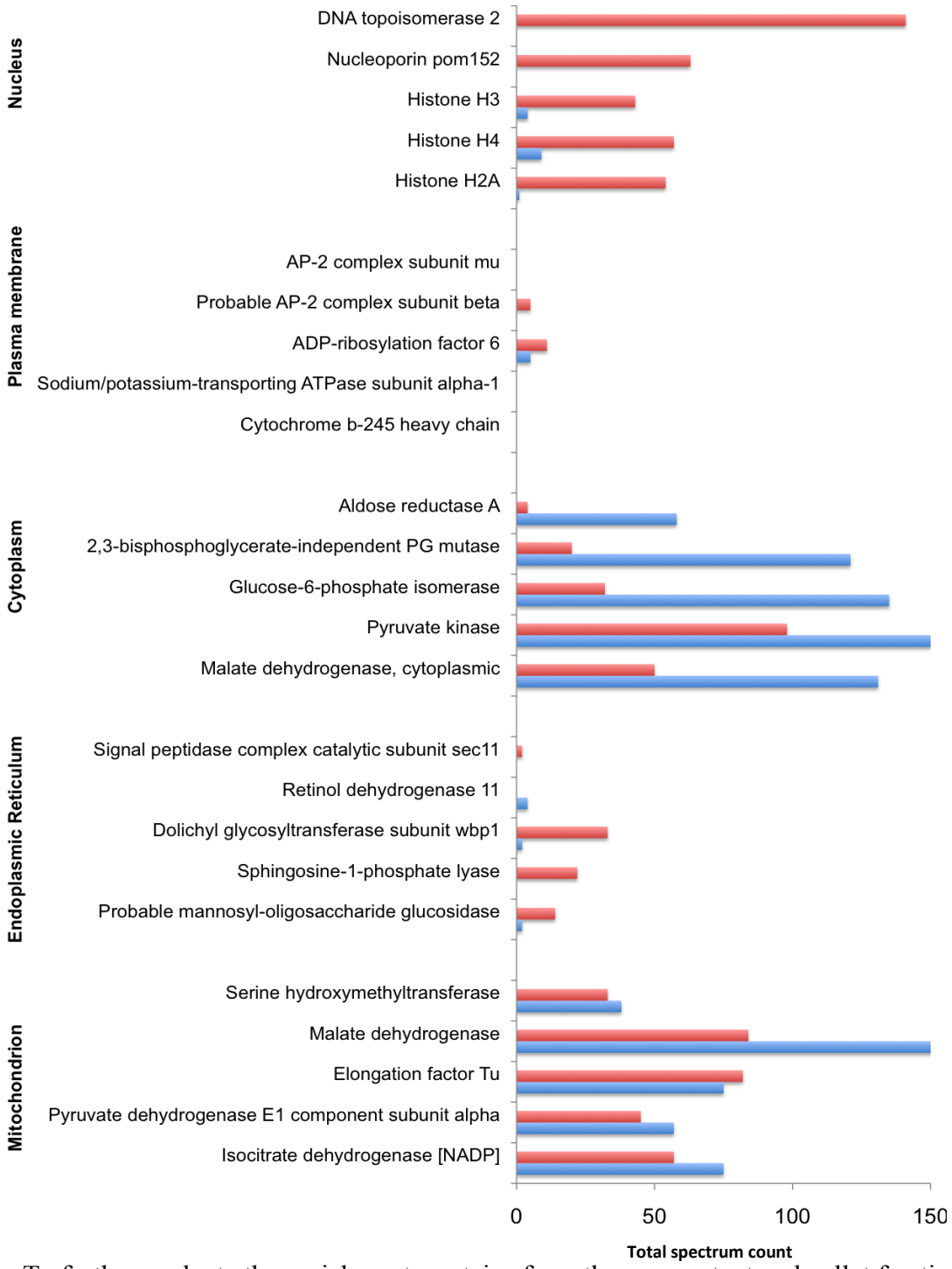

To further evaluate the enrichment, proteins from the supernatant and pellet fractions were analyzed by mass spectrometry. Experimentally determined, subcellular protein markers

(Andreyev et al. 2010) were used for comparing LC-MS/MS spectra matched to the protein sequences of *A. niger*. Figure 6 shows the relative abundance in the nuclear and supernatant fractions of five marker proteins specific for the nucleus, plasma membrane, cytoplasm, endoplasmic reticulum and mitochondrion. The results from mass spectrometric analysis suggest that although some proteins from other subcellular compartments were found in the pellet, this fraction contained a relatively high proportion of nuclear proteins. These data provide additional evidence that the pelleting procedure was successful in enriching nuclear materials.

3.1.2 Demonstration of suitable crosslinking conditions

Optimal chromatin crosslinking needs to be determined since insufficient crosslinking may result in loss of protein-DNA complexes and over-crosslinking will render the chromatin insoluble, unavailable for antibody capture and /or irreversible (Das et al. 2004; Haring et al. 2007). I generated chromatin samples crosslinked for a fixed time and with increasing formaldehyde concentrations. The samples were de-crosslinked (incubated overnight at 65°C in elution buffer) and resolved on an agarose gel for visualization of the DNA fragments. The starting material is over-crosslinked and irreversible if it is not recovered with the de-crosslinking step. Similarly, chromatin is under-crosslinked if recovered without de-crosslinking. Panel A of Figure 7 shows that at 1.0% formaldehyde, the crosslinking is irreversible and 0.75% formaldehyde is the highest concentration where crosslinked chromatin can be reversed. Panel B of Figure 7 shows that 0.75% formaldehyde is sufficient for crosslinking because at this concentration, DNA can only be recovered following de-crosslinking. Therefore, crosslinking with 0.75% formaldehyde was used for subsequent experiments.

Figure 7. Chromatin crosslinking and de-crosslinking

Panel A) Chromatin was crosslinked for a fixed time (8 minutes) with increasing formaldehyde concentrations (at 0%, 0.5%, 0.75% and 1% final concentration), subjected to a de-crosslinking step, then resolved on a 2% agarose gel stained with ethidium bromide. Panel B) Recovery of crosslinked and de-crosslinked chromatin. Lane 1, chromatin crosslinked at 0.75% formaldehyde; Lane 2, de-crosslinked chromatin following crosslinking at 0.75% formaldehyde; and Lane 3, chromatin that had not been subjected to crosslinking.

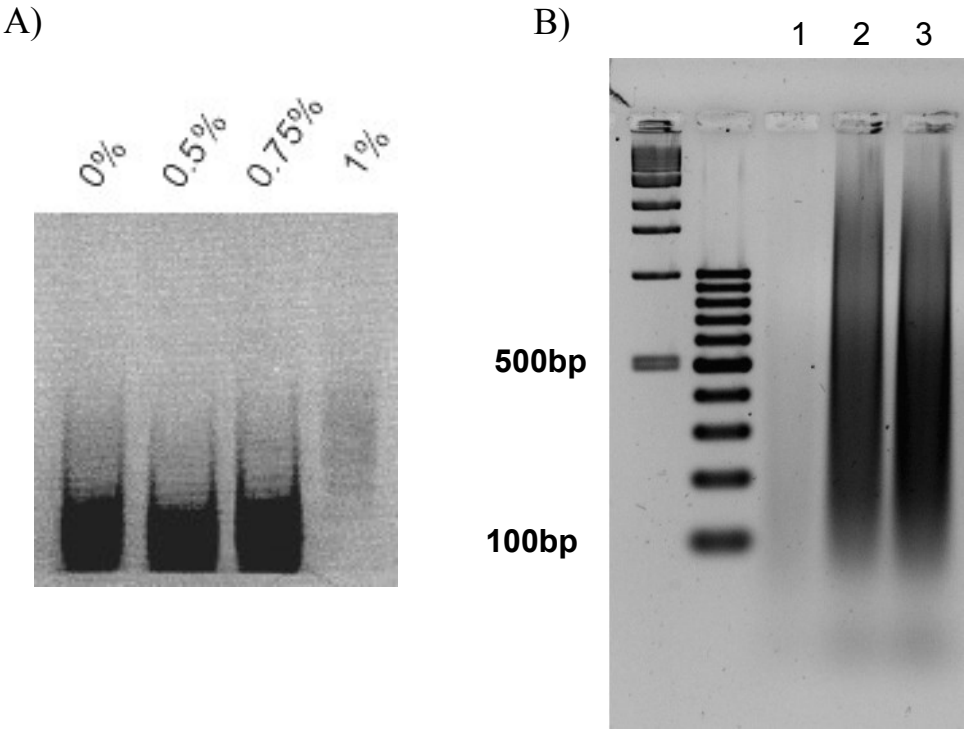

3.1.3 Determination of sonication conditions for crosslinked chromatin

To perform chromatin immunoprecipitation, it is necessary to obtain fragments of an appropriate size for downstream library size selection and sequencing. Resulting fragments from sonication should fall within the 200 – 600 bp range (Park, 2009). Using a microtip sonicator, I performed a sonication trial with increasing numbers of 10-second cycles. The sonicated DNA was resolved on an agarose gel and stained with ethidium bromide. Panel A of Figure 8 shows that sonication at 20% power output yielded fragments in the desired size range. Although the overall sizes of the fragments did not change significantly compared to those observed with fewer sonication cycles, the presence of the high molecular genomic DNA band was significantly reduced with more cycles. As a result, I selected six cycles of 10s for chromatin fragmentation by sonication for downstream sequence library preparation (Figure 8, Panel B).

3.1.4 H3K4me3 chromatin immunoprecipitation followed by sequencing (ChIP-seq)

A chromatin immunoprecipitation protocol was adapted from those of Johnson et al. (2007; updated protocol available at http://www.hudsonalpha.org/myers-lab/protocols/) and Saleh et al. (2008). Reactivity and specificity of anti-H3K4me3 antibody was determined by Western blot (Figure 9). With the crude nuclear extract, the Western blot showed a band at about 17 kDa, the expected molecular weight of the histone H3 protein and the signal increases with increasing amount of nuclear extract loaded. These results suggest that the anti-H3K4me3 antibody reacts specifically with *A. niger* histone H3. I then used the antibody to react with crosslinked chromatin. Following immunoprecipitation, the chromatin was subjected to Western blot analysis. The results suggested that the anti-H3K4me3 antibody binds specifically when incubated with crosslinked chromatin.

To identify H3K4me3-marked chromatin, *A. niger* mycelia were cultured independently with maltose or xylose as carbon sources. Two biological replicates were performed. The crosslinked chromatin from each of the four samples was immunoprecipitated with anti-H3K4me3 antibody and sequenced. Control DNA not subjected to immunoprecipitation from each of the four samples was sonicated to 200-600 bp and sequenced. Sequencing was performed at the Innovation Centre at McGill University (Montreal, QC, Canada) on an Illumina Hi-Seq

Figure 8. Determination of sonication conditions. Chromatin fragmentation size was determined by performing a series of sonication trials with increasing number of 10s cycles at 20% power output and visualizing the resulting DNA on an ethidium bromide stained agarose gel (Panel A). Sonicated chromatin from maltose and xylose growth replicates used for ChIP-seq in the current experiment is shown in Panel B.

A)

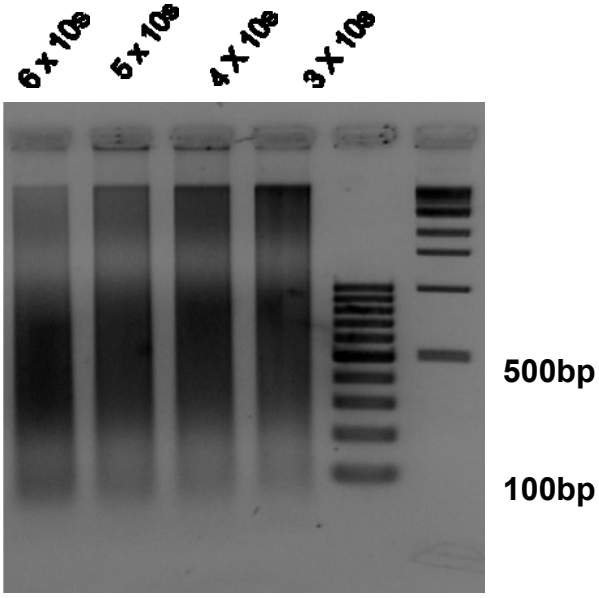

B)

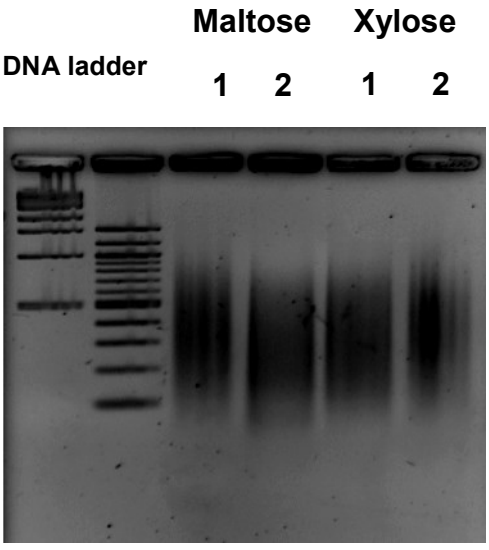

Figure 9. H3K4me3 antibody specificity. An immunoblot was performed using increasing amounts of crude nuclear lysate (starting material) and proteins eluted from chromatin immunoprecipitation using the antibody against H3K4me3 (Abcam, Ab8580). The dark band is observed at 17 kDa, the expected molecular weight for H3K4me3.

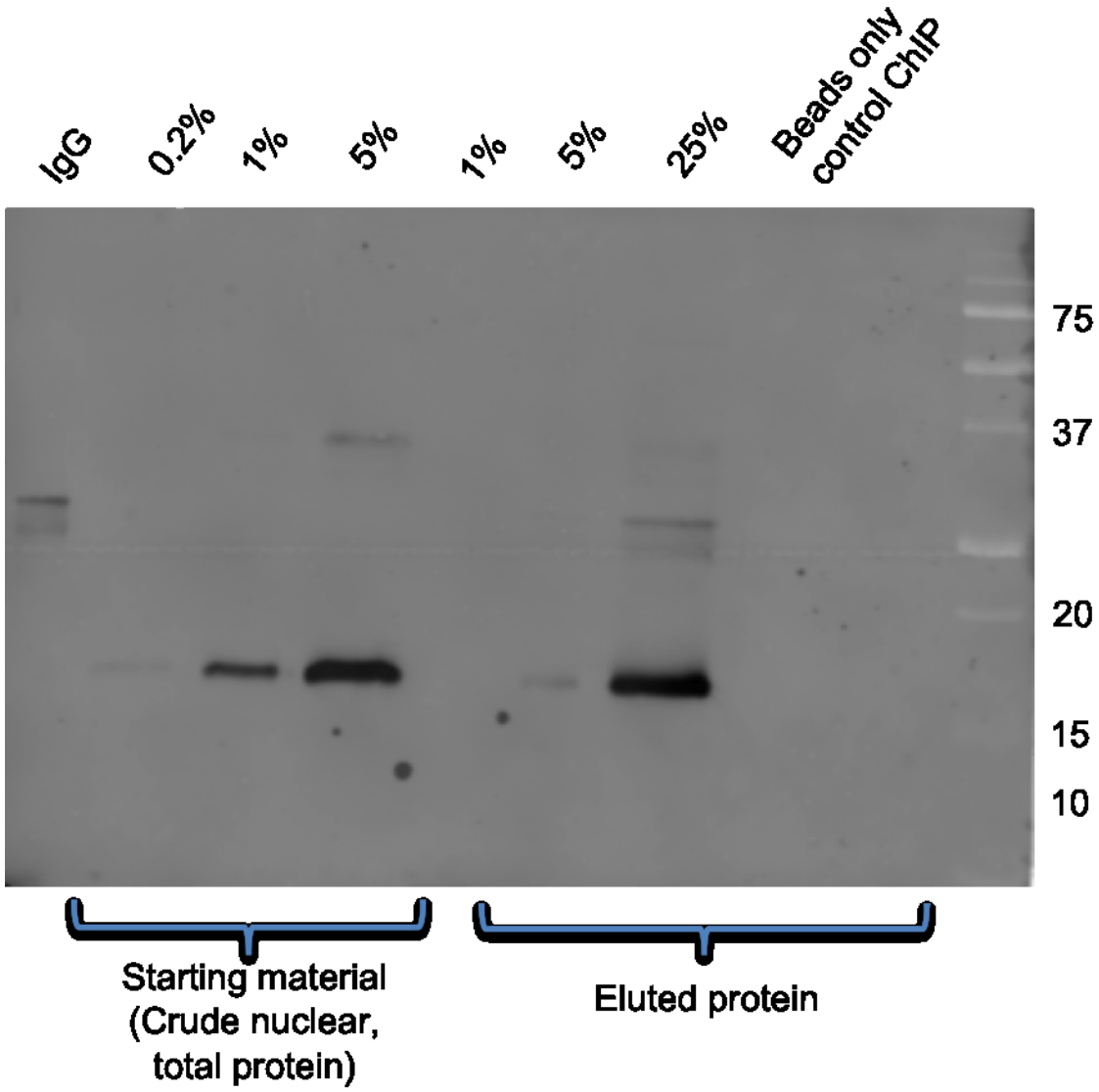

Sequencing System. Sequenced reads were then aligned to the genome using the Genomic Short-read Nucleotide Alignment Program (Wu and Nacu, 2010).

3.2 H3K4me3 ChIP-seq data processing

3.2.1 H3K4me3 peak finding

To locate regions showing significant H3K4me3 enrichment (or "peaks"), I tested a number of peak finding algorithms. Peak finding was first attempted using the CCAT algorithm (Control based ChIP-seq Analysis Tool, Xu et al. 2010; available at http://cmb.gis.a-star.edu.sg/ChIPSeq/paperCCAT.htm), reported as a reliable tool for identification of broad histone modification peaks (Kidder et al. 2011). I also used the Qeseq algorithm (Asp et al. 2011; available at http://sourceforge.net/projects/klugerlab/files/qeseq/). I examined results from CCAT and Qeseq by visualizing the peaks in the genome browser. Both CCAT and Qeseq failed to reliably identify peak regions that visually corresponded with the raw reads and instead identified intervals that bore no resemblance to the enriched mapped read regions (data not shown).

Peak finding was then attempted using the SICER (spatial clustering approach for identification of ChIP-enriched regions) peak finding algorithm (Zang et al. 2009; available at http://home.gwu.edu/~wpeng/Software.htm). Visual examination in the genome browser confirmed that SICER reliably identified peaks in locations enriched for H3K4me3 seen in the raw read mapping to the genome. The SICER method takes into account the tendency of histone modification ChIP-seq peaks to form "clusters". First, the genome is partitioned into windows of read counts and identifies peaks as clusters of windows that are unlikely to appear by chance. Once candidate regions have been identified, SICER uses a control DNA library (generated from total sonicated chromatin not subjected to immunoprecipitation) to determine the significance of enrichment on each candidate. SICER scales control read count to account for size differences in the control and ChIP libraries. Visualization of the mapped reads in the genome browser revealed that some regions mapped to the genome from control DNA also formed peaks. These overrepresented regions were eliminated from the final peaksets after performing SICER analysis (Figure 10).

Figure 10. Control sonicated DNA as a control for H3K4me3 ChIP-seq.

The effect of normalization of H3K4me3 ChIP-seq reads with control 'input' DNA (total sonicated chromatin not subjected to immunopreciptation) on the final peakset as determined by SICER (SICER peaks) on the final peakset as determined by using window size = 20bp and gap size = 60bp. Panels A) and B) are examples representing two different regions of the genome. Predicted gene models are displayed in the lower track.

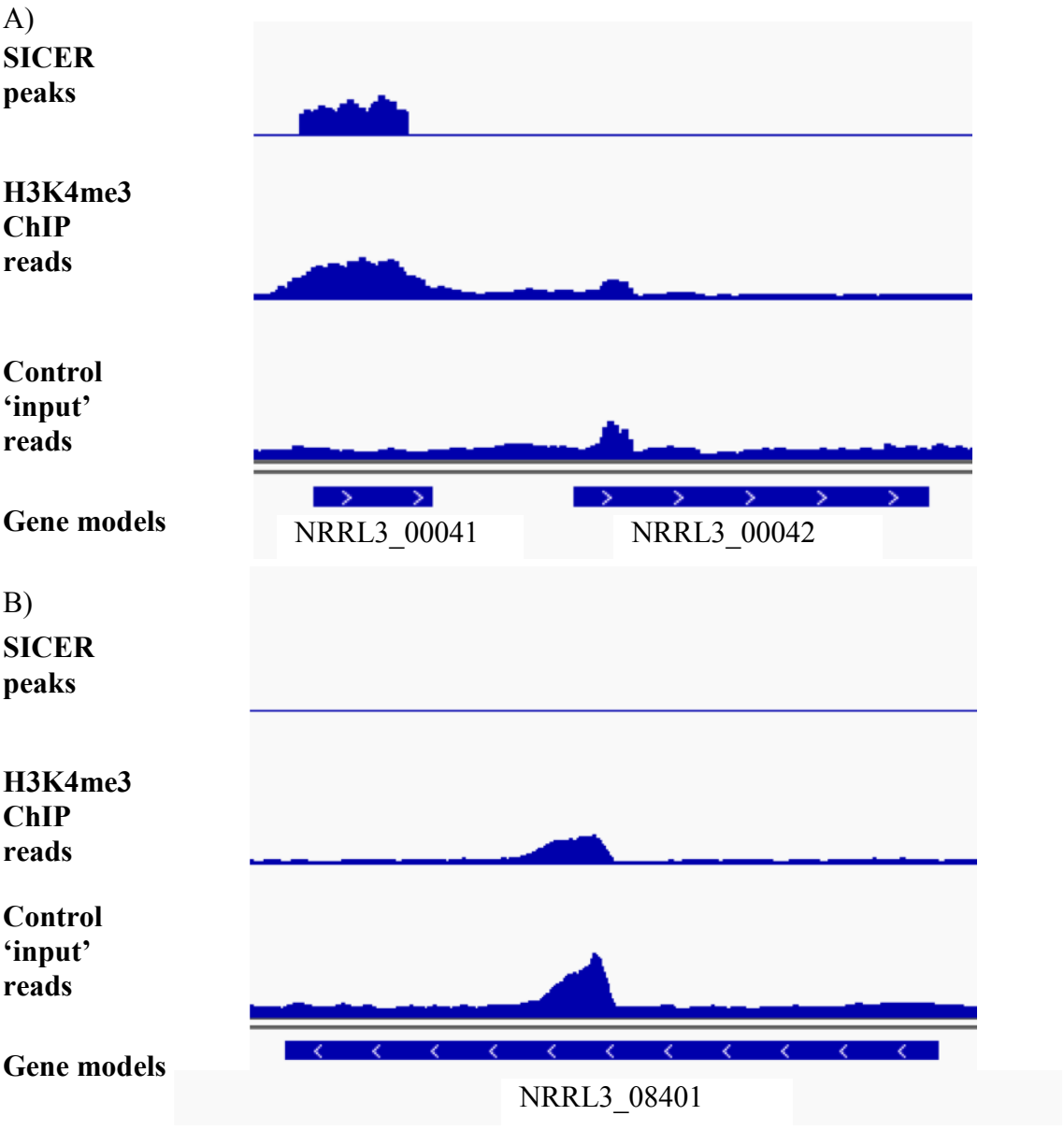

A key feature of SICER is the adjustable window and gap feature to account for read count fluctuations within an island and reliably separate distinct peaks. As the estimated size of a single nucleosome and its linker region is ~200bp, the authors recommended using a window size and gap size = 200 bp (W200-G200) for histone modification peak detection. As such, the first SICER peak finding trial was performed using these parameters. Visual examination in the genome browser for the W200-G200 data set in the genome browser revealed that some H3K4me3-enriched regions were missing in the final peakset. To determine whether this was occurring as a result of the choice in peak finding parameters, I attempted to use progressively smaller window and gap size (W100-G100, W40-40, W20-G20) and observed an increase in the numbers of peaks. I generated additional peaksets using the 20 bp windows with increasing gap sizes (W20-G40, W20-G60, W20-G80).

3.2.2 Analysis of SICER peakset correlation between replicates

To determine the consistency in peak finding between biological replicates for the various SICER peaksets, Pearson correlation scores based on peak occupancy were calculated using the DiffBind package for R Bioconductor (Stark and Brown, 2011). As shown in the heatmap in Figure 11, peaksets for the biological replicates form a cluster by growth condition. Clustering by growth condition was also seen for all other peaksets using the increasing window and gap sizes (Table 3). Although correlation values were similar for all SICER trials with increasing window and gap sizes, the W20-G60 and W20-G80 peaksets yielded the highest correlation between the biological replicates cultured on maltose or xylose.

3.2.3 SICER peakset analysis

When surveying each of the peaksets in the genome browser, I observed a number of issues, which could potentially affect the quality of the peaksets in downstream analyses. To address these issues, I further analyzed the peaksets to determine the following: 1) number of

Figure 11. Correlation heatmap of peaksets. Clustering of peaksets derived from biological replicates cultured on maltose (samples 1 and 2) and cultured on xylose (samples 3 and 4) as determined by Pearson correlation. Shown here is the result for the W20-G60 peak finding trial.

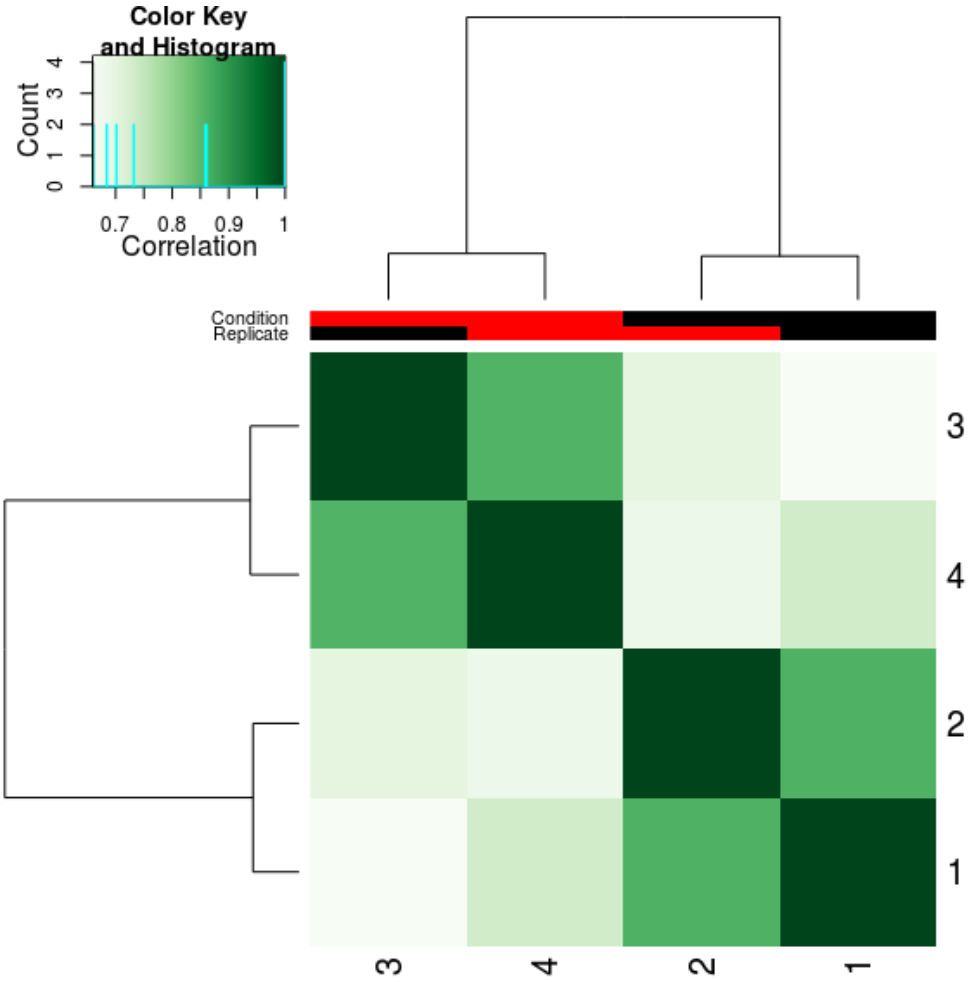

Table 3. **Pearson correlation values of SICER peaksets from sample replicates.** Window size (in base pairs) is denoted by 'W' and gap size by 'G'. Each table shows the correlation values between biological replicates (denoted by '1' or '2') from the various SICER peak finding trials.

W20-G20				
	xylose 1	**xylose 2**	**maltose 1**	**maltose 2**
xylose 1	1.00	0.82	0.66	0.69
xylose 2	0.82	1.00	0.70	0.67
maltose 1	0.667	0.70	1.00	0.83
maltose 2	0.69	0.67	0.83	1.00

W20-G40				
	xylose 1	**xylose 2**	**maltose 1**	**maltose 2**
xylose 1	1.00	0.84	0.67	0.70
xylose 2	0.84	1.00	0.71	0.69
maltose 1	0.70	0.71	1.00	0.85
maltose 2	0.70	0.69	0.85	1.00

W20-G60				
	xylose 1	**xylose 2**	**maltose 1**	**maltose 2**
xylose 1	1.00	0.86	0.70	0.66
xylose 2	0.86	1.00	0.68	0.73
maltose 1	0.70	0.68	1.00	0.86
maltose 2	0.66	0.73	0.86	1.00

W20-G80				
	xylose 1	**xylose 2**	**maltose 1**	**maltose 2**
xylose 1	1	0.86	0.68	0.72
xylose 2	0.86	1	0.74	0.71
maltose 1	0.68	0.74	1	0.86
maltose 2	0.72	0.71	0.86	1

W40-G40				
	xylose 1	**xylose 2**	**maltose 1**	**maltose 2**
xylose 1	1	0.84	0.67	0.71
xylose 2	0.84	1	0.72	0.70
maltose 1	0.67	0.72	1	0.83
maltose 2	0.71	0.70	0.83	1

W100-G100				
	xylose 1	**xylose 2**	**maltose 1**	**maltose 2**
xylose 1	1	0.85	0.67	0.71
xylose 2	0.85	1	0.75	0.70
maltose 1	0.67	0.75	1	0.84
maltose 2	0.71	0.70	0.84	1

W200-G200				
	xylose 1	**xylose 2**	**maltose 1**	**maltose 2**
xylose 1	1	0.86	0.68	0.73
xylose 2	0.86	1	0.75	0.71
maltose 1	0.68	0.75	1	0.84
maltose 2	0.73	0.71	0.84	1

genes intersecting peaks; 2) number of individual peaks overlapping more than one gene and 3) number of genes associated with more than one peak. Since decreasing the window and gap size increased the overall number of peaks, it was important to determine whether more peaks also corresponded to more genes containing H3K4me3. When using smaller window and gap sizes, the overall number of H3K4me3 modified genes increased (Figure 12, Panel A). Among peaksets generated with 20 bp windows and increasing gap sizes, the number of peaks intersecting with gene models was similar, although a notable drop was seen when gap size was 80 bp (Figure 12, Panel B). Regions that were omitted with larger window sizes were usually minor peaks and/or located next to another major peak (Figure 13).

I also evaluated the peaksets to determine the number of peaks that overlapped multiple gene models. Visual assessment of the peaks in the genome browser revealed that some peaks were not appropriately split between distinct gene models. I used the "count" feature from the BEDTools Suite Package (Quinlan and Hall, 2010, available at http://code.google.com/p/bedtools/) to determine the number of gene models overlapping single peak regions. The number of peaks that overlapped more than one gene model was significantly higher when window and gap sizes were larger (data not shown). However, even the smallest window and gap size peak finding parameters (W20-G20) were not able to perfectly split all ChIP enriched regions so that single peaks were coupled to single gene models. To resolve this issue, I employed PeakSplitter (Salmon-Divon et al. 2010; http://www.ebi.ac.uk/research/bertone/software), a utility of the PeakAnalyzer program. This tool performs a subdivision of aggregate peak regions (areas containing more than one peak "summit") into discrete subpeaks. The splitting operation is performed using a user-defined parameter, which can be adjusted for sequencing read depth. I examined the results from the application of PeakSplitter in the genome browser. I observed that PeakSplitter introduced a 20bp gap in regions where read depth decreased between gene models but were not split by the initial SICER peak finding. Finally, I re-evaluated the number of peaks overlapping more than one gene following the peak splitting operation. From this analysis, I determined that by using the PeakSplitter tool, I was able to reduce the number of ChIP regions overlapping more than one gene model from 673 regions to 57.

Figure 12. Peak finding parameters and the number of H3K4me3 modified genes detected. The number of peaks with intersecting gene models identified for maltose (red) and xylose (blue) peaksets as a function of window size (Panel A) and gap size (Panel B).

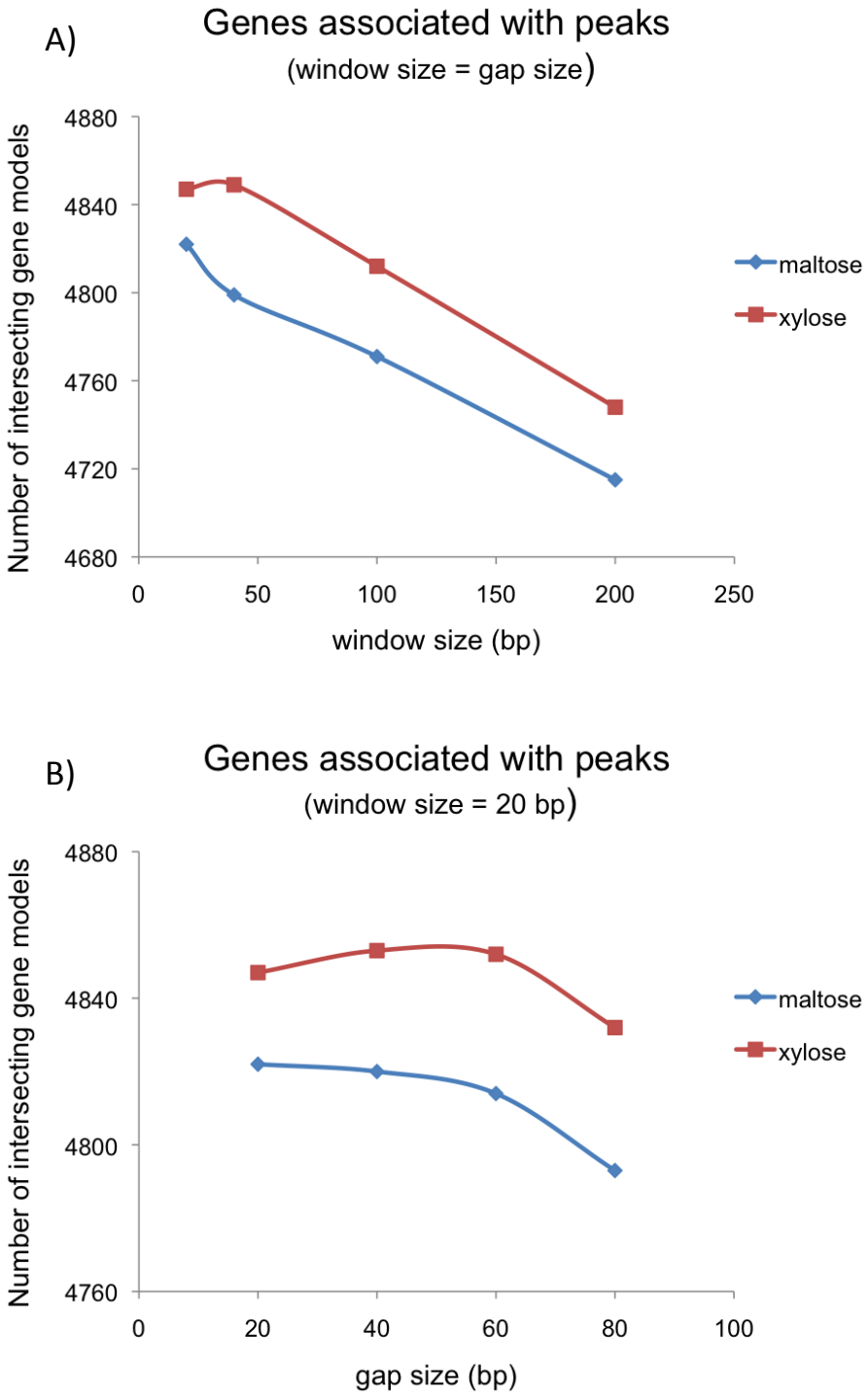

Figure 13. The effect of smaller window and gap sizes on peak detection. Panels A and B show two regions of the genome. Numbers 1 and 2 represent results from two biological samples cultured on xylose. The top two tracks show the mapping of raw reads; the third and fourth tracks, SICER peaks called with window size of 20 bp and gap size of 60 bp (W20-G60-1 and -2); the fifth and sixth tracks, SICER peaks called with window size and gap size of 200 bp (W200-G200-1 and -2); and the bottom track shows the positions of the gene models in the two regions.

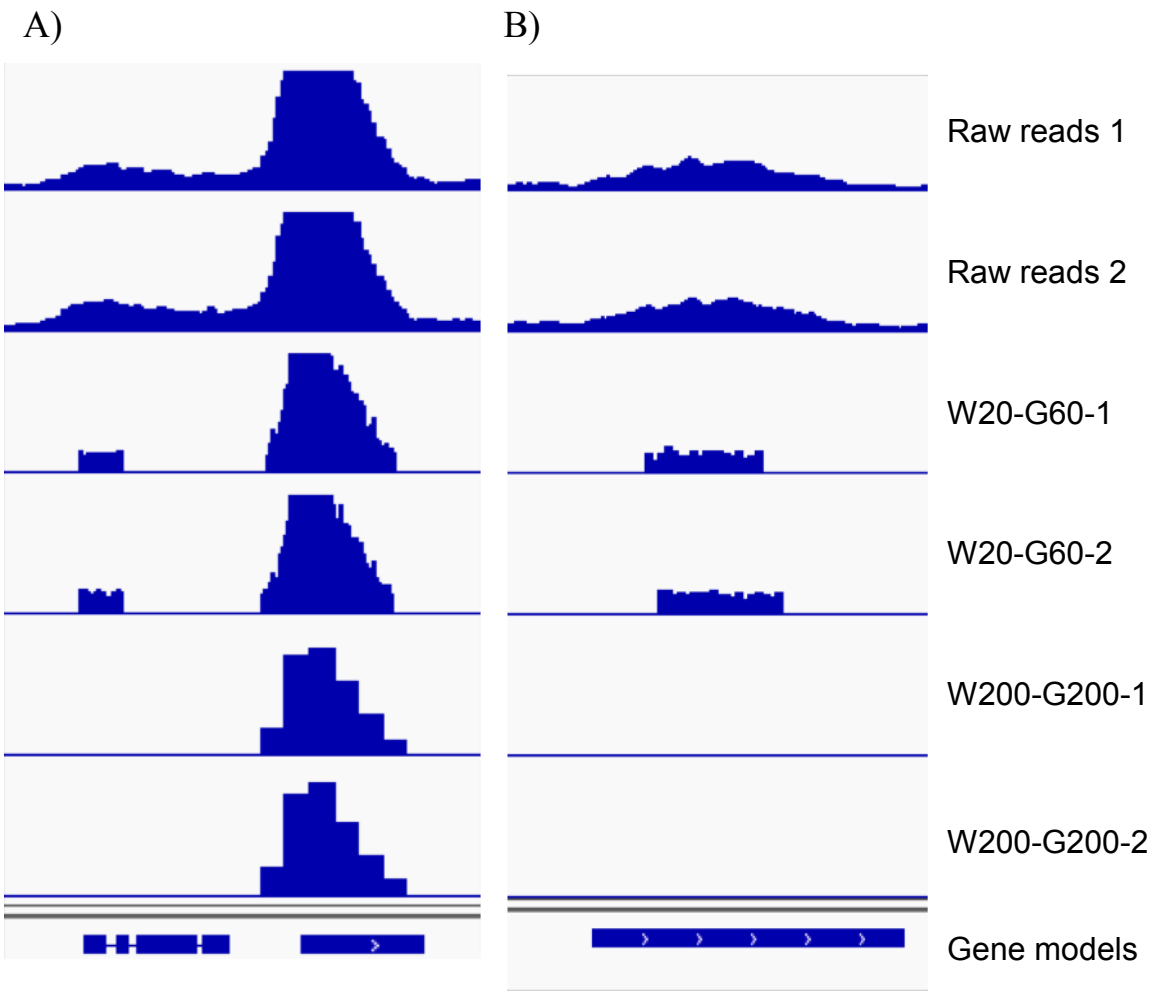

Finally, for the peaksets generated with 20 bp windows, I determined the number of fragmented or "split" peaks, where more than one peak was reported for a single gene model. These regions occasionally arose as a result of read fluctuations within a single peak. The number of split peaks was determined by counting the number of peak features overlapping each predicted gene model (here again with the BEDTools Suite package). The results from this analysis showed that the number of split peaks was largest when gap size was 20 bp, and the fewest were seen when gap size was 60 bp and 80 bp (Figure 14).

The results from the various analyses showed that, among the various peak finding trials, W20-G60 was the best performer. These parameters yielded a resulting peakset with few peaks overlapping multiple gene models, a minimal number of split peak regions, while maintaining maximum sensitivity in detecting H3K4me3 modified genes. As a result, the data set containing enriched intervals determined using W20-G60 was used for further analysis.

Figure 14. **Effects of gap size on fragmented peak regions.** The number of split or fragmented peak regions as a function of gap size.

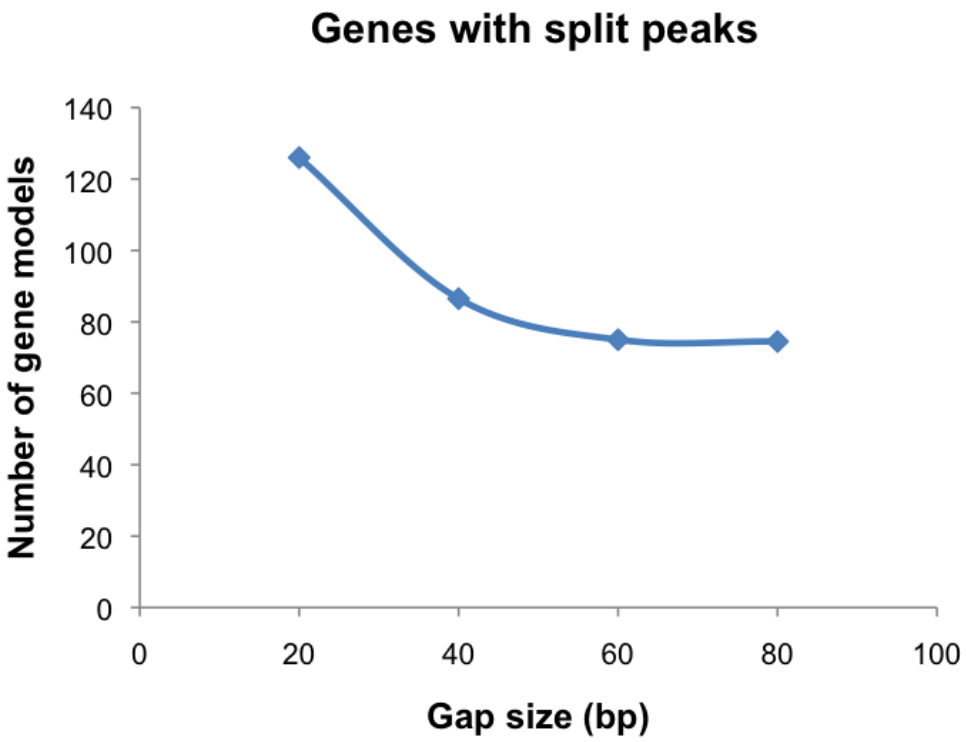

3.3 H3K4me3 patterns and distribution in the *Aspergillus niger* genome

3.3.1 A majority of actively transcribed genes contain H3K4me3

To examine the relationship between gene expression and presence of H3K4me3, I obtained RNA-seq data generated using the same growth conditions as the ChIP-seq experiment (data provided by Vanessa Blandford, unpublished). I plotted the $\log_2$ FPKM (fragments per kilobase of exon per million reads mapped) values from maltose growth against the $\log_2$ FPKM values of xylose growth and highlighted gene models containing an H3K4me3 peak (Figure 15, Panels A, B, C). As shown in the scatter plots, the presence of H3K4me3 correlates positively with active gene expression. Nearly all genes that have H3K4me3 peaks have FPKM values > 4 (Figure 15, Panel C). However, 1971 genes with FPKM > 4 were not marked with an H3K4me3 peak (Figure 15, Panel B), which suggests that the H3K4me3 chromatin modification is not necessarily required for gene expression.

While there is a strong trend for highly expressed genes to be epigenetically marked by H3K4me3 (median FPKM values for genes containing H3K4me3 are 40.8 and 41.4 for growth on xylose and maltose, respectively, compared with 1.1 and 1.3 for genes without H3K4me3), the correlation is not perfect. I therefore examined whether there is a correlation between gene function and H3K4me3 markers. Functional annotation of the predicted genes was described by Pel et al. (Pel et al. 2007). I compared genes with and without H3K4me3 in the following functional classes: genes encoding glycosyl hydrolases, components of the secretory pathway, enzymes of the central metabolism, fungal transcription factors and secondary metabolite genes. The genes from these functional classes are highlighted in the gene expression scatter plots in panels A-J of Figure 16. Median FPKM, mean FPKM, standard deviation, maximum and minimum FPKM values for these gene classes are listed in Table 4. In all cases, the correlation between gene activity and presence of the H3K4me3 modification is similar to that of the entire gene set. Due to the high variance seen in each of the functional classes, a Mann-Whitney rank sum test (suitable for non-normal distributions: Bauer, 1972; Hollander and Wolfe, 1973, 1999) was performed to determine the significance of differences between the FPKM distributions. For all protein function categtories, p values were <.0001, which indicates that the difference in distributions of the FPKM values between genes with and without H3K4me3 are significant.

Figure 15. **Comparing gene expression of *A. niger* and presence of H3K4me3 for growth on maltose and xylose.** Scatter plots of $\log_2$ FPKM values for all genes in *A. niger* for 2h growth on maltose vs. xylose is shown in Panel A). Panels B) and C) represent the genes without H3K4me3 and with H3K4me3, respectively.

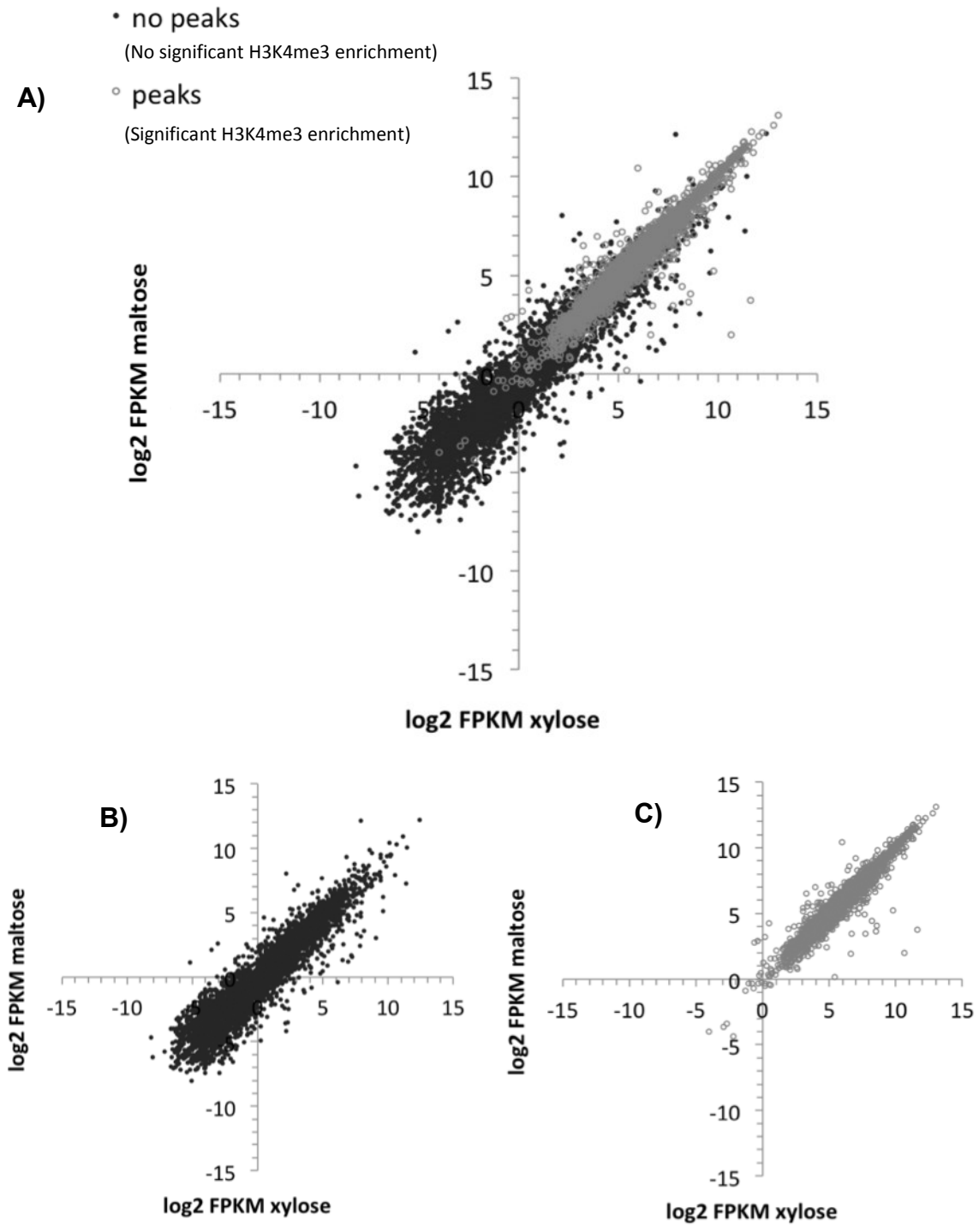

Figure 16. Comparing expression and presence of H3K4me3 across functional categories. Genes derived from various functional gene subsets without H3K4me3 are highlighted in orange. The panels on the left show genes without H3K4me3 (A,C,E,G,I) and those on the right show the genes with H3K4me3 (B,D,F,H,J).

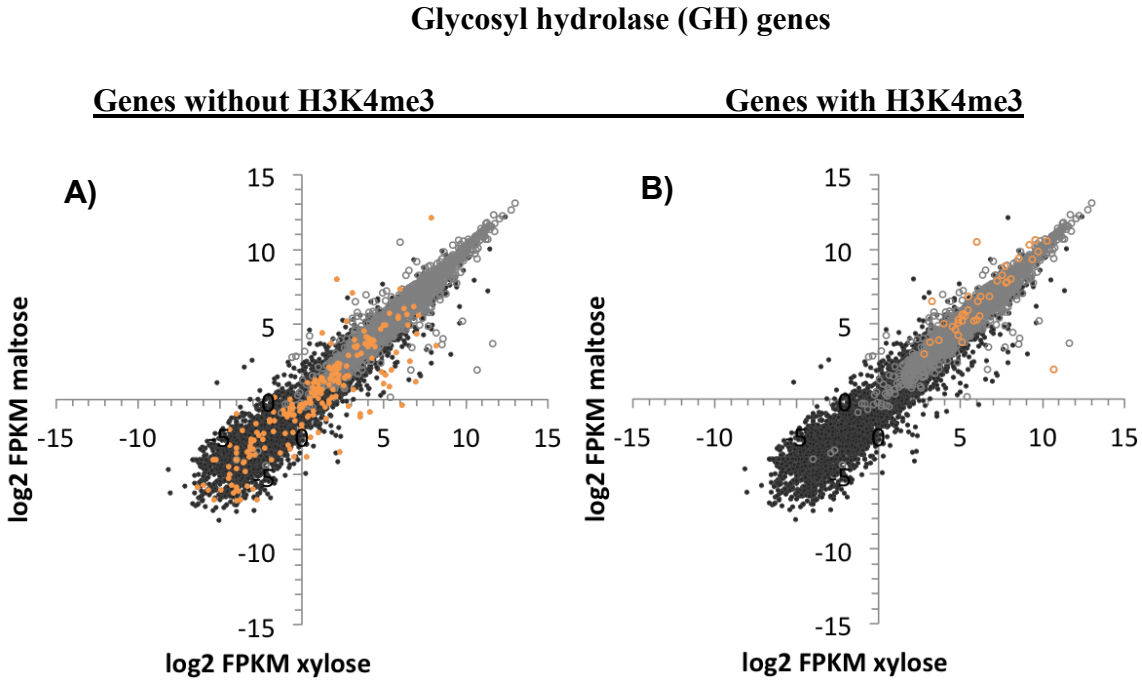

Secretory pathway genes

Genes without H3K4me3 **Genes with H3K4me3**

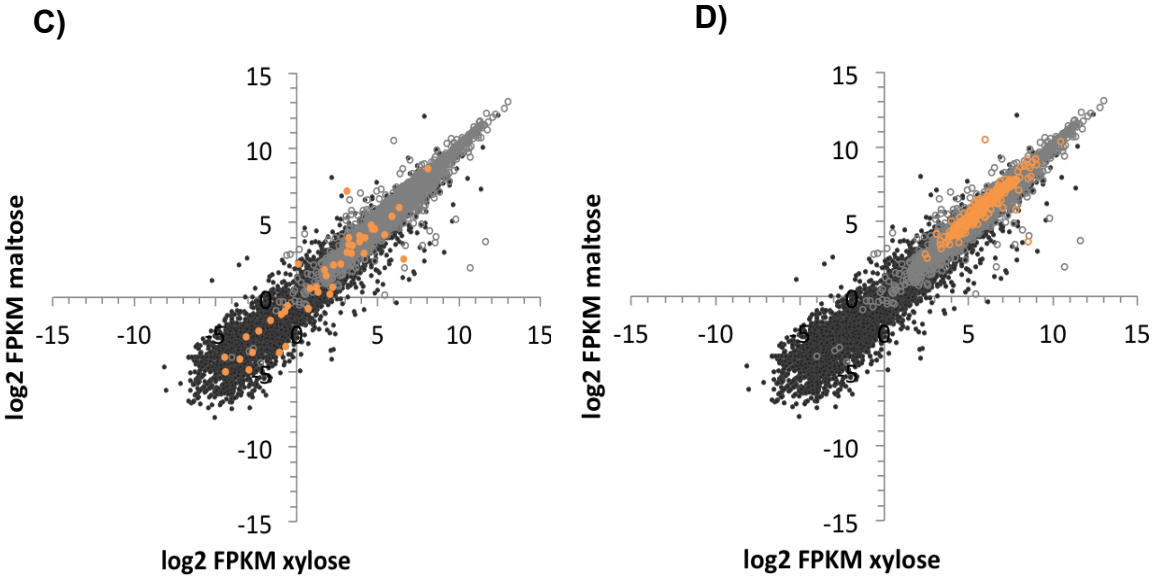

Central metabolism genes

Genes without H3K4me3 **Genes with H3K4me3**

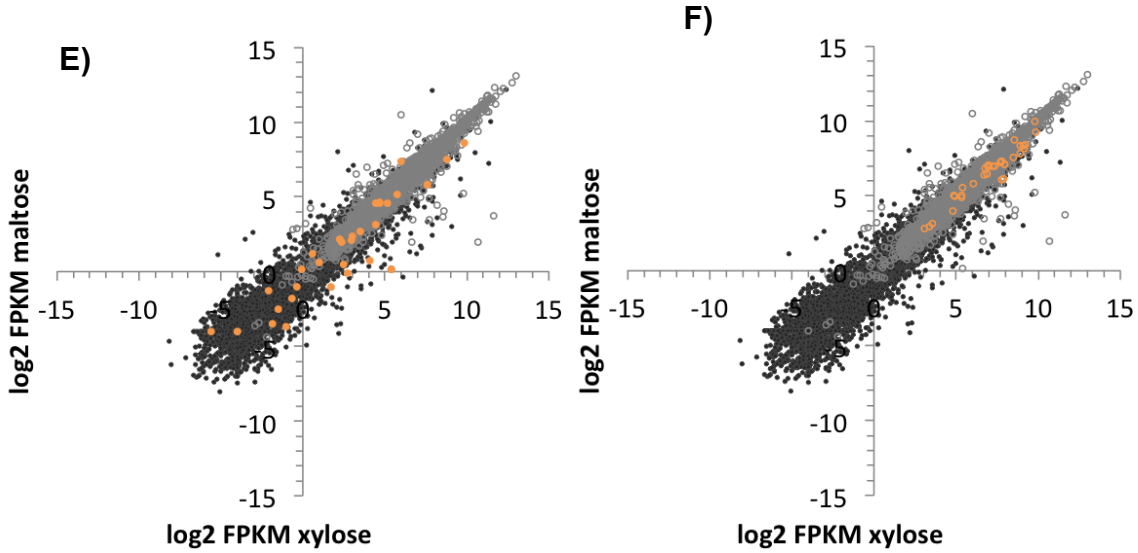

Fungal transcription factors

Genes without H3K4me3 **Genes with H3K4me3**

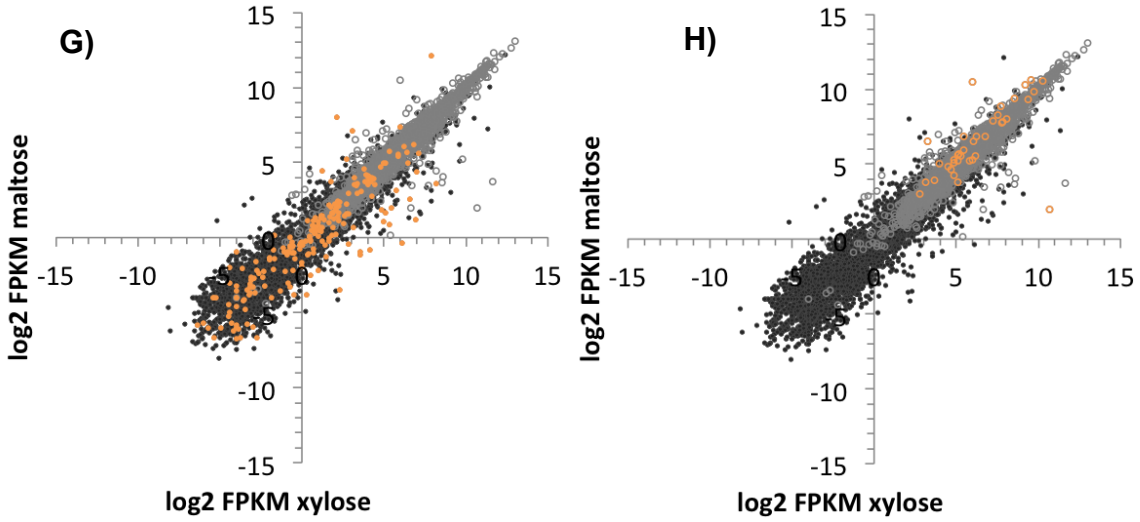

Secondary metabolism genes

Genes without H3K4me3 **Genes with H3K4me3**

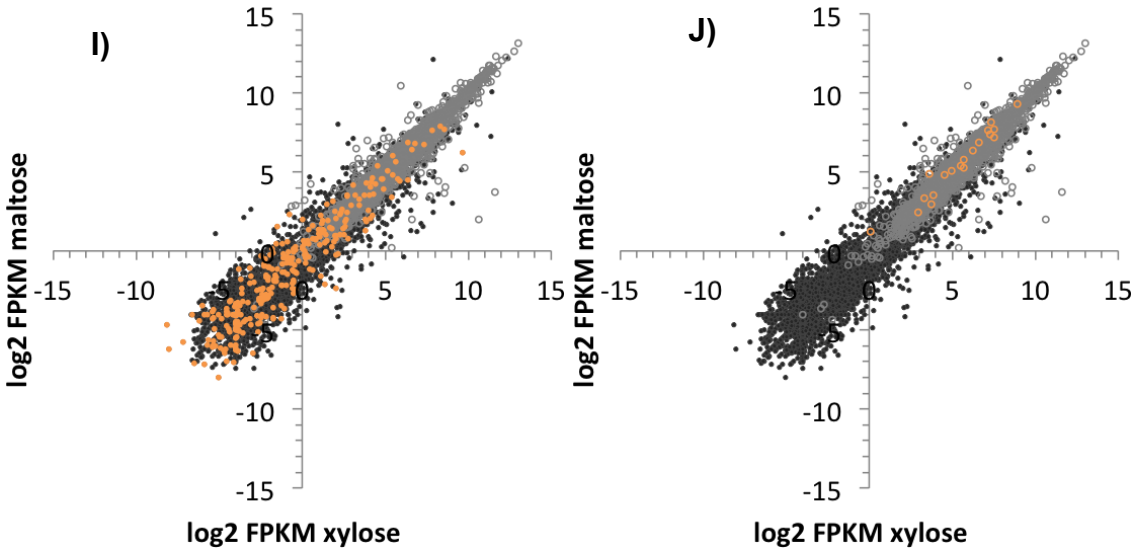

Table 4. Genes marked or unmarked by H3K4me3 as categorized by protein function.

For each protein function category (glycosyl hydrolases, central metabolism, secretory pathway, secondary metabolism, fungal transcription factors) the following are reported: median FPKM, mean FPKM, standard deviation (SD), minimum FPKM and maximum FPKM. The results from a Mann-Whitney U test (to determine whether the distributions of FPKM values differed between genes with H3K4me3 and genes without H3K4me3) are also reported. U value: product of the sample sizes for the two samples; *p* value: the probability that the distributions between the two groups, genes with H3K4me3 and genes without H3K4me3, are similar.

	Genes with H3K4me3						**Genes without H3K4me3**					
Protein Function	**No. genes**	**Median FPKM**	**Mean FPKM**	**SD**	**Min. FPKM**	**Max. FPKM**	**No. genes**	**Median FPKM**	**Mean FPKM**	**SD**	**Min. FPKM**	**Max. FPKM**
Glycosyl hydrolases	38	62.7	258	409	4.00	1620	207	1.38	21.3	222	0	4470
Central metabolism	37	131	202	217	6.92	1019	33	4.63	46.5	138	0	917
Secretory pathway	272	56.7	97.2	134	5.37	1435	44	3.93	19.4	54.3	0	397
Secondary metabolism	19	48.6	101	131	1.04	616	87	0.32	8.38	43.9	0	800
Fungal TF	20	17.7	29.2	34.5	2.32	188	309	3.87	5.71	5.22	0.05	23.3
All genes	5058	41.1	109	314	0	8847	6788	1.21	12.8	98.4	0	5475

Mann-Whitney U two sample rank-sum test outcomes	
Glycosyl hydrolases	U = 23454; p <.0001 (one-tailed), p <.0001 (two-tailed)
Central metabolism	U = 454; p <.0001 (one-tailed), p <.0001 (two-tailed)
Secretory pathway	U = 4105; p <.0001 (one-tailed), p <.0001 (two-tailed)
Secondary metabolism	U = 22058; p <.0001 (one-tailed), p <.0001 (two-tailed)
Fungal transcription factors	U = 5540; p <.0001 (one-tailed), p <.0001 (two-tailed)
All genes	U = 127335486; p <.0001 (one-tailed), p <.0001 (two-tailed)

I also examined the distribution of H3K4me3 in genes expected to be constitutively expressed. With one exception, all aminoacyl tRNA synthetase genes contained H3K4me3 peaks (Figure 17, Panel A). Similarly, all but one of the ribosomal protein genes were marked with H3K4me3 (Figure 17, Panel B). The mitochondrial ribosomal protein genes, transcribed at considerably lower levels than their cytoplasmic counterparts, are all marked by H3K4me3 (Figure 17, Panel C).

The integrated transcriptome and ChIP-seq data presented here demonstrate that although the majority of actively transcribed genes contained H3K4me3, the presence of this histone modification is not required for transcription of all *A. niger* genes.

3.3.2 Differential H3K4me3 binding analysis

To identify sites with significantly different levels of H3K4me3 binding, I performed an analysis using the DiffBind package for R Bioconductor (Stark and Brown, 2011). The package determines differential read counts in bound genomic intervals using a statistical model and builds on R graphics routines to generate plots and diagrams to support the binding analysis. DiffBind works with previously defined peaksets and then calculates a binding matrix based on scores generated by counting reads within the peaksets. Differentially bound sites are identified by counting the reads in overlapping intervals for each unique sample group to generate a normalized read count for each site, then re-clusters the samples using affinity rather than occupancy data. Using the SICER peaksets from the four samples (two from xylose growth and two from maltose growth) as an input, DiffBind identified 34 sites (0.7% of the total number of ChIP enriched sites) as differentially bound by H3K4me3 when comparing growth on maltose or xylose. The MA plot in Figure 18 (a representation of differences in log H3K4me3 read counts on maltose and xylose growth as a function of average log read concentration) shows sites with differential H3K4me3 binding and highlights those that also have a false discovery rate of <0.05. A list of these sites with their respective fold differences and associated gene models are listed in Table 5. Five of the sites identified as differentially bound did not intersect with a gene model. The sites were classified into categories based on the type of differential binding exhibited:

Figure 17. Presence of H3K4me3 in constitutively transcribed genes. Scatter plots representing the $\log_2$ FPKM values from growth on maltose vs growth on xylose and highligting the genes predicted to be constitutively expressed (orange). Aminoacyl tRNA synthetase proteins are shown in Panel A and ribosomal genes in Panel B. Panel C shows the $\log_2$ FPKM values for the cytoplasmic (orange) and mitochondrial (blue) ribosomal proteins. Genes highlighted in black did not contain H3K4me3.

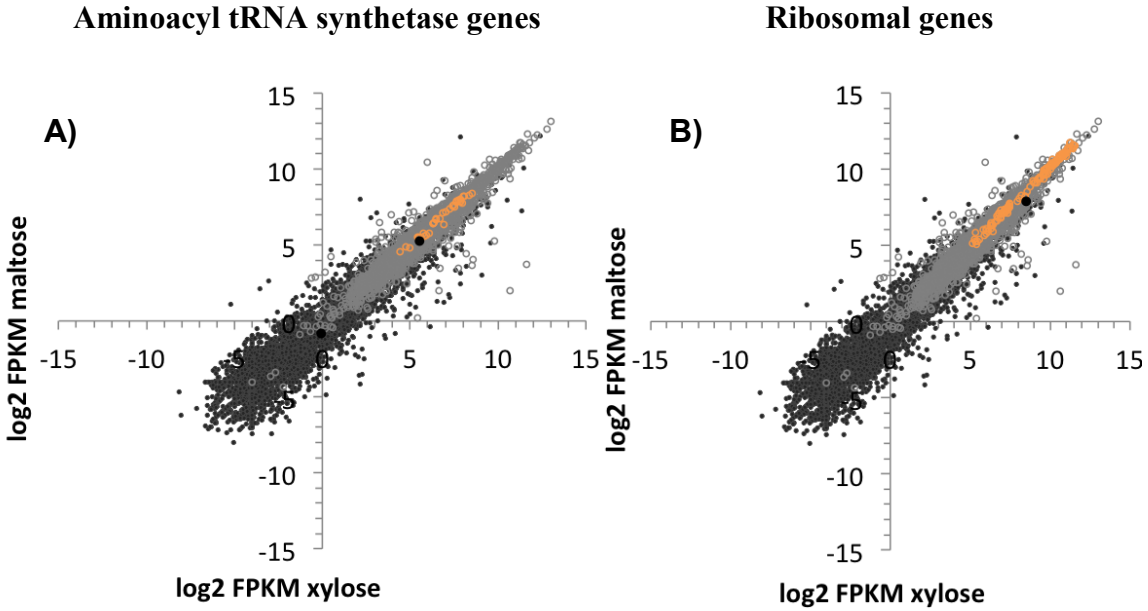

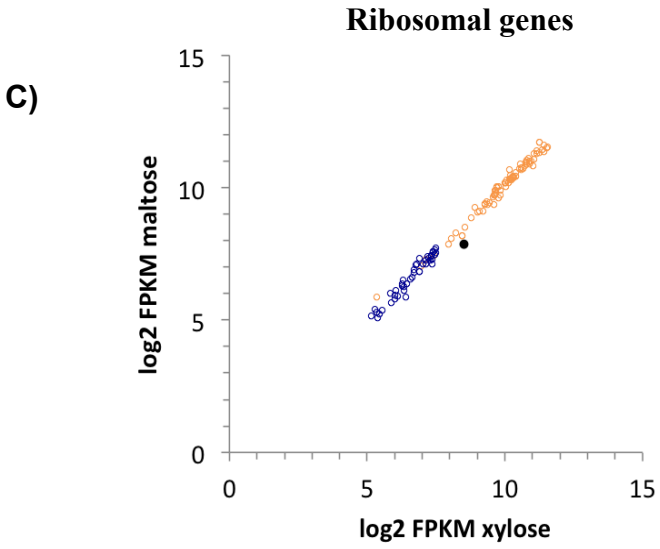

H3K4me3 enrichment occurring uniquely during growth on one of the carbon sources ("peaks exclusively detected in growth on xylose", "peaks exclusively in growth on maltose") or significantly higher H3K4me3 binding (read counts) during growth on one of the carbon sources ("higher counts in growth on maltose", "higher counts in growth on xylose").

I then compared the results from the differential binding analysis with a peak occupancy analysis. The Venn diagram in Figure 19 shows the number of sites that were uniquely occupied (as determined by the peak caller) by H3K4me3 for growth on maltose and growth on xylose. In total, 36 sites uniquely occupied sites on maltose growth and 124 sites on xylose growth. By using the DiffBind affinity analysis, associated with significance statistics, only 5 sites were determined as unique to maltose growth and 12 sites to xylose growth. Finally, the DiffBind analysis returned 17 sites that display significantly different binding affinities (Table 5). These results indicated that the binding affinity analysis is indispensable for the identification significantly differentially bound sites.

3.3.3 Comparison of differential H3K4me3 binding and levels of transcript accumulation

The next logical analysis is to compare the differential H3K4me3 binding results with the differentially expressed genes from the maltose and xylose growth. The differential gene expression analysis was provided by Vanessa Blandford (data unpublished) and was generated using the DESeq algorithm (Anders and Huber, 2010). The comparison of the two data sets revealed that the majority of genes determined as differentially expressed (188/233) do not contain an H3K4me3 peak, highlighted in the scatter plot shown in Panel A of Figure 20. Of the 45 genes that contain a ChIP peak (Figure 20, Panel B), only 11 genes (listed in Table 6) have significantly differential levels of H3K4me3. For these 11 genes, higher levels of transcription are associated with increased H3K4me3. Similarly, genes that have lower expression levels also have lower levels of H3K4me3. The GH31 alpha-glucosidase gene (NRRL3_07700) was the single exception to this trend: a lower transcript level is accompanied by an increase in H3K4me3 at this gene locus. These results demonstrated that genes differentially transcribed on maltose and xylose growth correlate weakly with the presence of H3K4me3 or with respective increases and decreases in H3K4me3 modification.

Figure 18. Visual representation of significantly differentially bound sites.

An MA plot was generated using the DiffBind package. The points on the plot represent individual sites that exhibited fold changes in H3K4me3 ChIP-seq read counts between maltose and xylose growth conditions. Sites determined as significantly differentially bound by H3K4me3 (highlighted in red) are those that have a log fold change of at least 2 and an FDR rate of <0.05

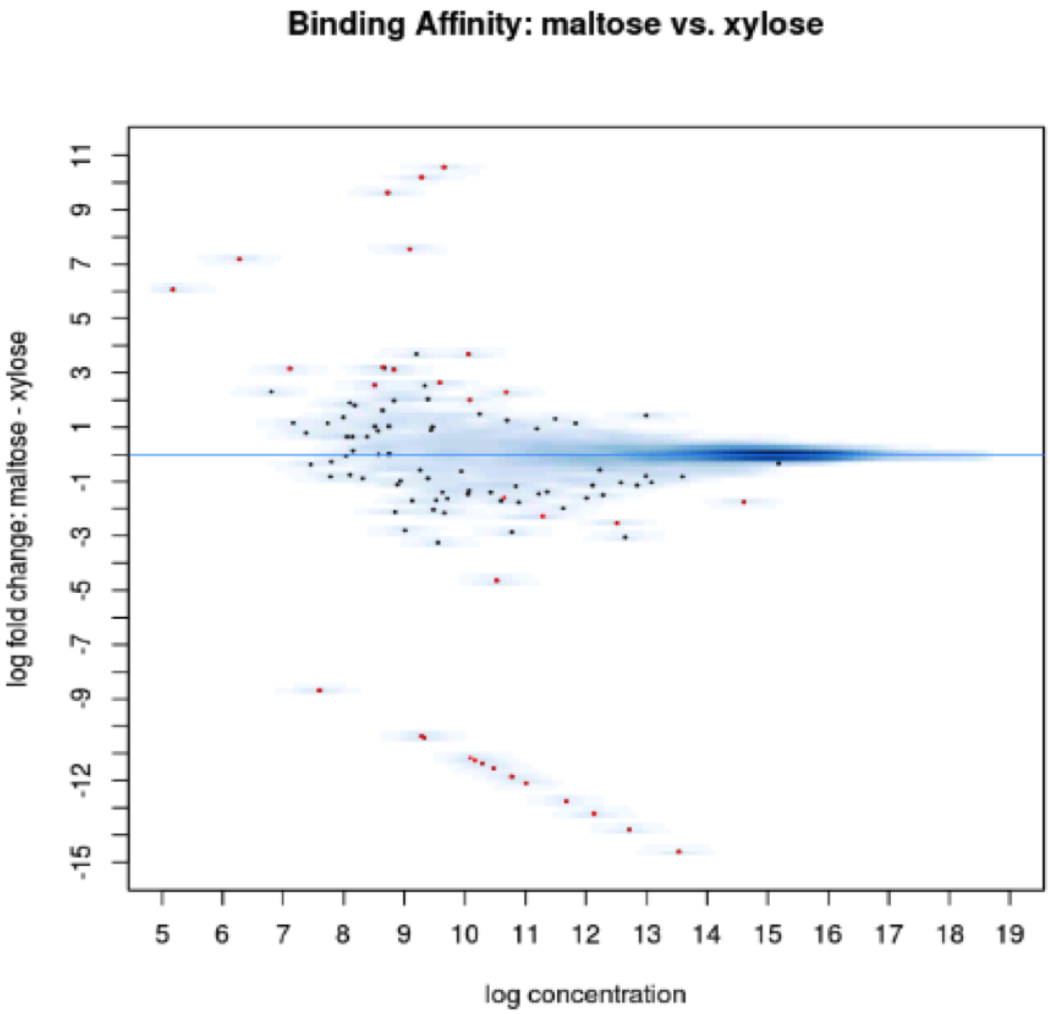

Table 5. Differentially bound sites identified in DiffBind. Significantly differential H3K4me3 ChIP regions and associated gene models, as determined by the DiffBind analysis. Genome coordinates are provided for regions where no gene model is predicted.

Gene model	Mean log2 read depth - maltose	Mean log2 read depth - xylose	Predicted protein
Peaks exclusively detected in growth on xylose			
NRRL3_07563	-0.086	14.536	unknown
NRRL3_09251	-0.086	13.718	Bifunctional protein gal10
NRRL3_04471	-0.086	13.133	D-xylulose kinase A
NRRL3_01952	-0.086	12.673	NAD(P)H-dependent D-xylose reductase xyl1
NRRL3_02450	-0.086	12.009	Uncharacterized protein YxeQ
NRRL3_07698	-0.086	11.773	Transcriptional activator of proteases prtT
NRRL3_05970	-0.086	11.470	Galactose-1-phosphate uridylyltransferase
NRRL3_02451	-0.086	11.166	beta-xylosidase GH3
NRRL3_04473	-0.086	11.085	Transaldolase
NRRL3_02937	-0.086	10.328	unknown
NRRL3_07700	-0.086	10.285	alpha-glucosidase GH31
NRRL3_09050	-0.086	8.594	Lactose regulatory protein LAC9
Peaks exclusively detected in growth on maltose			
NRRL3_01770	10.653	0.087	unknown
NRRL3_09399	10.285	0.087	Vacuolar calcium ion transporter
NRRL3_05625	9.722	0.087	Linoleate 10R-lipoxygenase
NO MODEL	7.267	0.087	chr_5_2:182420-182559
NO MODEL	6.157	0.087	chr_7_2:237680-237759
Higher counts in growth on xylose			
NRRL3_09204	13.479	15.233	D-xylulose reductase A
NRRL3_10884	10.754	13.281	Uncharacterized oxidoreductase
NRRL3_02934	11.292	12.860	unknown
NRRL3_01478	9.739	12.014	Putative NADP-dependent oxidoreductase YfmJ
NRRL3_03187	6.831	11.468	Initiation-specific alpha-1,6-mannosyltransferase
NRRL3_06477	5.227	8.349	UPF0187 protein sll1024
Higher counts in growth on maltose			
NRRL3_07785	11.413	9.121	unknown
NRRL3_04106	10.952	7.265	unknown
NO MODEL	10.759	8.753	chr_3_2:368420-368939
NRRL3_02744	10.371	7.725	unknown
NO MODEL	10.109	7.580	chr_2_2:1645480-1646119
NRRL3_01410	10.083	2.526	Putative succinate-semialdehyde dehydrogenase C
NRRL3_00397	9.668	6.553	60 kDa lysophospholipase
NRRL3_03297	9.535	5.804	Siderophore iron transporter mirB
NRRL3_04956	9.500	6.295	Maleylacetate reductase
NRRL3_02279	9.280	6.729	unknown
NO MODEL	7.953	4.799	chr_4_1:1132420-1132519

Figure 19. Maltose growth and xylose growth peak occupancy analysis

The number of H3K4me3-bound sites exclusive to maltose and xylose, based on peak occupancy data as determined by SICER peak calling.

Figure 20. Comparison of differentially expressed genes and H3K4me3 modification. A scatter plot of $\log_2$ FPKM values for all genes in *A. niger* for growth on maltose vs. xylose. The genes determined to be differentially expressed by the DESeq method are highlighted in orange.

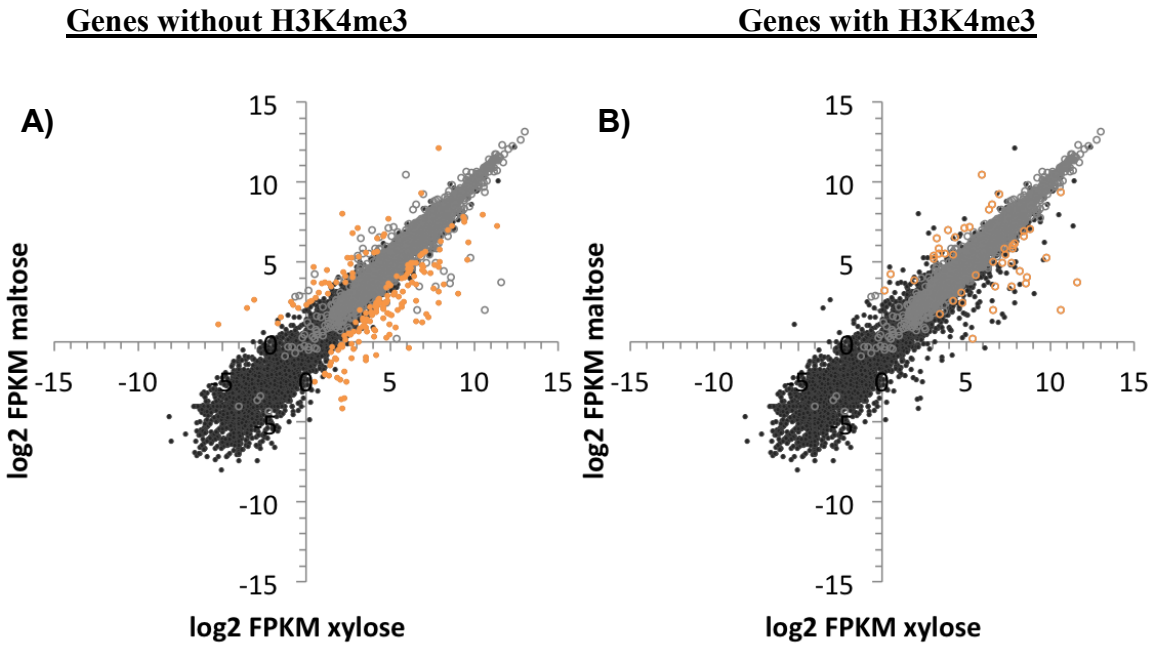

Table 6. Differentially transcribed genes with differential H3K4me3. Genes that display positive correlation in the differential RNA-seq and ChIP-seq analyses for growth on maltose and growth on xylose.

Gene model	Xylose FPKM	Maltose FPKM	Xylose log2 H3K4me3 mapped ChIP reads	Maltose log2 H3K4me3 mapped ChIP reads	Predicted protein
Peaks exclusively detected in growth on xylose					
NRRL3_09251	373.00	12.64	13.72	-0.086	Bifunctional protein gal10
NRRL3_04471	386.73	16.66	13.13	-0.086	D-xylulose kinase A
NRRL3_01952	3153.43	13.39	12.67	-0.086	NAD(P)H-dependent D-xylose reductase xyl1
NRRL3_02450	99.45	3.89	12.01	-0.086	Uncharacterized protein YxeQ
NRRL3_05970	221.65	56.86	11.47	-0.086	Galactose-1-phosphate uridylyltransferase
NRRL3_02451	1620.04	4.00	11.17	-0.086	beta-xylosidase GH3
NRRL3_04473	42.40	1.13	11.09	-0.086	Transaldolase
NRRL3_07700	62.65	1408.08	10.29	-0.086	alpha-glucosidase GH31
Peaks exclusively detected in growth on maltose					
NRRL3_05625	30.49	139.67	0.087	9.722	Linoleate 10R-lipoxygenase
Higher counts in growth on xylose					
NRRL3_09204	880.46	37.54	15.23	13.479	D-xylulose reductase A
NRRL3_10884	105.16	10.98	13.28	10.754	Uncharacterized oxidoreductase MexAM1

3.3.4 Genes with and without H3K4me3 are not randomly distributed along the chromosome

The eight *A. niger* chromosomes and the distribution of gene models with and without H3K4me3 along their lengths are plotted in Figure 21. In general, H3K4me3 distribution is not even throughout the length of the chromosome. At the centromere regions, H3K4me3 peaks were completely missing. H3K4me3 distribution abruptly ends on either side of this region, which also coincides with the last coding gene model predicted. In addition, H3K4me3 is not evenly distributed along the chromosome arms. This is particularly noticeable at the gene-coding regions near the centromeres and telomeres. A magnified view of the centromeric and telomeric regions of chromosomes 4 and 6 is shown in Figure 22 to illustrate the non-random distribution of H3K4me3 peaks. Table 7 summarizes the number of gene models in the 100-kb regions adjacent to the telomeres and centromeres associated with H3K4me3 peaks. At the regions near the telomeres, H3K4me3 is almost completely absent. The opposite is seen at the pericentromeric regions, where peaks appear at nearly every gene model. These observations suggest a preferential localization of H3K4me3 along the chromosome length.

Figure 21. Chromosomal distribution of H3K4me3.

Genes with H3K4me3 peaks (red) and without H3K4me3 (blue) were mapped to the eight *A. niger* chromosomes. The figure also shows a map of genes that are differentially expressed on maltose growth and xylose growth: black triangles represent the genes that were marked by H3K4me3 peaks and black circles represent the genes that did not contain H3K4me3.

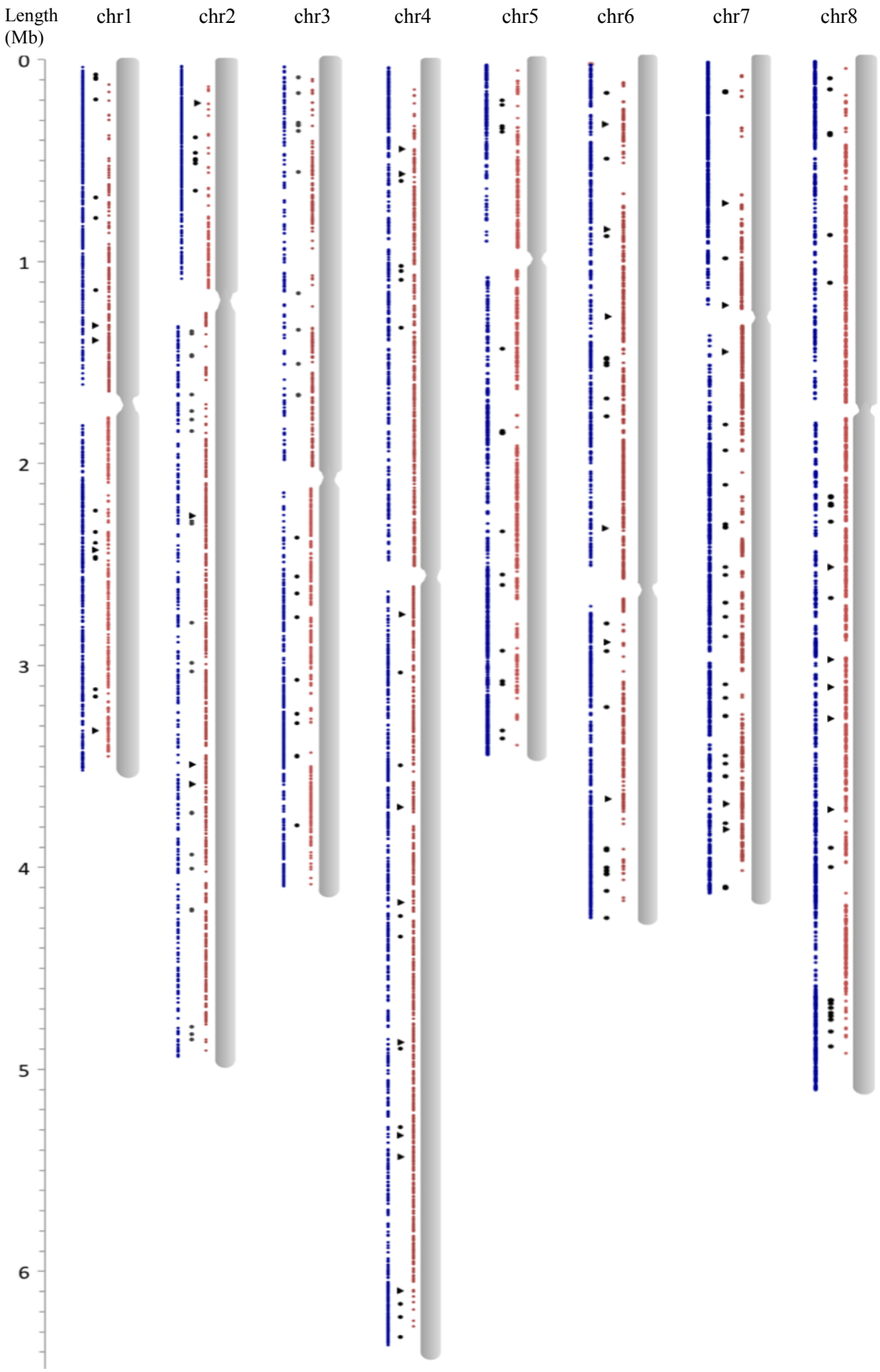
Length
(Mb)
chr1
chr2
chr3
chr4
chr5
chr6
chr7
chr8
0
1
2
3
4
5
6

Figure 22. Genes with and without H3K4me3 in regions near the centromeres and telomeres. Gene models with H3K4me3 (red) and without H3K4me3 (blue) are represented in the boxed regions displaying the 100 kb closest to the centromeres and telomeres.

Chromosome 4

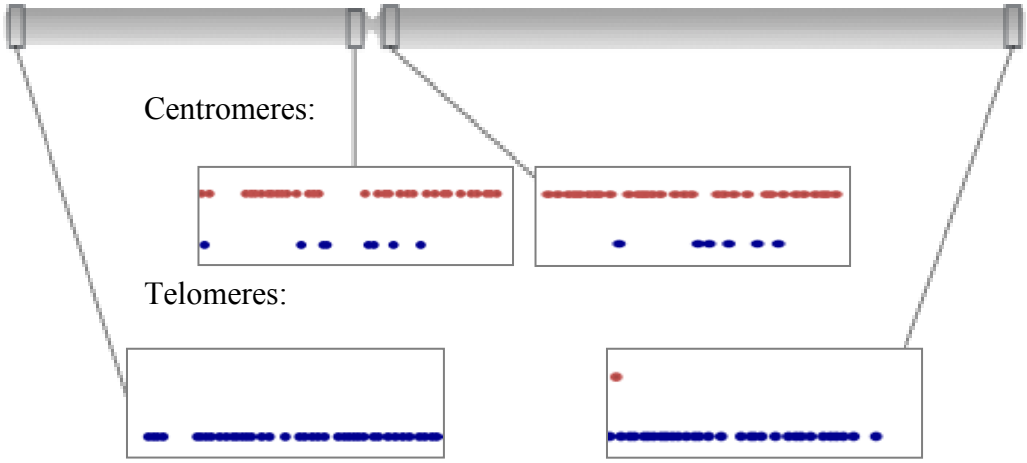

Chromosome 6

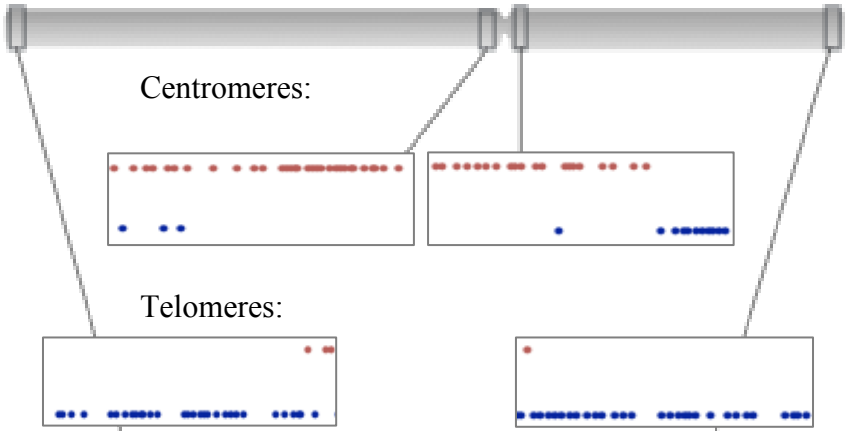

Table 7. H3K4me3 distribution at regions proximal to the centromeres and telomeres. Summarized here is the number of genes with H3K4me3 peaks in the 100 kb intervals closest to centromere and telomere regions of each of the eight *A. niger* chromosomes.

	Genes with H3K4me3 at **centromeres**	% of genes with H3K4me3 peaks	Genes with H3K4me3 at **telomeres**	% of genes with H3K4me3 peaks
chromosome 1	59/71	83.1	10/74	13.5
chromosome 2	44/58	75.9	1/77	1.30
chromosome 3	58/72	80.6	5/71	7.04
chromosome 4	66/77	85.7	1/73	1.37
chromosome 5	55/71	77.5	5/81	6.17
chromosome 6	54/72	75.0	2/70	2.86
chromosome 7	55/64	85.9	3/74	4.05
chromosome 8	57/81	70.4	1/72	1.39

3.3.5 H3K4me3 is associated with potential non-coding RNA

The peak finding analysis returned 60 H3K4me3-enriched ChIP sites that did not associate with a predicted gene model. I investigated the possible significance of these H3K4me3 peaks. In particular, I examined whether transcription may be occurring at these regions in the genome, a phenomenon that has been reported in yeast (van Dijk et al. 2011). I observed most of the ChIP peaks not associated with gene models are present at regions where there is transcript coverage, an example of which is shown in Figure 23. Five of these ChIP peaks were determined as differentially bound by H3K4me3 on maltose and xylose (shown in Table 5). A protein-coding gene model could not be predicted in the genomic sequence of any of these regions. Therefore, the transcription seen in these regions may be generating non-coding RNA species and their genomic loci contain the H3K4me3 chromatin modification.

Figure 23. H3K4me3 marks regions of non-coding transcripts

The H3K4me3 peak shown in the upper track (in green) was mapped to a genomic interval from chromosome 7 not predicted to contain a protein- or rRNA-coding gene. The lower track shows mapped RNA reads (red), generated by RNA-sequencing.

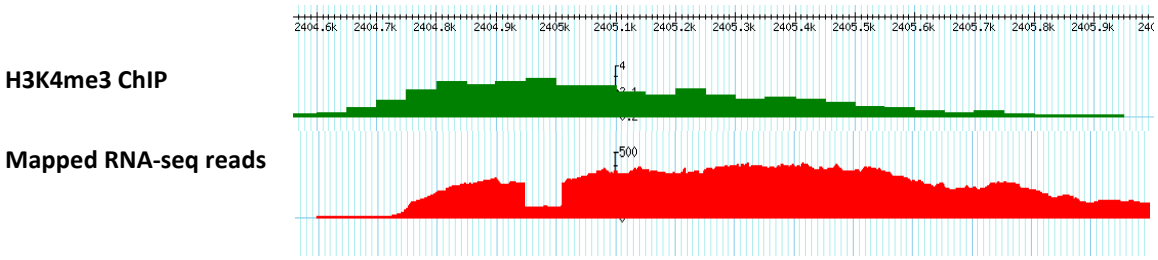

Table 8. Genome coordinates for ChIP-enriched regions not intersecting with a known gene model.

	Start	End
chr_1_1	926740	926919
chr_1_1	1223000	1224279
chr_1_1	1388040	1388279
chr_1_1	1596500	1597179
chr_1_2	1333260	1333419
chr_1_2	1339860	1340819
chr_2_1	263280	263759
chr_2_2	344720	345739
chr_2_2	1068560	1069259
chr_2_2	1361280	1362759
chr_2_2	1362960	1363079
chr_2_2	1401440	1401579
chr_2_2	1445640	1446159
chr_2_2	1645480	1646119
chr_2_2	2027360	2027759
chr_2_2	2941980	2942899
chr_2_2	3073640	3073999
chr_2_2	3266360	3266539
chr_3_1	230940	231699
chr_3_1	595900	597059
chr_3_1	1323700	1324459
chr_3_1	1324680	1325039
chr_3_1	1921080	1921799
chr_3_2	348360	349239
chr_3_2	368420	368939
chr_3_2	1689820	1691079
chr_3_2	1875560	1877419
chr_4_1	1132420	1132519
chr_4_1	1520140	1520319
chr_4_1	2282620	2282939
chr_4_2	239480	240799
chr_4_2	318480	319159
chr_4_2	1561780	1562019
chr_4_2	2550260	2551219
chr_4_2	3649080	3649279
chr_5_1	815380	815659
chr_5_1	925180	925719
chr_5_2	41020	41639
chr_5_2	182420	182559

chr_5_2	1044200	1044479
chr_5_2	1083100	1083519
chr_5_2	1404020	1404279
chr_5_2	1750740	1752279
chr_5_2	1885480	1886859
chr_5_2	2382060	2382899
chr_6_1	6560	6739
chr_6_1	1031260	1031879
chr_6_1	2433540	2433859
chr_7_1	745140	745799
chr_7_1	879400	880099
chr_7_2	237680	237759
chr_7_2	1501500	1501919
chr_7_2	1824800	1825119
chr_7_2	2404700	2405499
chr_8_1	423600	423959
chr_8_1	996880	997779
chr_8_2	419460	420599
chr_8_2	718020	718199
chr_8_2	1099480	1100379
chr_8_2	1584960	1586359

Section 4: Discussion

4.1 Development of a method for enrichment of nuclei in *Aspergillus niger*

I developed a method to obtain a nuclei-enriched cellular extract of *A. niger* for use in downstream chromatin immunoprecipitation experiments. The method was adapted from others previously described for use in *Neurospora crassa* with two modifications: 1) volumes in the protocol were scaled down for use with the smaller 2 g mycelial mats (the *N. crassa* protocol was for use with 7g of mycelia) and 2) centrifugation with the sucrose gradients was omitted to decrease the number of steps required to minimize loss. I validated the nuclei enrichment by determining the DNA content of the fractions generated and by mass spectrometry to detect marker proteins of various cellular compartments. The cellular fractionation procedure described here yields a pellet containing a high concentration of DNA. In addition, mass spectrometric analysis revealed a relatively high level of marker proteins specific for the nuclear compartment in the enriched extract. These included proteins located in the nuclear envelope (nucleoporins), soluble nuclear proteins (topoisomerases) and chromatin bound proteins (histones), suggesting that whole, intact nuclei were pelleted. The separation method was crude, as the nuclei-enriched fraction also contained some proteins from the mitochondrion, endoplasmic reticulum and cytoplasm. However, other previously described procedures for organelle fractionation, even those reporting high purity, have shown varying degree of contamination of proteins from other cellular compartments (Mootha et al. 2003; Taylor et al. 2003; Andreyev et al. 2010). Although other membrane bound organelles (endoplasmic reticulum, mitochondria) were co-purified along with the nuclear fraction in the current experiment, their presence did not affect the chromatin immunoprecipitation: only a single, specific band was detected in the immunoblot performed with the anti-H3K4me3 antibody. Overall, this protocol is a fast and efficient method for the isolation of an enriched nuclei fraction from *A. niger* mycelia for use in chromatin immunoprecipitation.

4.2 Technical considerations for *A. niger* ChIP-sequencing and data analysis

The results from the ChIP-seq experiment performed here in *A. niger* highlight the importance of technical issues to consider for obtaining high quality data. First, it is important to select an appropriate control for sequencing normalization. I selected total "input" DNA (chromatin not subjected to immunoprecipitation) as negative control for ChIP-seq, in favour of

performing a mock immunoprecipitation with non-specific IgG. Native genomic DNA is regarded as a more effective negative control than a mock immunoprecipitation (Kidder et al. 2011) for two reasons. First, since IgG from the same animal used to produce the antibody against the target protein is not usually available. Thus, DNA immunoprecipitated in this way cannot be considered as a "true" background. Secondly, the mock immunoprecipiation method is often ineffective in pulling down enough DNA for sequencing. In the current experiment, I witnessed that the using the input DNA control was important for eliminating peaks in regions where sheared chromatin was overrepresented (Figure 13). These regions likely arise from open chromatin or nucleosome-free structures that can fragment more easily during the sonication process. These peaks were seen in the ChIP samples and could have otherwise been considered as true ChIP peaks. This suggests that native genomic DNA was an effective control for chromatin immunoprecipitation in *A. niger*.

In the data analysis step of the ChIP-seq experiment, choices of peak finding algorithm and parameters for determining significant peaks are also important factors. I attempted peak finding with three programs that have been reviewed in the literature as reliable for this purpose. Two of these methods were unable to accurately identify peaks that corresponded to ChIP enriched regions, which was confirmed by comparing the results in the genome browser. The SICER algorithm (Zang et al. 2009) was an effective method for detecting significant H3K4me3 enrichment with this data set, as the results corresponded well to peaks seen in the raw reads mapped to the genome. SICER has been reviewed as suitable for the detection of broad regions characteristic of certain histone modifications (Kidder et al. 2011). This method is also among the best performers in a recent study of several algorithms developed over the past several years in an unbiased evaluation of algorithmic performance selectivity and sensitivity (Micsinai et al. 2012). To my knowledge, the ChIP-seq experiment performed in the current experiment is the first report of the application of this peak finding algorithm in a non-mammalian genome.

An in-depth analysis for each generated peakset using different window and gap sizes in SICER was useful for determining which parameters were suitable for peak finding in this experiment. I demonstrated that reducing window size from the recommended 200bp to 20bp was essential for detecting a greater number of genes containing H3K4me3 peaks. The regions that were undetected with larger window and gap sizes were regions with smaller peaks and

lower levels of mapped ChIP reads. By performing peak finding with smaller windows, these less prominent peak regions could be detected as significant by the algorithm. Along with the use of smaller windows, I determined the effects of modifying gap size in SICER peak finding. As expected, a smaller gap size increased the sensitivity to fluctuations in read density. Peaksets generated using small gap sizes had the highest number of fragmented peaks associated with a single gene model. When window size was 20bp and gap size was 60bp, peaksets between biological replicates showed the highest levels of correlation, a maximum number of ChIP enriched genes was detected, and fragmented peak regions were kept to a minimum. However, there were still a number of regions in this peakset that overlapped more than one gene. This was a potential concern, since some smaller, less highly enriched regions could be obscured as a result of being merged with another broader or taller peak. The issue was resolved by using a peak splitting program, which effectively detected the vast majority of significant read fluctuations that occurred between gene models that were not detected as gaps in the original peak finding with SICER. The peak splitting method introduced a gap in these regions and the resulting peakset contained distinct peaks for individual gene models. Taken together, the analysis demonstrated that the choice of methods for data analysis is important to consider in ChIP-seq analysis. The genome of *A. niger* is densely packed, with a mean spacing of ~1 gene per 3 kbp (close together when compared with that of higher eukaryotes like human and mouse, which have an average spacing of 1 gene per ~ 144 kbp and ~130 kbp, respectively; Ensembl Genome Reference Consortium, 2013). This provides a rationale for determining optimal peak finding parameters that may differ from those recommended by the authors of a peak finding algorithm. Moreover, the application of another data analysis tool (for example, an application for peak splitting) was useful in further improving the resulting peakset. This suggests that integration of multiple methods for generating peaksets from ChIP-seq data could be a useful approach for obtaining optimal results.

4.3 H3K4me3 is not a definitive marker of active gene transcription in *A. niger*

H3K4me3 has been reported to correlate positively with actively transcribed genes. To examine the relationship between gene expression and presence of H3K4me3 in *A. niger*, I integrated the results from the ChIP-seq experiment with RNA-seq data generated using the

same growth conditions. The results obtained in the current study are only somewhat similar to reports of patterns and distribution of H3K4me3 for other species. One study in rice (*Oryza sativa*) reported that H3K4me3 modified 61.4% of all non-transposable element genes and 82.6% of all transcribed genes (He et al. 2010). In mouse, H3K4me3 mapped to 68% and 74% of genes in cerebrum and testis tissues, respectively, and 15% of actively transcribed genes lacked H3K4me3 (Cui et al. 2012). A recent report of H3K4me3 in CD4+ regulatory T cells reported the presence of this histone modification in 76% of all genes (He et al. 2014). In yeast the presence of H3K4me3 is associated with as many as 87% of all genes (Guillemette et al. 2011) and at most +1 nucleosome sites (occuring at gene transcription start sites in the yeast genome; Weiner et al. 2012). Notably, there is mounting evidence that H3K4me3 is also associated with transcriptional repression by promoting antisense transcription (van Dijk et al. 2011; Weiner et al. 2012; Margaritis et al. 2013). The complex picture of H3K4me3 in the yeast genome is an active area of ongoing investigation

Other studies have integrated genome-wide expression data and shown a positive correlation of H3K4me3 with increase in gene activity in response to changes in experimental treatments. In rice, in response to dehydration stress 89.3% of genes that are up-regulated also have increased levels of H3K4me3 and 90.6% of the down-regulated genes have lower levels of H3K4me3 (Zong et al. 2013). These results were similar to those from a dehydration stress experiment performed in *Arabidopsis thaliana* (van Dijk et al. 2010). In human mammary cells undergoing epithelial-mesenchymal transition, a gain of H3K4me3 is associated with increased mRNA accumulation (Malouf et al. 2013).

I show in the present study that in *A. niger* H3K4me3 is not associated with all active gene loci. Though the majority of actively transcribed regions (5058 genes) were associated with H3K4me3, 1971 genes that are actively transcribed (28% of all actively transcribed genes) from the maltose and xylose growth RNA-seq data sets do not contain an H3K4me3 peak. In total, H3K4me3 modified regions are mapped to 42.7% of all known coding regions in the *A. niger* genome. When compared with the reports in other species, H3K4me3 appears less frequently in the genome of *A. niger*. In addition, the analysis from the current experiment shows that only 10 out of 255 genes with increased expression on either growth condition is accompanied by an increase in H3K4me3. In fact, the majority of genes differentially transcribed between growth on

maltose and growth on xylose do not contain H3K4me3 on either carbon source, as this modified histone marks only 45 of the 233 differentially regulated genes. Amongst the differentially regulated genes not marked by H3K4me3 during growth on maltose or xylose, there were some highly expressed genes. These included the glucoamylase gene, known to be strongly repressed during growth on xylose and strongly induced during growth on maltose (Barton et al. 1972).

The analysis of transcription on maltose or xylose growth in relation to H3K4me3 resulted in other notable observations. Though nearly a third of all actively transcribed genes do not contain H3K4me3, there is nonetheless an apparent relationship between the presence of the H3K4me3 modification and genes with higher levels of transcription in *A. niger*. Although the threshold values differ, this pattern is conserved in classes of genes with different functional properties. For example, mean transcript levels for the central metabolic genes containing H3K4me3 (202±217) are much higher than for fungal transcription factors containing H3K4me3 (29.2±34.5). I examined the presence of H3K4me3 at ribosomal genes and aminoacyl tRNA synthetases, classes of genes that are predicted to be highly and constitutively expressed. Nearly all of these loci contained the H3K4me3 modification. These results indicate that although H3K4me3 does not appear to be required for transcription of nearly a third of the genome, there may be a role for H3K4me3 for highly expressed genes, including constitutively transcribed genes.

Interestingly, there are some regions (23 in total) that exhibit differential levels of H3K4me3 between maltose and xylose growth, but are not differentially transcribed. The reason for these differential levels of H3K4me3, or the possible significance of the proteins coded at these loci, is not clear. Another exception is the presence of H3K4me3 at 57 gene loci that are not actively transcribed on either growth condition. There are reports of similar occurrences in the literature from other species. One explanation is the suggestion that H3K4me3 can mark genes "poised" for transcription (Black et al. 2012). Another reason could be that H3K4me3 is acting in combination with other epigenetic modifications: studies in pluripotent cells have reported that activating marks can occur alongside a repressive mark, such as H3K27me3, in what are termed "bivalent promoters" (Bernstein et al. 2006; Azuara et al. 2006). Expression of genes with bivalent promoters can be repressed despite the presence of the activating H3K4me3 mark. Yet another possibility is that gene expression is silenced by way of H3K4me3 promotion

of anti-sense transcription, a phenomenon that has been observed in yeast (Margaritis et al. 2012). H3K4me3 has also been shown to be involved in a type of epigenetic "memory" of recent transcriptional activity, transmittable through generations in yeast from mother to daughter cells (Ng et al. 2003; Muramoto et al. 2010) and could explain the presence of this histone modification at silent genes. Given that a significant number of genes undergoing active expression do not contain any H3K4me3, these scenarios are difficult to predict. The results I obtained in this study suggest that the epigenome of *A. niger* requires further exploration to better understand the role of H3K4me3 in *A. niger* gene expression.

Taken together, the comparisons made with reports from other species suggest that there are differences in the function and distribution of H3K4me3 in the *A. niger* genome. In particular, the data suggest that H3K4me3 does not function as a characteristic transcription activating marker, as demonstrated in other species. To further examine a possible cause for these differences, I mined the *A. niger* genome for proteins that make up this protein complex responsible for tri-methylation of lysine 4 on histone H3 (Set1/COMPASS). The sequences used for comparison were obtained from well-characterized genes that make up this complex in the yeast *S. cerevisiae*. The *A. niger* genome contains proteins with sequence similarity to six of the seven Set1/COMPASS complex subunits, but I was not able to locate an ortholog for the Shg1 gene. Although this subunit is not apparently essential for H3K4me3 deposition, Shg1 may influence efficiency or accuracy of K4 trimethylation (Krogan et al. 2002; Nagy et al. 2002; Mersman et al. 2012). The possible effects of the lack of a Shg1 ortholog in *A. niger* should be further examined.

4.4 Non-random distribution of H3K4me3 in the chromosome

H3K4me3 density increases at the pericentromeric region, where nearly every gene model contains an H3K4me3 peak. The opposite is seen in the regions preceding the telomeres, and this occurs independently of gene density or GC content. As well, H3K4me3 is not evenly distributed over the lengths of the chromosome arms. An interesting observation that requires further investigation is the appearance of many differentially expressed genes in intervals where H3K4me3 is largely depleted both on maltose and xylose. Patterns in chromosomal distribution are not yet well understood, although some models have been hypothesized. For example, the "genome compartmentalization" theory (Naumova and Dekker, 2010) proposes that the local

state of chromatin, including patterns of histone modifications along the chromosome, can be integrated with three-dimensional chromatin folding and spatial co-localization of other factors to gain a full understanding of genome regulation. The uneven distribution of H3K4me3 in *A. niger* chromosomes, sometimes over long intervals of the genome in gene-dense regions and in regions proximal to the telomeres and centormeres, raises the possibility that regions in chromosomes in *A. niger* are compartmentalized. This result could provide an interesting avenue for investigating the role of higher order chromatin structures in *A. niger* gene expression.

4.5 H3K4me3 supports the annotation of genomic features

The H3K4me3 map of *A. niger* chromosomes also reveals that this histone modification is completely absent in the centromere region. The lack of H3K4me3 peaks observed in centromeric regions, typically associated with heterochromatin, is consistent with findings by Smith et al. (2011), which demonstrated a lack of H3K4 di- and tri-methylation in centromere regions of the filamentous fungus *N. crassa*. In *N. crassa*, canonical H3 is replaced by a centromere-specific histone variant, CenH3. Although centromeric regions are typically associated with heterochromatin, other euchromatic markers generally associated with transcriptionally active genes have been found in human centromeres (Lam et al. 2006; Sullivan et al. 2004). Euchromatic modifications, including H3K4me3, are not seen in the *N. crassa* centromeres. This raises the possibility that similar to *N. crassa*, the *A. niger* centromere boundaries occur where an abrupt discontinuation of H3K4me3 peaks is observed, and thereby marking the precise location of the *A. niger* centromeres.

A number of H3K4me3 peaks do not intersect with a predicted gene model, but may mark a previously unrecognized coding region or other genomic features. Indeed, during a recent manual curation of the newly assembled NRRL3 *A. niger* genome, the H3K4me3 ChIP-seq data is useful in supporting the presence of gene models (data unpublished). A similar approach was recently used in improving the rice genome (Du et al. 2013). As shown in the current experiment, in rare instances H3K4me3 marks regions where coding gene models cannot be predicted but where there is transcript coverage. This observation suggests that H3K4me3 could be a marker for regions of non-coding RNA. Several studies have demonstrated the co-localization of histone modifications, including H3K4me3, with non-coding RNA. These observations, combined with the availability of RNA sequencing data, have facilitated the

annotation of non-coding RNA species in the genome (Marchese and Huarte, 2013). An analysis of the location of peak summits of H3K4me3 regions have been useful in annotating transcription start sites in a number of organisms, including mouse (Mikkelsen et al. 2007), *Arabidopsis* (van Dijk et al. 2010), and *Rhesus macaque* (Liu et al. 2011). Precise locations of transcription start sites in *A. niger* have not been widely identified in the genome, although a number of highly transcribed and well-assembled full-length transcripts are available from several expression data sets. This relationship is currently being investigated.

Section 5: Conclusion

In the present study, I have generated a map of H3K4me3 distribution in a high-quality assembly of the *Aspergillus niger* genome. H3K4me3 marks genes undergoing active transcription, but a significant number of expressed genes do not contain H3K4me3. These include the majority of genes that are differentially expressed between growth on maltose and xylose. Overall, distribution of H3K4me3 is non-random along the length of the chromosome, with high levels at pericentromeric regions and low levels near the telomeres. The results presented here also highlight the considerations involved in ChIP-seq data analysis and the importance of relating epigenetic information with gene expression data. The integration of transcriptome and epigenome data can reveal novel trends and targets for further investigation.

References

Allis, C. D., & Muir, T. W. (2011). Spreading chromatin into chemical biology. *Chembiochem : A European Journal of Chemical Biology*, *12*, 264–279. doi:10.1002/cbic.201000761

Alon, U. (2009). How To Choose a Good Scientific Problem. *Molecular Cell*, *35*(6), 726–728.

Ameyar-Zazoua, M., Rachez, C., Souidi, M., Robin, P., Fritsch, L., Young, R., … Harel-Bellan, A. (2012). Argonaute proteins couple chromatin silencing to alternative splicing. *Nature Structural & Molecular Biology*. doi:10.1038/nsmb.2373

Anders, S., & Huber, W. (2010). Differential expression analysis for sequence count data. *Genome Biology*, *11*, R106. doi:10.1186/gb-2010-11-10-r106

Andreyev, A. Y., Shen, Z., Guan, Z., Ryan, A., Fahy, E., Subramaniam, S., … Dennis, E. A. (2010). Application of proteomic marker ensembles to subcellular organelle identification. *Molecular & Cellular Proteomics : MCP*, *9*, 388–402. doi:10.1074/mcp.M900432-MCP200

Archer, D., & Turner, G. (2006). Genomics of protein secretion and hyphal growth in Aspergillus. In A. J. P. Brown (Ed.), *The Mycota XIII* (pp. 75–96). Springer, Berlin Heidelberg.

Azuara, V., Perry, P., Sauer, S., Spivakov, M., Jørgensen, H. F., John, R. M., … Fisher, A. G. (2006). Chromatin signatures of pluripotent cell lines. *Nature Cell Biology*, *8*, 532–538. doi:10.1038/ncb1403

Baker, S. E. (2006). Aspergillus niger genomics: past, present and into the future. *Medical Mycology*, *44*, S17–21. doi:10.1080/13693780600921037

Bannister, A. J., & Kouzarides, T. (2011). Regulation of chromatin by histone modifications. *Cell Research*, *21*, 381–395. doi:10.1038/cr.2011.22

Barski, A., Cuddapah, S., Cui, K., Roh, T. Y., Schones, D. E., Wang, Z., … Zhao, K. (2007). High-Resolution Profiling of Histone Methylations in the Human Genome. *Cell*, *129*, 823–837. doi:10.1016/j.cell.2007.05.009

Barton, L. L., Georgi, C. E., & Lineback, D. R. (1972). Effect of maltose on glucoamylase formation by Aspergillus niger. *Journal of Bacteriology*, *111*, 771–777.

Batta, K., Zhang, Z., Yen, K., Goffman, D. B., & Pugh, B. F. (2011). Genome-wide function of H2B ubiquitylation in promoter and genic regions. *Genes & Development*. doi:10.1101/gad.177238.111

Bauer, D. F. (1972). Constructing Confidence Sets Using Rank Statistics. *Journal of the American Statistical Association*, *67*, 687–690. doi:10.2307/2284469

Bernstein, B. E., Humphrey, E. L., Erlich, R. L., Schneider, R., Bouman, P., Liu, J. S., … Schreiber, S. L. (2002). Methylation of histone H3 Lys 4 in coding regions of active genes. *Proceedings of the National Academy of Sciences of the United States of America*, *99*, 8695–8700. doi:10.1073/pnas.082249499

Bernstein, B. E., Kamal, M., Lindblad-Toh, K., Bekiranov, S., Bailey, D. K., Huebert, D. J., … Lander, E. S. (2005). Genomic maps and comparative analysis of histone modifications in human and mouse. *Cell*, *120*, 169–181. doi:10.1016/j.cell.2005.01.001

Bernstein, B. E., Mikkelsen, T. S., Xie, X., Kamal, M., Huebert, D. J., Cuff, J., … Lander, E. S. (2006). A Bivalent Chromatin Structure Marks Key Developmental Genes in Embryonic Stem Cells. *Cell*, *125*, 315–326. doi:10.1016/j.cell.2006.02.041

Biology, S. (1978). *Progress in Molecular and Subcellular Biology*. (F. E. Hahn, H. Kersten, W. Kersten, & W. Szybalski, Eds.) (Vol. 6). Berlin, Heidelberg: Springer Berlin Heidelberg. doi:10.1007/978-3-642-66856-2

Black, J. C., Van Rechem, C., & Whetstine, J. R. (2012). Histone Lysine Methylation Dynamics: Establishment, Regulation, and Biological Impact. *Molecular Cell*. doi:10.1016/j.molcel.2012.11.006

Boa, S., Coert, C., & Patterton, H.-G. (2003). Saccharomyces cerevisiae Set1p is a methyltransferase specific for lysine 4 of histone H3 and is required for efficient gene expression. *Yeast (Chichester, England)*, *20*(9), 827–35. doi:10.1002/yea.995

Bohle, K., Jungebloud, a, Göcke, Y., Dalpiaz, a, Cordes, C., Horn, H., & Hempel, D. C. (2007). Selection of reference genes for normalisation of specific gene quantification data of Aspergillus niger. *Journal of Biotechnology*, *132*(4), 353–8. doi:10.1016/j.jbiotec.2007.08.005

Bonnet-Garnier, A., Feuerstein, P., Chebrout, M., Fleurot, R., Jan, H.-U., Debey, P., & Beaujean, N. (2012). Genome organization and epigenetic marks in mouse germinal vesicle oocytes. *The International Journal of Developmental Biology*, *56*(10-12), 877–87. doi:10.1387/ijdb.120149ab

Borun, T. W., Pearson, D., & Paik, W. K. (1972). Studies of histone methylation during the HeLa S-3 cell cycle. *The Journal of Biological Chemistry*, *247*(13), 4288–98. Retrieved from http://www.ncbi.nlm.nih.gov/pubmed/5035694

Boyer, L. A., Mathur, D., & Jaenisch, R. (2006). Molecular control of pluripotency. *Current Opinion in Genetics and Development*. doi:10.1016/j.gde.2006.08.009

Celniker, S. E., Dillon, L. A. L., Gerstein, M. B., Gunsalus, K. C., Henikoff, S., Karpen, G. H., … Waterston, R. H. (2009). Unlocking the secrets of the genome. *Nature*, *459*, 927–930. doi:10.1038/459927a

Chen, X., Xu, H., Yuan, P., Fang, F., Huss, M., Vega, V. B., … Ng, H. H. (2008). Integration of External Signaling Pathways with the Core Transcriptional Network in Embryonic Stem Cells. *Cell*, *133*, 1106–1117. doi:10.1016/j.cell.2008.04.043

Chen, X., & Zhou, D. X. (2013). Rice epigenomics and epigenetics: Challenges and opportunities. *Current Opinion in Plant Biology*. doi:10.1016/j.pbi.2013.03.004

Christensen, J., Agger, K., Cloos, P. A. C., Pasini, D., Rose, S., Sennels, L., … Helin, K. (2007). RBP2 Belongs to a Family of Demethylases, Specific for Tri-and Dimethylated Lysine 4 on Histone 3. *Cell*, *128*, 1063–1076. doi:10.1016/j.cell.2007.02.003

Cirillo, L. A., Lin, F. R., Cuesta, I., Friedman, D., Jarnik, M., & Zaret, K. S. (2002). Opening of compacted chromatin by early developmental transcription factors HNF3 (FoxA) and GATA-4. *Molecular Cell*, *9*, 279–289. doi:10.1016/S1097-2765(02)00459-8

Cui, P., Liu, W., Zhao, Y., Lin, Q., Ding, F., Xin, C., … Yu, J. (2012). The association between H3K4me3 and antisense transcription. *Genomics, Proteomics & Bioinformatics*, *10*(2), 74–81. doi:10.1016/j.gpb.2012.05.001

Cui, P., Liu, W., Zhao, Y., Lin, Q., Zhang, D., Ding, F., … Hu, S. (2012). Comparative Analyses of H3K4 and H3K27 Trimethylations Between the Mouse Cerebrum and Testis. *Genomics, Proteomics and Bioinformatics*, *10*, 82–93. doi:10.1016/j.gpb.2012.05.007

Culleton, H., McKie, V., & de Vries, R. P. (2013). Physiological and molecular aspects of degradation of plant polysaccharides by fungi: What have we learned from Aspergillus? *Biotechnology Journal*, *8*, 884–94. doi:10.1002/biot.201200382

Cumming, G., Fidler, F., & Vaux, D. L. (2007). Error bars in experimental biology. *The Journal of Cell Biology*, *177*(1), 7–11.

Das, P. M., Ramachandran, K., vanWert, J., & Singal, R. (2004). Chromatin immunoprecipitation assay. *BioTechniques*, *37*, 961–969.

De Oliveira, J. M. P. F., van Passel, M. W. J., Schaap, P. J., & de Graaff, L. H. (2011). Proteomic analysis of the secretory response of Aspergillus niger to D-maltose and D-xylose. *PloS One*, *6*, e20865. doi:10.1371/journal.pone.0020865

De Vries, R. P., & Visser, J. (2001). Aspergillus Enzymes Involved in Degradation of Plant Cell Wall Polysaccharides. *Microbiology and Molecular Biology Reviews*, *65*, 497–522. doi:10.1128/MMBR.65.4.497-522.2001

Dehé, P.-M., Dichtl, B., Schaft, D., Roguev, A., Pamblanco, M., Lebrun, R., … Géli, V. (2006). Protein interactions within the Set1 complex and their roles in the regulation of histone 3 lysine 4 methylation. *The Journal of Biological Chemistry*, *281*(46), 35404–12. doi:10.1074/jbc.M603099200

Dekker, J., Rippe, K., Dekker, M., & Kleckner, N. (2002). Capturing chromosome conformation. *Science (New York, N.Y.)*, *295*, 1306–1311. doi:10.1126/science.1067799

Deng, W., & Blobel, G. A. (2010). Do chromatin loops provide epigenetic gene expression states? *Current Opinion in Genetics and Development*. doi:10.1016/j.gde.2010.06.007

Du, Z., Li, H., Wei, Q., Zhao, X., Wang, C., Zhu, Q., … Su, Z. (2013). Genome-wide analysis of histone modifications: H3K4me2, H3K4me3, H3K9ac, and H3K27ac in Oryza sativa L. Japonica. *Molecular Plant*, *6*, 1463–72. doi:10.1093/mp/sst018

Ebringerova, A., & Heinze, T. (2000). Xylan and xylan derivatives - biopolymers with valuable properties, 1 - Naturally occurring xylans structures, procedures and properties. *Macromolecular Rapid Communications*, *21*, 542–556. doi:10.1002/1521-3927(20000601)21:9<542::aid-marc542>3.3.co;2-z

Eissenberg, J. C., & Shilatifard, A. (2010). Histone H3 lysine 4 (H3K4) methylation in development and differentiation. *Developmental Biology*. doi:10.1016/j.ydbio.2009.08.017

Fischle, W. (2012). One, two, three: how histone methylation is read. *Epigenomics*, *4*, 641–653. doi:10.2217/epi.12.56

Flipphi, M., Sun, J., Robellet, X., Karaffa, L., Fekete, E., Zeng, A. P., & Kubiecek, C. P. (2009). Biodiversity and evolution of primary carbon metabolism in Aspergillus nidulans and other Aspergillus spp. *Fungal Genetics and Biology : FG & B*, *46 Suppl 1*. doi:10.1016/j.fgb.2008.07.018

Fuchs, J., Demidov, D., Houben, A., & Schubert, I. (2006). Chromosomal histone modification patterns--from conservation to diversity. *Trends in Plant Science*, *11*, 199–208. doi:10.1016/j.tplants.2006.02.008

Fuda, N. J., Ardehali, M. B., & Lis, J. T. (2009). Defining mechanisms that regulate RNA polymerase II transcription in vivo. *Nature*, *461*, 186–192. doi:10.1038/nature08449

Gacek, A., & Strauss, J. (2012). The chromatin code of fungal secondary metabolite gene clusters. *Applied Microbiology and Biotechnology*. doi:10.1007/s00253-012-4208-8

Galbe, M., & Zacchi, G. (2007). Pretreatment of lignocellulosic materials for efficient bioethanol production. *Advances in Biochemical Engineering/biotechnology*, *108*, 41–65. doi:10.1007/10

Gangloff, Y. G., Pointud, J. C., Thuault, S., Carré, L., Romier, C., Muratoglu, S., … Davidson, I. (2001). The TFIID components human TAF(II)140 and Drosophila BIP2 (TAF(II)155) are novel metazoan homologues of yeast TAF(II)47 containing a histone fold and a PHD finger. *Molecular and Cellular Biology*, *21*, 5109–5121. doi:10.1128/MCB.21.15.5109-5121.2001

Gardner, K. E., Allis, C. D., & Strahl, B. D. (2011). Operating on chromatin, a colorful language where context matters. *Journal of Molecular Biology*. doi:10.1016/j.jmb.2011.01.040

Gershey, E. L., Haslett, G. W., Vidali, G., & Allfrey, G. (1969). MACROMOLECULES : Chemical Studies of Histone Methylation : EVIDENCE FOR THE OCCURRENCE OF 3-METHYLHISTIDINE IN AVIAN ERYTHROCYTE HISTONE of Histone Methylation.

Greenberg, R. A. (2011). Histone tails: Directing the chromatin response to DNA damage. *FEBS Letters*. doi:10.1016/j.febslet.2011.05.037

Greer, E. L., & Shi, Y. (2012). Histone methylation: a dynamic mark in health, disease and inheritance. *Nature Reviews Genetics*, *13*(5), 343–357. doi:10.1038/nrg3173

Grigoryev, S. a, & Woodcock, C. L. (2012). Chromatin organization - the 30 nm fiber. *Experimental Cell Research*, *318*(12), 1448–55. doi:10.1016/j.yexcr.2012.02.014

Guccione, E., Martinato, F., Finocchiaro, G., Luzi, L., Tizzoni, L., Dall' Olio, V., … Amati, B. (2006). Myc-binding-site recognition in the human genome is determined by chromatin context. *Nature Cell Biology*, *8*, 764–770. doi:10.1038/ncb1434

Guillemette, B., Drogaris, P., Lin, H.-H. S., Armstrong, H., Hiragami-Hamada, K., Imhof, A., … Festenstein, R. J. (2011). H3 lysine 4 is acetylated at active gene promoters and is regulated by H3 lysine 4 methylation. *PLoS Genetics*, *7*(3), e1001354. doi:10.1371/journal.pgen.1001354

Ha, M. (2013). Understanding the chromatin remodeling code. *Plant Science : An International Journal of Experimental Plant Biology*, *211*, 137–45. doi:10.1016/j.plantsci.2013.07.006

Haring, M., Offermann, S., Danker, T., Horst, I., Peterhansel, C., & Stam, M. (2007). Chromatin immunoprecipitation: optimization, quantitative analysis and data normalization. *Plant Methods*, *3*, 11. doi:10.1186/1746-4811-3-11

Haynes, B. C., Skowyra, M. L., Spencer, S. J., Gish, S. R., Williams, M., Held, E. P., … Doering, T. L. (2011). Toward an integrated model of capsule regulation in Cryptococcus neoformans. *PLoS Pathogens*, *7*. doi:10.1371/journal.ppat.1002411

He, G., Zhu, X., Elling, A. A., Chen, L., Wang, X., Guo, L., … Deng, X.-W. (2010). Global epigenetic and transcriptional trends among two rice subspecies and their reciprocal hybrids. *The Plant Cell*, *22*, 17–33. doi:10.1105/tpc.109.072041

He, H., Ni, B., Tian, Y., Tian, Z., Chen, Y., Liu, Z., … Zhang, Y. (2014). Histone methylation mediates plasticity of human FOXP3(+) regulatory T cells by modulating signature gene expressions. *Immunology*, *141*(3), 362–76. doi:10.1111/imm.12198

Henikoff, S., & Shilatifard, A. (2011). Histone modification: cause or cog? *Trends in Genetics : TIG*, *27*(10), 389–96. doi:10.1016/j.tig.2011.06.006

Højfeldt, J. W., Agger, K., & Helin, K. (2013). Histone lysine demethylases as targets for anticancer therapy. *Nature Reviews. Drug Discovery*, *12*, 917–30. doi:10.1038/nrd4154

Hollander, M., & Wolfe, D. A. (n.d.). *Nonparametric Statistical Methods* (pp. 27–33; 68–75). New York: John Wiley & Sons.

Hondmann, D., & Visser, J. (1994). Carbon metabolism. *Prog Ind Microbiol*, *29*, 61–139.

Hong, C. I., Jolma, I. W., Loros, J. J., Dunlap, J. C., & Ruoff, P. (2008). Simulating dark expressions and interactions of frq and wc-1 in the Neurospora circadian clock. *Biophysical Journal*, *94*, 1221–1232. doi:10.1529/biophysj.107.115154

Huang, Y., Fang, J., Bedford, M. T., Zhang, Y., & Xu, R.-M. (2006). Recognition of histone H3 lysine-4 methylation by the double tudor domain of JMJD2A. *Science (New York, N.Y.)*, *312*, 748–751. doi:10.1126/science.1125162

Jacobs, D. I., Olsthoorn, M. M. A., Maillet, I., Akeroyd, M., Breestraat, S., Donkers, S., … Sagt, C. M. J. (2009). Effective lead selection for improved protein production in Aspergillus niger based on integrated genomics. *Fungal Genetics and Biology : FG & B*, *46 Suppl 1*. doi:10.1016/j.fgb.2008.08.012

Johnson, D. S., Mortazavi, A., Myers, R. M., & Wold, B. (2007). Genome-wide mapping of in vivo protein-DNA interactions. *Science (New York, N.Y.)*, *316*, 1497–1502. doi:10.1126/science.1141319

Johnson, L. M., Cao, X., & Jacobsen, S. E. (2002). Interplay between two epigenetic marks: DNA methylation and histone H3 lysine 9 methylation. *Current Biology*, *12*, 1360–1367. doi:10.1016/S0960-9822(02)00976-4

Jørgensen, T. R., Goosen, T., Hondel, C. a M. J. J. Van Den, Ram, A. F. J., & Iversen, J. J. L. (2009). Transcriptomic comparison of Aspergillus niger growing on two different sugars reveals coordinated regulation of the secretory pathway. *BMC Genomics*, *10*, 44. doi:10.1186/1471-2164-10-44

Jothi, R., Cuddapah, S., Barski, A., Cui, K., & Zhao, K. (2008). Genome-wide identification of in vivo protein-DNA binding sites from ChIP-Seq data. *Nucleic Acids Research*, *36*, 5221–5231. doi:10.1093/nar/gkn488

Karimi-Aghcheh, R., Bok, J. W., Phatale, P. a, Smith, K. M., Baker, S. E., Lichius, A., … Kubicek, C. P. (2013). Functional analyses of Trichoderma reesei LAE1 reveal conserved and contrasting roles of this regulator. *G3 (Bethesda, Md.)*, *3*(2), 369–78. doi:10.1534/g3.112.005140

Keller, A., Nesvizhskii, A. I., Kolker, E., & Aebersold, R. (2002). Empirical statistical model to estimate the accuracy of peptide identifications made by MS/MS and database search. *Analytical Chemistry*, *74*, 5383–5392. doi:10.1021/ac025747h

Kharchenko, P. V, Tolstorukov, M. Y., & Park, P. J. (2008). Design and analysis of ChIP-seq experiments for DNA-binding proteins. *Nature Biotechnology*, *26*, 1351–1359. doi:10.1038/nbt.1508

Kidder, B. L., Hu, G., & Zhao, K. (2011). ChIP-Seq: technical considerations for obtaining high-quality data. *Nature Immunology*. doi:10.1038/ni.2117

Kirmizis, A., Santos-Rosa, H., Penkett, C. J., Singer, M. A., Vermeulen, M., Mann, M., … Kouzarides, T. (2007). Arginine methylation at histone H3R2 controls deposition of H3K4 trimethylation. *Nature*, *449*(7164), 928–32. doi:10.1038/nature06160

Kouzarides, T. (2007). Chromatin Modifications and Their Function. *Cell*. doi:10.1016/j.cell.2007.02.005

Krogan, N. J., Dover, J., Khorrami, S., Greenblatt, J. F., Schneider, J., Johnston, M., & Shilatifard, A. (2002). COMPASS, a histone H3 (Lysine 4) methyltransferase required for telomeric silencing of gene expression. *The Journal of Biological Chemistry*, *277*, 10753–10755. doi:10.1074/jbc.C200023200

Laajala, T. D., Raghav, S., Tuomela, S., Lahesmaa, R., Aittokallio, T., & Elo, L. L. (2009). A practical comparison of methods for detecting transcription factor binding sites in ChIP-seq experiments. *BMC Genomics*, *10*, 618. doi:10.1186/1471-2164-10-618

Lam, A. L., Boivin, C. D., Bonney, C. F., Rudd, M. K., & Sullivan, B. A. (2006). Human centromeric chromatin is a dynamic chromosomal domain that can spread over noncentromeric DNA. *Proceedings of the National Academy of Sciences of the United States of America*, *103*, 4186–4191. doi:10.1073/pnas.0507947103

Lanctôt, C., Cheutin, T., Cremer, M., Cavalli, G., & Cremer, T. (2007). Dynamic genome architecture in the nuclear space: regulation of gene expression in three dimensions. *Nature Reviews. Genetics*, *8*, 104–115. doi:10.1038/nrg2041

Landt, S. G., Marinov, G. K., Kundaje, A., Kheradpour, P., Pauli, F., Batzoglou, S., … Snyder, M. (2012). ChIP-seq guidelines and practices of the ENCODE and modENCODE consortia. *Genome Research*. doi:10.1101/gr.136184.111

Lauberth, S. M., Nakayama, T., Wu, X., Ferris, A. L., Tang, Z., Hughes, S. H., & Roeder, R. G. (2013). H3K4me3 interactions with TAF3 regulate preinitiation complex assembly and selective gene activation. *Cell*, *152*(5), 1021–36. doi:10.1016/j.cell.2013.01.052

Li, F., Mao, G., Tong, D., Huang, J., Gu, L., Yang, W., & Li, G. M. (2013). The histone mark H3K36me3 regulates human DNA mismatch repair through its interaction with MutSα. *Cell*, *153*, 590–600. doi:10.1016/j.cell.2013.03.025

Liu, Y., Han, D., Han, Y., Yan, Z., Xie, B., Li, J., … Han, J.-D. J. (2011). Ab initio identification of transcription start sites in the Rhesus macaque genome by histone modification and RNA-Seq. *Nucleic Acids Research*, *39*, 1408–1418. doi:10.1093/nar/gkq956

Loros, J. J., & Dunlap, J. C. (1991). Neurospora crassa clock-controlled genes are regulated at the level of transcription. *Molecular and Cellular Biology*, *11*, 558–563. doi:10.1128/MCB.11.1.558.Updated

Lu, X., Sun, J., Nimtz, M., Wissing, J., Zeng, A.-P., & Rinas, U. (2010). The intra- and extracellular proteome of Aspergillus niger growing on defined medium with xylose or maltose as carbon substrate. *Microbial Cell Factories*, *9*, 23. doi:10.1186/1475-2859-9-23

Luger, K., Mäder, A. W., Richmond, R. K., Sargent, D. F., & Richmond, T. J. (1997). Crystal structure of the nucleosome core particle at 2.8 A resolution. *Nature*, *389*, 251–260. doi:10.1038/38444

Luo, C., Loros, J. J., & Dunlap, J. C. (1998). Nuclear localization is required for function of the essential clock protein FRQ. *The EMBO Journal*, *17*, 1228–1235. doi:10.1093/emboj/17.5.1228

Malouf, G. G., Taube, J. H., Lu, Y., Roysarkar, T., Panjarian, S., Estecio, M. R., … Issa, J.-P. J. (2013). Architecture of epigenetic reprogramming following Twist1-mediated epithelial-mesenchymal transition. *Genome Biology*, *14*(12), R144. doi:10.1186/gb-2013-14-12-r144

Maltby, V. E., Martin, B. J. E., Brind'Amour, J., Chruscicki, A. T., McBurney, K. L., Schulze, J. M., … Howe, L. J. (2012). Histone H3K4 demethylation is negatively regulated by histone H3 acetylation in Saccharomyces cerevisiae. *Proceedings of the National Academy of Sciences*. doi:10.1073/pnas.1202070109

Marchese, F. P., & Huarte, M. (2013). Long non-coding RNAs and chromatin modifiers: Their place in the epigenetic code. *Epigenetics : Official Journal of the DNA Methylation Society*, *9*, 21–26. doi:10.4161/epi.27472

Margaritis, T., Oreal, V., Brabers, N., Maestroni, L., Vitaliano-Prunier, A., Benschop, J. J., … Holstege, F. C. P. (2012). Two distinct repressive mechanisms for histone 3 lysine 4 methylation through promoting 3'-end antisense transcription. *PLoS Genetics*, *8*(9), e1002952. doi:10.1371/journal.pgen.1002952

Mersman, D. P., Du, H.-N., Fingerman, I. M., South, P. F., & Briggs, S. D. (2012). Charge-based Interaction Conserved within Histone H3 Lysine 4 (H3K4) Methyltransferase Complexes Is Needed for Protein Stability, Histone Methylation, and Gene Expression. *Journal of Biological Chemistry*. doi:10.1074/jbc.M111.280867

Metzker, M. L. (2010). Sequencing technologies - the next generation. *Nature Reviews. Genetics*, *11*(1), 31–46.

Micsinai, M., Parisi, F., Strino, F., Asp, P., Dynlacht, B. D., & Kluger, Y. (2012). Picking ChIP-seq peak detectors for analyzing chromatin modification experiments. *Nucleic Acids Research*, *40*, e70. doi:10.1093/nar/gks048

Mikkelsen, T. S., Ku, M., Jaffe, D. B., Issac, B., Lieberman, E., Giannoukos, G., … Bernstein, B. E. (2007). Genome-wide maps of chromatin state in pluripotent and lineage-committed cells. *Nature*, *448*, 553–560. doi:10.1038/nature06008

Miller, T., Krogan, N. J., Dover, J., Erdjument-Bromage, H., Tempst, P., Johnston, M., … Shilatifard, A. (2001). COMPASS: a complex of proteins associated with a trithorax-related SET domain protein. *Proceedings of the National Academy of Sciences of the United States of America*, *98*, 12902–12907. doi:10.1073/pnas.231473398

Mootha, V. K., Bunkenborg, J., Olsen, J. V., Hjerrild, M., Wisniewski, J. R., Stahl, E., … Mann, M. (2003). Integrated Analysis of Protein Composition, Tissue Diversity, and Gene Regulation in Mouse Mitochondria. *Cell*, *115*, 629–640. doi:10.1016/S0092-8674(03)00926-7

Morillon, A., Karabetsou, N., Nair, A., & Mellor, J. (2005). Dynamic lysine methylation on histone H3 defines the regulatory phase of gene transcription. *Molecular Cell*, *18*(6), 723–34. doi:10.1016/j.molcel.2005.05.009

Muramoto, T., Müller, I., Thomas, G., Melvin, A., & Chubb, J. R. (2010). Methylation of H3K4 Is Required for Inheritance of Active Transcriptional States. *Current Biology*, *20*, 397–406. doi:10.1016/j.cub.2010.01.017

Nagy, P. L., Griesenbeck, J., Kornberg, R. D., & Cleary, M. L. (2002). A trithorax-group complex purified from Saccharomyces cerevisiae is required for methylation of histone H3. *Proceedings of the National Academy of Sciences of the United States of America*, *99*, 90–94. doi:10.1073/pnas.221596698

Naumova, N., & Dekker, J. (2010). Integrating one-dimensional and three-dimensional maps of genomes. *Journal of Cell Science*, *123*, 1979–1988. doi:10.1242/jcs.051631

Nesvizhskii, A. I., Keller, A., Kolker, E., & Aebersold, R. (2003). A statistical model for identifying proteins by tandem mass spectrometry. *Analytical Chemistry*, *75*, 4646–4658. doi:10.1021/ac0341261

Ng, H. H., Robert, F., Young, R. a, & Struhl, K. (2003). Targeted recruitment of Set1 histone methylase by elongating Pol II provides a localized mark and memory of recent transcriptional activity. *Molecular Cell*, *11*(3), 709–19. Retrieved from http://www.ncbi.nlm.nih.gov/pubmed/12667453

Ng, R. K., & Gurdon, J. B. (2008). Epigenetic inheritance of cell differentiation status. *Cell Cycle (Georgetown, Tex.)*, *7*, 1173–1177. doi:10.4161/cc.7.9.5791

Novozymes. (2008). *The Novozymes Report 2007*.

Park, P. J. (2009). ChIP-seq: advantages and challenges of a maturing technology. *Nature Reviews. Genetics*, *10*, 669–680. doi:10.1038/nrg2641

Pedersen, M. T., & Helin, K. (2010). Histone demethylases in development and disease. *Trends in Cell Biology*. doi:10.1016/j.tcb.2010.08.011

Pel, H. J., de Winde, J. H., Archer, D. B., Dyer, P. S., Hofmann, G., Schaap, P. J., … Stam, H. (2007). Genome sequencing and analysis of the versatile cell factory Aspergillus niger CBS 513.88. *Nature Biotechnology*, *25*, 221–231. doi:10.1038/nbt1282

Pepke, S., Wold, B., & Mortazavi, A. (2009). Computation for ChIP-seq and RNA-seq studies. *Nature Methods*, *6*, S22–S32. doi:10.1038/nmeth.1371

Petersen, K. L., Lehmbeck, J., & Christensen, T. (1999). A new transcriptional activator for amylase genes in Aspergillus. *Molecular & General Genetics : MGG*, *262*, 668–676.

Pokholok, D. K., Harbison, C. T., Levine, S., Cole, M., Hannett, N. M., Tong, I. L., … Young, R. A. (2005). Genome-wide map of nucleosome acetylation and methylation in yeast. *Cell*, *122*, 517–527. doi:10.1016/j.cell.2005.06.026

Pradeepa, M. M., Sutherland, H. G., Ule, J., Grimes, G. R., & Bickmore, W. a. (2012). Psip1/Ledgf p52 binds methylated histone H3K36 and splicing factors and contributes to the regulation of alternative splicing. *PLoS Genetics*, *8*(5), e1002717. doi:10.1371/journal.pgen.1002717

Punt, P. J., Van Biezen, N., Conesa, A., Albers, A., Mangnus, J., & Van Den Hondel, C. (2002). Filamentous fungi as cell factories for heterologous protein production. *Trends in Biotechnology*. doi:10.1016/S0167-7799(02)01933-9

Quinlan, A. R., & Hall, I. M. (2010). BEDTools: a flexible suite of utilities for comparing genomic features. *Bioinformatics (Oxford, England)*, *26*, 841–842. doi:10.1093/bioinformatics/btq033

R Development Core Team, R. (2011). R: A Language and Environment for Statistical Computing. (R. D. C. Team, Ed.)*R Foundation for Statistical Computing*. R Foundation for Statistical Computing. doi:10.1007/978-3-540-74686-7

Reyes-Dominguez, Y., Bok, J. W., Berger, H., Shwab, E. K., Basheer, A., Gallmetzer, A., … Strauss, J. (2010). Heterochromatic marks are associated with the repression of secondary metabolism clusters in Aspergillus nidulans. *Molecular Microbiology*, *76*, 1376–1386. doi:10.1111/j.1365-2958.2010.07051.x

Richmond, R. K., Sargent, D. F., Richmond, T. J., Luger, K., & Ma, A. W. (1997). Crystal structure of the nucleosome ˚ resolution core particle at 2 . 8 A, *7*, 251–260.

Robertson, G., Hirst, M., Bainbridge, M., Bilenky, M., Zhao, Y., Zeng, T., … Jones, S. (2007). Genome-wide profiles of STAT1 DNA association using chromatin immunoprecipitation and massively parallel sequencing. *Nature Methods*, *4*, 651–657. doi:10.1038/nmeth1068

Robinson, M. D., McCarthy, D. J., & Smyth, G. K. (2010). edgeR: a Bioconductor package for differential expression analysis of digital gene expression data. *Bioinformatics (Oxford, England)*, *26*, 139–140. doi:10.1093/bioinformatics/btp616

Rozowsky, J., Euskirchen, G., Auerbach, R. K., Zhang, Z. D., Gibson, T., Bjornson, R., … Gerstein, M. B. (2009). PeakSeq enables systematic scoring of ChIP-seq experiments relative to controls. *Nature Biotechnology*, *27*, 66–75. doi:10.1038/nbt.1518

Ruijter, G. J. ., Kubicek, C. P., & Visser, J. (2002). *Production of organic acids by fungi. in The Mycota X Industrial Applications (ed. Osiewacz, H.D.)* (pp. 213–230). Springer Berlin Heidelberg.

Saleh, A., Alvarez-Venegas, R., & Avramova, Z. (2008). An efficient chromatin immunoprecipitation (ChIP) protocol for studying histone modifications in Arabidopsis plants. *Nature Protocols*, *3*, 1018–1025. doi:10.1038/nprot.2008.66

Salmon-Divon, M., Dvinge, H., Tammoja, K., & Bertone, P. (2010). PeakAnalyzer: genome-wide annotation of chromatin binding and modification loci. *BMC Bioinformatics*, *11*, 415. doi:10.1186/1471-2105-11-415

Santos-Rosa, H., Schneider, R., Bannister, A. J., Sherriff, J., Bernstein, B. E., Emre, N. C. T., … Kouzarides, T. (2002). Active genes are tri-methylated at K4 of histone H3. *Nature*, *419*, 407–411. doi:10.1038/nature01080

Scharf, A. N. D., & Imhof, A. (2011). Every methyl counts--epigenetic calculus. *FEBS Letters*, *585*, 2001–2007. doi:10.1016/j.febslet.2010.11.029

Schneider, R., Bannister, A. J., Myers, F. A., Thorne, A. W., Crane-Robinson, C., & Kouzarides, T. (2004). Histone H3 lysine 4 methylation patterns in higher eukaryotic genes. *Nature Cell Biology*, *6*, 73–77. doi:10.1038/ncb1076

Seiboth, B., Karimi, R. A., Phatale, P. a, Linke, R., Hartl, L., Sauer, D. G., … Kubicek, C. P. (2012). The putative protein methyltransferase LAE1 controls cellulase gene expression in Trichoderma reesei. *Molecular Microbiology*, *84*, 1150–64. doi:10.1111/j.1365-2958.2012.08083.x

Sérandour, A. A., Avner, S., Percevault, F., Demay, F., Bizot, M., Lucchetti-Miganeh, C., … Eeckhoute, J. (2011). Epigenetic switch involved in activation of pioneer factor FOXA1-dependent enhancers. *Genome Research*, *21*, 555–565. doi:10.1101/gr.111534.110

Shi, Y., Lan, F., Matson, C., Mulligan, P., Whetstine, J. R., Cole, P. A., … Shi, Y. (2004). Histone demethylation mediated by the nuclear amine oxidase homolog LSD1. *Cell*, *119*, 941–953. doi:10.1016/j.cell.2004.12.012

Sims, R. J., Nishioka, K., & Reinberg, D. (2003). Histone lysine methylation: A signature for chromatin function. *Trends in Genetics*, *19*, 629–639. doi:10.1016/j.tig.2003.09.007

Sims, R. J., & Reinberg, D. (2006). Histone H3 Lys 4 methylation: caught in a bind? *Genes & Development*, *20*, 2779–2786. doi:10.1101/gad.1468206

Smith, E., & Shilatifard, A. (2010). The Chromatin Signaling Pathway: Diverse Mechanisms of Recruitment of Histone-Modifying Enzymes and Varied Biological Outcomes. *Molecular Cell*. doi:10.1016/j.molcel.2010.11.031

Smith, K. M., Phatale, P. A., Sullivan, C. M., Pomraning, K. R., & Freitag, M. (2011). Heterochromatin is required for normal distribution of Neurospora crassa CenH3. *Molecular and Cellular Biology*, *31*, 2528–2542. doi:10.1128/MCB.01285-10

Stark, R., & Brown, G. (2011). DiffBind: differential binding analysis of ChIP-Seq peak data. R Foundation for Statistical Computing. Retrieved from http://bioconductor.org/packages/release/bioc/vignettes/DiffBind/inst/doc/DiffBind.pdf

Strahl, B. D., & Allis, C. D. (2000). The language of covalent histone modifications. *Nature*, *403*, 41–45. doi:10.1038/47412

Strahl, B. D., Ohba, R., Cook, R. G., & Allis, C. D. (1999). Methylation of histone H3 at lysine 4 is highly conserved and correlates with transcriptionally active nuclei in Tetrahymena. *Proceedings of the National Academy of Sciences of the United States of America*, *96*, 14967–14972. doi:10.1073/pnas.96.26.14967

Sullivan, B. A., & Karpen, G. H. (2004). Centromeric chromatin exhibits a histone modification pattern that is distinct from both euchromatin and heterochromatin. *Nature Structural & Molecular Biology*, *11*, 1076–1083. doi:10.1038/nsmb845

Tamaru, H., & Selker, E. U. (2001). A histone H3 methyltransferase controls DNA methylation in Neurospora crassa. *Nature*, *414*, 277–283. doi:10.1038/35104508

Tang, J., Cho, N. W., Cui, G., Manion, E. M., Shanbhag, N. M., Botuyan, M. V., … Greenberg, R. a. (2013). Acetylation limits 53BP1 association with damaged chromatin to promote homologous recombination. *Nature Structural & Molecular Biology*, *20*, 317–25. doi:10.1038/nsmb.2499

Taverna, S. D., Li, H., Ruthenburg, A. J., Allis, C. D., & Patel, D. J. (2007). How chromatin-binding modules interpret histone modifications: lessons from professional pocket pickers. *Nature Structural & Molecular Biology*, *14*, 1025–1040. doi:10.1038/nsmb1338

Taylor, S. W., Fahy, E., Zhang, B., Glenn, G. M., Warnock, D. E., Wiley, S., … Ghosh, S. S. (2003). Characterization of the human heart mitochondrial proteome. *Nature Biotechnology*, *21*, 281–286. doi:10.1038/nbt793

The ENCODE Project Consortium 2004. (ENCyclopedia Of DNA Elements). (2004). *Science (New York, N.Y.)*, *306*, 636–640.

The ENCODE Project Consortium 2011. A user's guide to the encyclopedia of DNA elements (ENCODE). (n.d.). *PLoS Biology*, *9*(e1001046).

Thornton, J. L., Westfield, G. H., Takahashi, Y.-H., Cook, M., Gao, X., Woodfin, A. R., … Shilatifard, A. (2014). Context dependency of Set1/COMPASS-mediated histone H3 Lys4 trimethylation. *Genes & Development*, *28*(2), 115–20. doi:10.1101/gad.232215.113

Thurtle, D. M., & Rine, J. (2014). The molecular topography of silenced chromatin in Saccharomyces cerevisiae. *Genes & Development*, *28*, 245–258. doi:10.1101/gad.230532.113

Trewick, S. C., McLaughlin, P. J., & Allshire, R. C. (2005). Methylation: lost in hydroxylation? *EMBO Reports*, *6*, 315–320. doi:10.1038/sj.embor.7400379

Tu, S., Teng, Y.-C., Yuan, C., Wu, Y.-T., Chan, M.-Y., Cheng, A.-N., … Tsai, M.-D. (2008). The ARID domain of the H3K4 demethylase RBP2 binds to a DNA CCGCCC motif. *Nature Structural & Molecular Biology*, *15*, 419–421. doi:10.1038/nsmb.1400

Valouev, A., Johnson, D. S., Sundquist, A., Medina, C., Anton, E., Batzoglou, S., … Sidow, A. (2008). Genome-wide analysis of transcription factor binding sites based on ChIP-Seq data. *Nature Methods*, *5*, 829–834. doi:10.1038/nmeth.1246

Van Dijk, E. L., Chen, C. L., d'Aubenton-Carafa, Y., Gourvennec, S., Kwapisz, M., Roche, V., … Morillon, A. (2011). XUTs are a class of Xrn1-sensitive antisense regulatory non-coding RNA in yeast. *Nature*, *475*, 114–117. doi:10.1038/nature10118

Van Dijk, K., Ding, Y., Malkaram, S., Riethoven, J.-J. M., Liu, R., Yang, J., … Fromm, M. (2010). Dynamic changes in genome-wide histone H3 lysine 4 methylation patterns in response to dehydration stress in Arabidopsis thaliana. *BMC Plant Biology*, *10*, 238. doi:10.1186/1471-2229-10-238

Vermeulen, M., Mulder, K. W., Denissov, S., Pijnappel, W. W. M. P., van Schaik, F. M. A., Varier, R. A., … Timmers, H. T. M. (2007). Selective Anchoring of TFIID to Nucleosomes by Trimethylation of Histone H3 Lysine 4. *Cell*, *131*, 58–69. doi:10.1016/j.cell.2007.08.016

Vermeulen, M., & Timmers, H. M. (2010). Grasping trimethylation of histone H3 at lysine 4. *Epigenomics*. doi:10.2217/epi.10.11

Vongsangnak, W., Salazar, M., Hansen, K., & Nielsen, J. (2009). Genome-wide analysis of maltose utilization and regulation in aspergilli. *Microbiology*, *155*, 3893–3902. doi:10.1099/mic.0.031104-0

Waddington, C. H. (1942). The epigenotype. *Endeavour*, 18–20. doi:10.1093/ije/dyr184

Wasiak, S., Legendre-Guillemin, V., Puertollano, R., Blondeau, F., Girard, M., de Heuvel, E., … McPherson, P. S. (2002). Enthoprotin: a novel clathrin-associated protein identified through subcellular proteomics. *The Journal of Cell Biology*, *158*, 855–862. doi:10.1083/jcb.200205078

Weiner, A., Chen, H. V., Liu, C. L., Rahat, A., Klien, A., Soares, L., … Rando, O. J. (2012). Systematic dissection of roles for chromatin regulators in a yeast stress response. *PLoS Biology*, *10*, 17. doi:10.1371/journal.pbio.1001369

Wiemann, P., Sieber, C. M. K., von Bargen, K. W., Studt, L., Niehaus, E. M., Espino, J. J., … Tudzynski, B. (2013). Deciphering the Cryptic Genome: Genome-wide Analyses of the Rice Pathogen Fusarium fujikuroi Reveal Complex Regulation of Secondary Metabolism and Novel Metabolites. *PLoS Pathogens*, *9*. doi:10.1371/journal.ppat.1003475

Wilbanks, E. G., & Facciotti, M. T. (2010). Evaluation of algorithm performance in ChIP-seq peak detection. *PLoS ONE*, *5*. doi:10.1371/journal.pone.0011471

Wu, T. D., & Nacu, S. (2010). Fast and SNP-tolerant detection of complex variants and splicing in short reads. *Bioinformatics (Oxford, England)*, *26*, 873–881. doi:10.1093/bioinformatics/btq057

Xu, H., Handoko, L., Wei, X., Ye, C., Sheng, J., Wei, C.-L., … Sung, W.-K. (2010). A signal-noise model for significance analysis of ChIP-seq with negative control. *Bioinformatics (Oxford, England)*, *26*, 1199–1204. doi:10.1093/bioinformatics/btq128

Yuan, C., Matthews, A. G. W., Jin, Y., Chen, C. F., Brad, A., Ohsumi, T. K., … Oettinger, M. A. (2012). NIH Public Access, *1*(2), 83–90. doi:10.1016/j.celrep.2011.12.008.Histone

Yuan, X.-L., van der Kaaij, R. M., van den Hondel, C. A. M. J. J., Punt, P. J., van der Maarel, M. J. E. C., Dijkhuizen, L., & Ram, A. F. J. (2008). Aspergillus niger genome-wide analysis reveals a large number of novel alpha-glucan acting enzymes with unexpected expression profiles. *Molecular Genetics and Genomics : MGG*, *279*, 545–561. doi:10.1007/s00438-008-0332-7

Zang, C., Schones, D. E., Zeng, C., Cui, K., Zhao, K., & Peng, W. (2009). A clustering approach for identification of enriched domains from histone modification ChIP-Seq data. *Bioinformatics (Oxford, England)*, *25*(15), 1952–8. doi:10.1093/bioinformatics/btp340

Zhang, Y., Liu, T., Meyer, C. A., Eeckhoute, J., Johnson, D. S., Bernstein, B. E., … Liu, X. S. (2008). Model-based analysis of ChIP-Seq (MACS). *Genome Biology*, *9*, R137. doi:10.1186/gb-2008-9-9-r137

Zong, W., Zhong, X., You, J., & Xiong, L. (2013). Genome-wide profiling of histone H3K4-tri-methylation and gene expression in rice under drought stress. *Plant Molecular Biology*, *81*(1-2), 175–88. doi:10.1007/s11103-012-9990-2